NTNU – Trondheim
Norwegian University of
Science and Technology

Estimation of Anisotropy Parameters and AVO modeling of the Troll Field, North Sea

Hilde Haktorson

Abstract

In the work of this Master's thesis, the anisotropy parameters, ε and δ, for the reservoir and the cap rock on the Troll Field have been estimated. This was done using well logs from 35 wells, including the P-wave sonic log and the inclination angle log of the wellbore. The velocity from the sonic log and the inclination angle were applied to a second order polynomial equation, which includes the anisotropy parameters.

The Matlab software was utilized to perform the calculations and to generate plots necessary to estimate the parameters. To obtain more reliable results, different filters were applied to the data set for both the reservoir and the cap rock. The filters consisted of different intervals of porosity, acoustic impedance and depth, both individually and combined in different ways. In advance of the filtering, histograms were made for porosity, acoustic impedance and depth to look at the distribution of each, in order to find reasonable ranges for filtering on the different parameters.

This process resulted in the following estimations of the anisotropy parameters for the reservoir: ε = -0.081 and δ = -0.026. The anisotropy parameters for the cap rock, which is a shale in most of the wells, was estimated as follows: ε = 0.106 and δ = 0.055. These parameters were applied in an AVO analysis, performed for the vertical well 31/2-L-41. An approximation using the 3-term Shuey equation was applied for this purpose. The anisotropic case was compared with the isotropic case. This showed that there is an evident difference between the isotropic and the anisotropic model at large offsets. The exact solution from the Zoeppritz's equations was also included for comparison. This proved to be very close to the approximate solution.

Amplitude values from seismic gathers were included in the AVO analysis. This showed that the amplitude values from the gathers increased with in-

cidence angle, as for the isotropic and the anisotropic model. However, the increase in amplitude was much less than for the models.

From this work, the estimation of the anisotropy parameters were shown to have a large uncertainty, even after filtering. To make the estimation of δ more stable, more deviated wells to cover the whole inclination angle range, especially from $27 - 40\,°$, are required. ε is dependent on the vertical and the horizontal P-wave velocity only, thus there should be less uncertainty in estimating this parameter.

From the AVO analysis, including the amplitude values from the gathers, no conclusive statements could be established due to the fact that the amplitude values had to be scaled to fit the amplitude values with the models. The amplitude values of the gathers were scaled to the amplitude values of the isotropic case at far offset, thus the result could have been altered if scaled to the anisotropic case.

Sammendrag

I denne masteroppgaven har anisotropiparametrene, ε og δ, blitt estimert for reservoaret og takbergarten på Troll-feltet. Dette har blitt gjort ved hjelp av P-bølge sonic-logg fra 35 brønner og helningsvinkel-logg fra brønnbanen. Hastigheten fra sonic-loggen og helningsvinkelen ble brukt i en annenordens polynomligning, som inneholder anisotropiparametrene.

Programvaren Matlab, ble brukt til å utføre beregninger og til å generere plott som er nødvendig for å estimere parametrene. For å oppnå mer pålitelige resultater, ble ulike filtre brukt på datasettet for både reservoaret og takbergarten. Filtrene består av forskjellige intervaller av porøsitet, akustisk impedans og dyp, både individuelt og kombinert på forskjellige måter. I forkant av filtreringen, ble histogrammer laget for porøsitet, akustisk impedans og dyp for å se på fordelingen av hver, og dermed for å finne rimelige verdier for filtreringen på de forskjellige parametrene.

Dette resulterte i følgende estimeringer av anisotropiparametrene for reservoaret: ε = -0.081 og δ = -0.026. Anisotropiparametrene for takbergarten, som er en skifer i de fleste brønnene, ble estimert som følger: ε = 0.106 og δ = 0.055. Disse parametrene ble anvendt i en AVO-analyse for den vertikale brønnen 31/2-L-41. Den tilnærmede 3-term Shuey ligningen ble brukt i AVO-analysen, der det anisotrope tilfellet ble sammenlignet med det isotrope tilfellet. Dette viste en tydelig forskjell mellom den isotrope og den anisotrope modellen ved store offset. Den eksakte løsningen fra Zoeppritz's ligninger ble også inkludert og sammenlignet. Dette viste seg å være svært nær den tilnærmede løsningen.

Amplitudeverdier fra seismiske gathere inngikk i AVO-analysen. Dette viste at amplitudene fra gatherne økte med innfallsvinkel, som det gjorde for den isotrope og den anisotrope modellen. Imidlertid var økningen i amplitude

mye mindre enn for modellene.

Estimeringen av anisotropiparametrene viste seg å ha stor usikkerhet, selv etter filtrering. For å gjøre estimeringen av δ mer stabil, trengs flere avviksbrønner for å dekke alle helningsvinkler, spesielt mellom 27 og 40°. Siden ε kun er avhengig av vertikal og horisontal P-bølge hastighet, burde det være mindre usikkerhet i estimeringen av denne parameteren.

Siden amplitudeverdiene fra gatherne måtte skaleres for å passe amplitudeverdiene for modellene i AVO-analysen, kunne det ikke sies noe kvantitativt om gatherne ligger nærmest den isotrope eller den anisotrope modellen. Amplitudeverdiene fra gatherne ble skalert til amplitudeverdiene til det isotrope tilfellet ved fjern offset, dermed kunne resultatet ha blitt et annet hvis amplitudeverdiene hadde blitt skalert til det anisotrope tilfellet i stedet for.

Contents

List of Figures

List of Tables

Preface

This report is the result of my work in the subject TPG 4930 – Petroleum Geophysics, Master's Thesis at the Norwegian University of Science and Technology (NTNU). The problem was described by Martin Landrø, Professor in Applied Geophysics at NTNU, in cooperation with Kenneth Duffaut, Principal Researcher Reservoir Geophysics at Statoil Research Center and Jakob Andreas Gjengedal, Discipline Leader Reservoir Geophysics at the Troll Department in Statoil ASA.

The exporting and preparation of the well logs, the calculations and the Matlab scripts were written and done by me.

I would like to give my acknowledgements to Statoil ASA for giving me access to the Statoil network and permission to use the data and software I needed. I would also like to thank Martin Landrø and Kenneth Duffaut for their guidance and informative discussion throughout the work of this thesis and for providing articles and background information. In addition I would like to thank Jakob Andreas Gjengedal for his assistance with software, the seismic gathers and for proofreading, and Frank Hauge, Reservoir Geophysics at Odin Petroleum AS, for his assistance with Matlab. Furthermore, I want to thank my family and friends for supporting me during this semester.

Trondheim, June 28$^{\text{th}}$ 2012

Hilde Haktorson

Chapter 1

Introduction

1.1 Motivation

The Earth, as usually assumed, is not isotropic. This is often assumed due to
the complexity the anisotropy yields in equations regarding the Earth. The
Earth is anisotropic with a lot of variation in stresses due to movements of
the mantle. The movements of the mantle is caused by heat trying to escape
into the atmosphere. Taking the anisotropy into account will lead to a more
correct model of the Earth and thereby give more correct results concern-
ing a lot of different techniques and analyses within geophysics, including an
amplitude versus offset (AVO) analysis.

In AVO analyses, the controlling factors are lithology, fluid and anisotropy.
Usually the anisotropy is regarded as a small effect, which can be neglected,
but this may not be the case. The anisotropy may even have a larger effect on
the amplitudes than fluids. The anisotropy is described by three anisotropy
parameters, in which two of them, ε and δ, will be discussed in this study.
An AVO analysis is done across a boundary, thus a prerequisite for an AVO
analysis is that these parameters must be calculated for two layers. In this
case, the two layers are the reservoir (a sandstone) and the cap rock (a shale
in most of the wells). The anisotropy parameters, ε and δ, are generally neg-
ative for sandstone (Walsh et al., 2006) and positive for shale (Walsh et al.,
2007). Taking the anisotropy into account will induce larger amplitude val-
ues than for an isotropic case, especially since the AVO analysis includes the
differences $\Delta\varepsilon$ and $\Delta\delta$ across the boundary (see Equation 2.32 and 2.33).

One of the anisotropy parameters, ε, has previously been estimated for the Troll Field using well logs. This was done by Richard Tøndel in 2005 (Tøndel, 2005). He used 25 wells, in which 14 wells are located in Troll West and 11 wells are located in Troll East. The result was found to be stable at approximately 8 % (-0.08).

The purpose of this study is to estimate ε and δ in detail, for both the reservoir and the cap rock in Troll West. The result of ε for the reservoir in this work will be compared with the result from Tøndel's report. Further on, an AVO analysis will be performed for the anisotropic case and the isotropic case for comparison. This will lead to an indication of how important including the anisotropy in AVO analyses can be. Real seismic gathers will be compared to both the isotropic and the anisotropic case and will be expected to be closer to the anisotropic case. In an ideal case, the amplitude values from the seismic gathers will overlap with the anisotropic case.

This work is motivated by the facts that the anisotropy gives us a more correct model of the Earth and that it may play a bigger role in AVO analysis than generally thought. A better understanding of anisotropy is also important for seismic imaging, seismic interpretation and reservoir characterization (Li and Pickford, 2002).

1.2   The development of the Troll Field

This subchapter is modified from the introduction of the specialization project "Seismic interpretation of an alternative top 4-series on the Troll Field" by Hilde Haktorson (Haktorson, 2011).

The Troll Field is located in the northern North Sea, near the west coast of Norway, about 100 km north-west of Bergen (Leiknes and Osvoll, 2005) (see Figure 1.1). The field is on the Horda Platform close to the eastern margin of the Viking Graben. Troll is the largest producing oil and gas field on the Norwegian continental shelf, and covers an area of 750 km^2. The reservoir consists of an oil layer of varying thickness, between a large gas cap and the aquifer. The field is divided into three segments, Troll West Oil Province (TWOP), Troll West Gas Province (TWGP) and Troll East. These segments are separated by large north-south trending faults, created by rifting during

the Upper Jurassic and the Lower Cretaceous period. The initial oil column on TWOP was between 22 and 27 m with an overlying gas cap of up to 43 m, and on TWGP about 11 to 13 m, with an overlying gas cap of 0-210 m. On Troll East, the initial oil column was only 1 to 6 m, but the gas cap is up to 250 m, so this is why it is mainly an area for gas production (Bolle, 1992). Figure 1.2 shows a structural map of the top of the reservoir indicating the different segments.
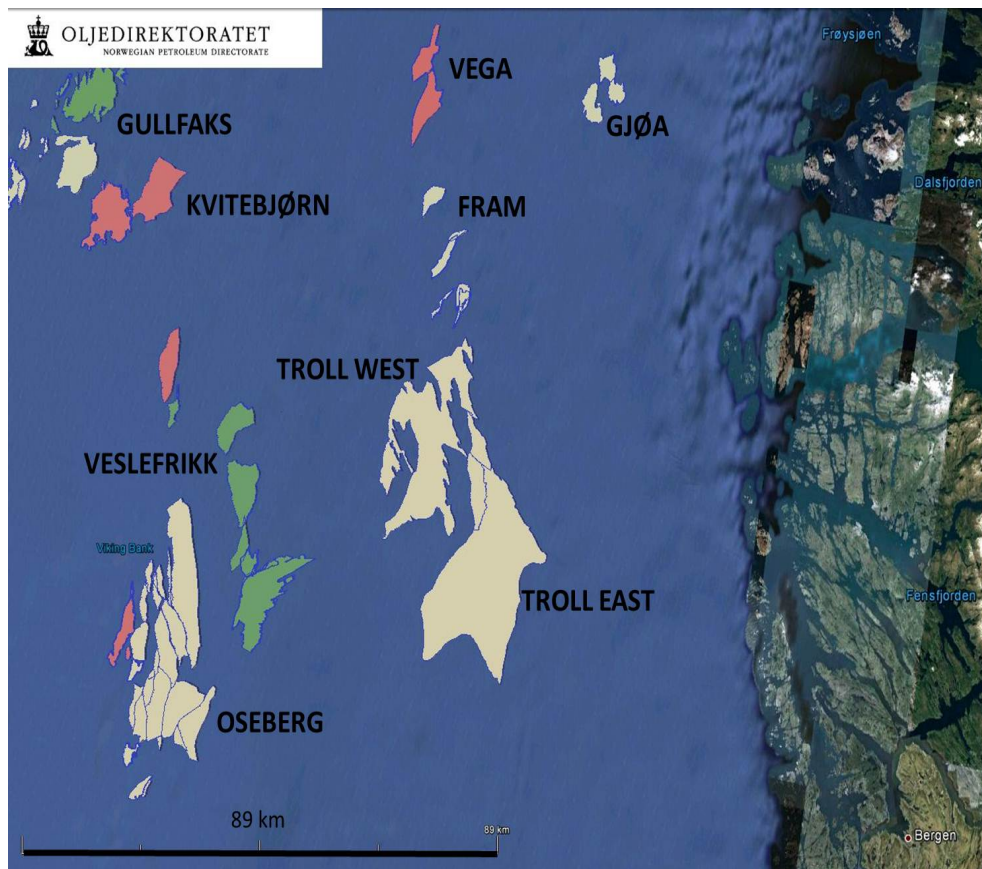
Figure 1.1: The Troll Field is located in the North Sea near the west coast of Norway. (From Norwegian Petroleum Directorate's website).

The Troll West was discovered in 1979 and the Troll East in 1983 (Dreyer et al., 2005). It is a field with 1,700 billions Sm3 of gas and four billion barrels of oil in place, and the expected recoverable oil reserves is 1.4 billion barrels (Mikkelsen et al., 2005). The decision to develop the oil reserves was taken in 1991 and the first production well was drilled in 1995 on Troll West (Madsen and Abtahi, 2005). In 2005, two thirds of the total oil reserves had been produced. Since the oil column is relatively thin, development of

horizontal drilling technology has been important for this field. More than 170 horizontal producers have been drilled on Troll West and the number of wells is still increasing. The scope of this work will be on Troll West.
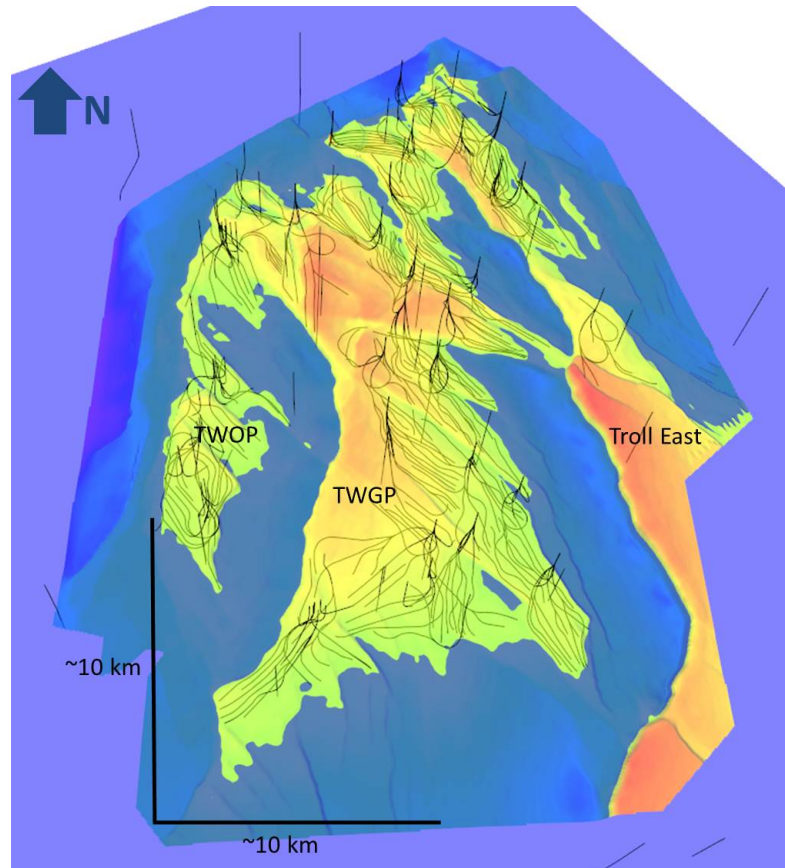
Figure 1.2: A structural map of top reservoir cut by the initial oil-water-contact. Shown in the figure are also all the horizontal wells drilled on the field. (Generated in the Irap RMS software).

Chapter 2

Background theory

The next two subchapters are modified from the introduction of the specialization project "Seismic interpretation of an alternative top 4-series on the Troll Field" by Hilde Haktorson (Haktorson, 2011).

2.1 Geological history

All through the Permian-Triassic period, most of the North Sea was an area of continental deposition within a rift system (Bolle, 1992). This is where the Viking Graben is situated today. Fluvial deposits accumulated near the margins of the rifts, and alluvial and lacustrine sediments were deposited towards the centers of the basins. On the flanks of the Viking Graben, shallow marine conditions developed during the middle to the late stages of the Upper Jurassic period, creating a thick sequence of high quality reservoir sandstone, which today is the Troll reservoir. This thick sequence of sandstone consists of alternations of progradational–retrogradational cyclothems. The progradational to aggradational parasequences formed sandstone wedges belonging to the Sognefjord Fm., while the transgressive parasequences formed fine-grained sandstones and siltstones deposited in between the sandstone wedges. This sequence of progradational to transgressive parasequences was controlled by regional sea level fluctuations which is a part of an overall regional transgression from the stages of late Callovian to early Volgian.

The reservoir succession represents an extensive coastal spit system with sedi-

mentary input from the north-east, creating a spit-strandplain in the western and central parts of the field. The shallow marine system is characterized by wave and tidal environments, with a high-energy coastal zone to the west, a tidal backbasin to the south-east and more marine conditions to the south. Figure 2.1 shows a depositional model for the Sognefjord Fm. There is a pinchout of successive sandstone units westwards, with the distal parts being thought of as shelf-shoreface deposits and the proximal sandier parts representing delta-front, estuarine and barrier bar environments (Dreyer et al., 2005).
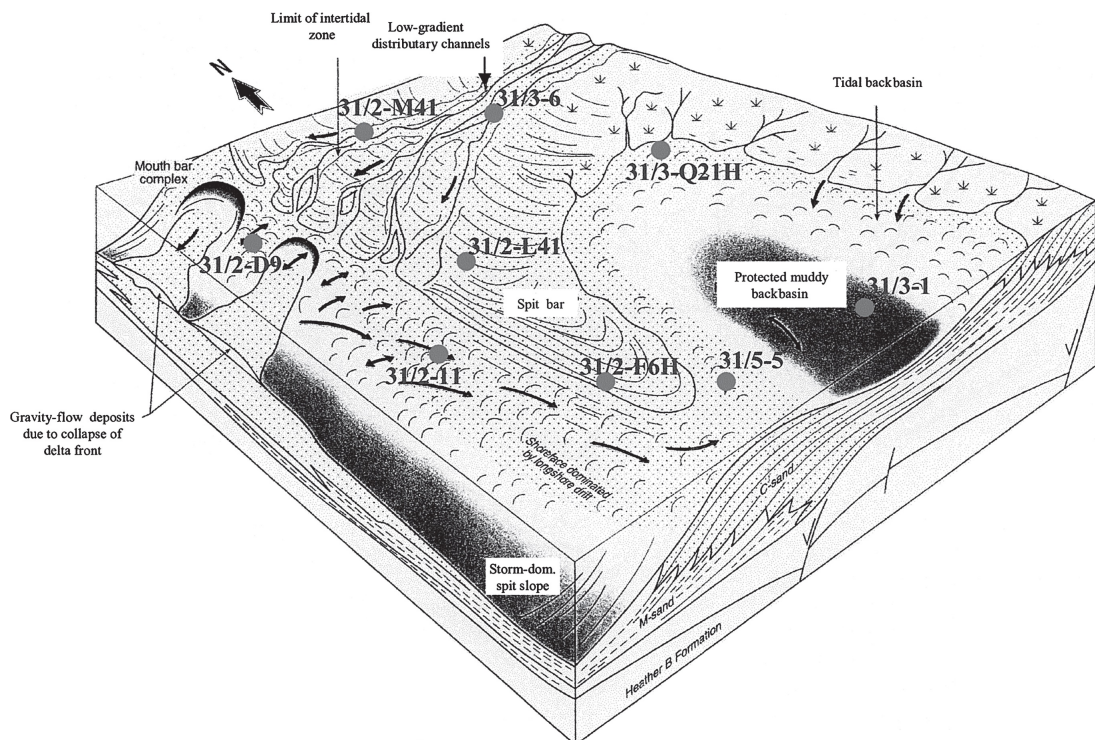
Figure 2.1: A depositional model for the Sognefjord Fm. in the Troll Field (Dreyer et al., 2005).

2.2 The petroleum system

The main reservoir on the Troll Field belongs to the Upper Jurassic Sognefjord Fm. (Madsen and Abtahi, 2005). It consists of stacked off-lapping

shallow marine sandstones with siltstones in between. The sandstone in the reservoir comprises of alternating m-sand and c-sand lithologies. The m-sands are mica rich, fine grained sands with permeabilities between 10 to several hundred milliDarcies. The c-sands are clean, medium to coarse grained sands with permeabilities in the range of 1-30 Darcy (Leiknes and Osvoll, 2005). The porosity is 35 % on average for the m- and c-sands. The reservoir has an excellent geology with no shale interbeddings (Bolle, 1992), but about 10 % of the reservoir is calcite cemented (Gibbons et al., 1993).

The source rock for the hydrocarbons on the Troll Field is the organic-rich shales of the Draupne Fm. located to the west-northwest of the field in the deeper parts of the Viking Graben. Migration pathways have been influenced by major faults and the migration of hydrocarbons is an ongoing process (Bolle, 1992). The cap rock in most part of the field belongs to the Upper Jurassic Draupne Fm., which is a shale. In some areas in the northwest the cap rock is from the Shetland Gp. and and in some areas in the west the cap rock is the Lista Fm. The cap rock from the Shetland Gp. is a mix of limestone, marl and claystone, while the Lista Fm. cap rock is a claystone. The Draupne Fm. cap rock is immature and does not provide hydrocarbon generation (Bolle, 1992).

Stratigraphically, the formations below the reservoir are the Middle Jurassic Fensfjord Fm. and the Krossfjord Fm. These formations are part of the Lower Viking Gp. Figure 2.2 shows the stratigraphy of the reservoir.

CHRONOSTRATIGRAPHY		LITHOSTRATIGRAPHY	
PERIOD	STAGE	GROUP	FORMATION
EARLY TERTIARY	EOCENE	ROGALAND	BALDER
	PALEOCENE		SELE
			LISTA
			MAUREEN
LATE CRETACEOUS		SHETLAND	
EARLY CRETACEOUS		CROMER KNOLL	
	RYAZANIAN	VIKING	DRAUPNE
LATE JURASSIC	VOLGIAN		U. HEATHER
	KIMMERIDGIAN		SOGNE
	OXFORDIAN		MID. FJORD. HEATHER
MIDDLE JURASSIC	CALLOVIAN		FENSFJORD
	BATHONIAN		KROSS- FJORD. LOWER HEATHER
	BAJOCIAN AALENIAN	BRENT	TARBERT
			NESS
			ETIVE
EARLY JURASSIC	TOARCIAN	DUNLIN	DRAKE
	PLIENSBACHIAN		COOK
			U. AMUNDSEN
	SINEMURIAN		JOHANSEN
			L. AMUNDSEN
	HETTANGIAN		STATFJORD
TRIASSIC	RHAETIAN		
			HEGRE

Figure 2.2: The stratigraphy of the Troll reservoir (Bolle, 1992).

2.3 Anisotropy

A material is anisotropic if the properties of the material depend on direction. Seismic anisotropy is an expression for the directional dependence of seismic wave velocity in rocks (Thomsen, 2002). This applies to both P- and S-wave velocity (and other types of waves), but only anisotropy of the P-wave will be considered in this thesis. The seismic velocities depend on elastic moduli (and density), such as bulk and shear moduli, hence the seismic anisotropy is in fact the elastic moduli varying with angle. The elastic anisotropy in the Earth is caused by joints or microcracks, or by layered bedding in sedimentary formations (clay, sandstone etc.). The cracks are again caused by stresses in the Earth. Knowlegde of the anisotropy will give rise to an indication of the direction of the stresses within the stress field, which again is important to consider while drilling a well.

The anisotropy can have different symmetries, whereas the hexagonal symmetry is the one considered in this case due to the fact that it is the simplest realistic case. This symmetry has five independent elastic constants, compared to the isotropic case which has only two independent elastic constants (and the fully anisotropic case which has 21 independent elastic constants) (Mavko et al., 2009). The hexagonal symmetry is also referred to as transversely isotropic (TI) or polar anisotropic. The TI symmetry is symmetric about an axis that is normal to a plane of isotropy. In geophysics, the axis of symmetry is usually the vertical direction, hence the name vertical transversely isotropic (VTI) (Thomsen, 2002). For the VTI case, the anisotropy is given by three parameters discussed in Section 2.4. For this thesis, concerning the seismic anisotropy, the anisotropy is assumed to be weak. This means that the anisotropy parameters are $\ll 1$. This makes the formulas shown in Section 2.4 simpler to use.

2.4   The anisotropy parameters

Wave propagation through a weakly anisotropic medium is characterized by P- and S-wave velocity and three anisotropy parameters which are shown in the following equations; Equation 2.1, 2.2, 2.3, 2.4, and 2.5 (Slawinski, 2002; Thomsen, 1986).

$$V_{PV} = \sqrt{\frac{C_{33}}{\rho}}, \tag{2.1}$$

$$V_{SV} = \sqrt{\frac{C_{44}}{\rho}}, \tag{2.2}$$

$$\gamma = \frac{C_{66} - C_{44}}{2C_{44}}, \tag{2.3}$$

$$\delta = \frac{(C_{13} + C_{44})^2 - (C_{33} - C_{44})^2}{2C_{33}(C_{33} - C_{44})}, \tag{2.4}$$

$$\varepsilon = \frac{C_{11} - C_{33}}{2C_{33}}, \tag{2.5}$$

where V_{PV} is the vertical P-wave velocity, V_{SV} is the vertical S-wave velocity, and γ, δ and ε are dimensionless anisotropy parameters. ρ is the density, and the C_{xx} are the five independent elastic constants. Only ε and δ are needed for the AVO analysis, so γ will not be discussed further.

ε is expressed by C_{11} and C_{33}, which are shown in Equation 2.6 and Equation 2.7 (Hornby et al., 2002).

$$C_{11} = \rho V_{PH}^2, \tag{2.6}$$

$$C_{33} = \rho V_{PV}^2, \tag{2.7}$$

where V_{PH} is the horizontal P-wave velocity and the rest of the variables are the same as defined above. From Equation 2.5, using Equation 2.6 and 2.7, ε can be written as Equation 2.8, where ρ gets canceled.

$$\varepsilon = \frac{V_{PH}^2 - V_{PV}^2}{2V_{PV}^2}, \tag{2.8}$$

where again the variables are the same as in the equations above. This equation can also be written as Equation 2.9.

$$\varepsilon = \frac{\left(\frac{V_{PH}}{V_{PV}}\right)^2 - 1}{2} \tag{2.9}$$

As can be seen, ε depends only on the horizontal and vertical P-wave velocity. This is why it is called the P-wave anisotropy parameter.

Seen from Equation 2.4 and 2.5, δ is more complicated than ε. This is why a different approach is needed to solve for both ε and δ. The method used is based on Equation 2.10 (Mavko et al., 2009).

$$V_p(\theta) \approx \alpha \left(1 + \delta \sin^2 \theta \cos^2 \theta + \varepsilon \sin^4 \theta\right), \tag{2.10}$$

where V_p is the phase velocity, α is the vertical P-wave velocity (the same as V_{PV}), δ and ε are the previously defined anisotropy parameters and θ is the angle of the wave vector relative to the x_3-axis, which is also called the polar angle (Thomsen, 2002). This angle is the same as the inclination angle of

the well path. The velocity calculated from the P-wave sonic log is assumed to be the phase velocity. As can be seen from the equation, V_p is equal to α when the inclination angle, θ, is zero, which means that the well is vertical. To make Equation 2.10 easier to implement, Equation 2.11 is inserted into Equation 2.10 to get Equation 2.12.

$$\cos^2 \theta = 1 - \sin^2 \theta, \tag{2.11}$$

$$V_p\left(\theta\right) \approx \alpha \left(1 + \delta \sin^2 \theta + (\varepsilon - \delta) \sin^4 \theta\right) \tag{2.12}$$

From the sonic logs and the inclination angle logs, different velocities at different inclination angles will be available. The vertical velocity, α, (at zero inclination) will also be given. To solve Equation 2.12 for δ and ε, the equation can be compared with a general second order equation. This is given by Equation 2.13.

$$y = A + Bx + Cx^2, \tag{2.13}$$

where y indicates a function, A,B and C are constants and x is the variable. Comparing Equation 2.13 with Equation 2.12 where $y = V_p\left(\theta\right)$ and $x = sin^2\theta$, gives Equation 2.14, 2.15 and 2.16.

$$A = \alpha, \tag{2.14}$$

$$B = \alpha\delta, \tag{2.15}$$

$$C = \alpha\left(\varepsilon - \delta\right), \tag{2.16}$$

where A, B and C are the coefficients from the second order polynomial function. From this, formulas for δ and ε are the following Equation 2.17 and Equation 2.18.

$$\delta = \frac{B}{\alpha}, \tag{2.17}$$

$$\varepsilon = \frac{C}{\alpha} + \delta \tag{2.18}$$

In the book written by Mavko et al. (2009), it is stated that $\varepsilon > \delta$ and that δ is smaller in sandtones than in shales. As mentioned in Chapter 1, the anisotropy parameters are expected to be negative for sandstone. Since $|\varepsilon| > |\delta|$ and the anisotropy parameters are negative, the coefficients B and C must be negative. The anisotropy parameters are expected to be positive for shales, thus the coefficients B and C must be positive. This gives an idea of what shape to expect for the fitted curve from the second order polynomial function for each formation. This will be discussed further in Chapter 5.

These preceding equations will be used to find the anisotropy parameters using Matlab, which will be descibed in further detail in Chapter 3.

2.5   The standard deviation of ε

In this analysis, it is valuable to calculate the standard deviation of ε and δ. An integrated function in Matlab will return the standard deviation of the velocity, but not ε or δ given the data set in this work. Since ε is a function of the vertical and the horizontal velocity, calculating the standard deviation of ε is achievable and can be done without too much complicated mathematics. Since δ is more complex, the standard deviation of this parameter is challenging to achieve, therefore only a qualitative analysis of this standard deviation will be done. To calculate the standard deviation of ε when the standard deviation of its variables are known, Equation 2.19 can be applied. This is the equation for the variance, which is a measure of the spread of a data set. From now on, the V_{PV} and the V_{PH} will be written as V_v and V_h to make the coming equations appear tidier.

$$\sigma_\varepsilon^2 = \left(\frac{\partial \varepsilon}{\partial V_v}\right)^2 \sigma_{V_v}^2 + \left(\frac{\partial \varepsilon}{\partial V_h}\right)^2 \sigma_{V_h}^2 + 2\left(\frac{\partial \varepsilon}{\partial V_v}\right)\left(\frac{\partial \varepsilon}{\partial V_h}\right)\sigma_{V_v V_h}, \qquad (2.19)$$

where σ_ε^2, $\sigma_{V_v}^2$ and $\sigma_{V_h}^2$ are the variances of ε, the vertical and the horizontal P-wave velocity respectively (σ_ε, σ_{V_v} and σ_{V_h} are the standard deviations). $\sigma_{V_v V_h}$ is the covariance of the vertical and the horizontal P-wave velocity. $(\partial \varepsilon / \partial V_v)$ and $(\partial \varepsilon / \partial V_h)$ are the partial derivative of ε with respect to each of the variables. Assuming that the variables, V_v and V_h, are independent of each other, the covariance is equal to zero, so the last term is canceled. This is the worst case scenario when calculating the standard deviation. The standard deviation is a measure on how much variation there is from the

average, and is equal to the square root of the variance. When the last term in Equation 2.19 is canceled, the standard deviation is shown in Equation 2.20.

$$\sigma_\varepsilon = \sqrt{\left(\frac{\partial \varepsilon}{\partial V_v}\right)^2 \sigma_{V_v}^2 + \left(\frac{\partial \varepsilon}{\partial V_h}\right)^2 \sigma_{V_h}^2}, \tag{2.20}$$

where σ_ε is the standard deviation of ε and the rest of the variables are the same as defined above. To do the partial derivation, Equation 2.8 is easier written as Equation 2.21.

$$\varepsilon = \frac{V_h^2}{2V_v^2} - \frac{1}{2} \tag{2.21}$$

Equation 2.22 and Equation 2.23 are the partial derivatives of ε with respect to the horizontal and the vertical P-wave velocity respectively.

$$\frac{\partial \varepsilon}{\partial V_h} = \frac{V_h}{V_v^2}, \tag{2.22}$$

$$\frac{\partial \varepsilon}{\partial V_v} = -\frac{V_h^2}{V_v^3} \tag{2.23}$$

Inserting Equation 2.22 and 2.23 into Equation 2.20 gives Equation 2.24.

$$\sigma_\varepsilon = \sqrt{\left(\frac{V_h^4}{V_v^6}\right) \sigma_{V_v}^2 + \left(\frac{V_h^2}{V_v^4}\right) \sigma_{V_h}^2}, \tag{2.24}$$

which is the same as Equation 2.25.

$$\sigma_\varepsilon = \frac{V_h}{V_v} \sqrt{\left(\frac{V_h^2}{V_v^4}\right) \sigma_{V_v}^2 + \left(\frac{1}{V_v^2}\right) \sigma_{V_h}^2}, \tag{2.25}$$

This final equation is applied to get the results for the standard deviation of ε for the different filters (explained in Chapter 3 and Chapter 4).

2.6   Amplitude versus offset (AVO)

This subchapter is modified from the background theory of the specialization project "Seismic interpretation of an alternative top 4-series on the Troll Field" by Hilde Haktorson (Haktorson, 2011).

AVO depends on differences in the P-wave velocity, the S-wave velocity and the density of a rock. The responses for the P- and S-wave velocities are different for fluids/no fluids in the pore spaces. P-wave velocities are sensitive to changes in the pore fluids. Only a small amount (5 %) of gas in the pores will decrease the velocity significantly (Hilterman, 2001). S-waves do not propagate in fluids, and thus the change of fluids in the pores will have an insignificant effect on the S-wave velocity. S-wave velocities depend mainly on the framework of the rocks. The change in lithology affects both the P-wave and the S-wave velocity, while the change in fluid mainly affects the P-wave velocity. AVO is widely used in subsurface characterization. In this thesis only the AVO analysis for the PP reflection will be discussed, both for the isotropic case and the anisotropic case.

2.6.1   AVO for isotropic case

One of the many formulas used to calculate the reflection coefficient as a function of incidence angle is the 3-term Shuey equation, which is the same as the Smith & Gidlow's approximation. This equation is an approximation of the PP reflection coefficient from the exact and complex Zoeppritz's equations. Equation 2.26 is for the isotropic case (Thomsen, 2002).

$$R_p \left(\theta \right) = R_0 + R_2 \sin^2 \theta + R_4 \sin^2 \theta \tan^2 \theta, \tag{2.26}$$

where R_p is the P-wave reflection coefficient and θ is the incidence angle. R_0, R_2 and R_4 are defined in Equation 2.27, 2.28 and 2.29.

$$R_0 = \frac{1}{2} \left[\frac{\Delta V_P}{V_P} + \frac{\Delta \rho}{\rho} \right], \tag{2.27}$$

$$R_2 = \frac{1}{2} \left[\frac{\Delta V_P}{V_P} - \frac{4 V_S^2}{V_P^2} \left(\frac{\Delta \rho}{\rho} + \frac{2 \Delta V_S}{V_S} \right) \right], \tag{2.28}$$

$$R_4 = \frac{1}{2} \left[\frac{\Delta V_P}{V_P} \right], \tag{2.29}$$

where V_P is the P-wave velocity averaged over an interface, V_S is the S-wave velocity averaged over an interface and ρ is the density also averaged over an interface. ΔV_P, ΔV_S and $\Delta \rho$ are the changes over an interface in the P-wave velocity, the S-wave velocity and the density respectively. In AVO analysis, the last term in Equation 2.26 can be cancelled, thus making the Equation linear where R_0 is the intercept and R_2 is the slope or gradient.

When there is a lithologic transition when crossing the interface, the ($\Delta\rho/\rho + 2\Delta V_S/V_S$) term is usually twice as large as the $\Delta V_P/V_P$ term, thus leading to R_2 having a minus sign, which is opposite of R_0. If there is a fluid transition when crossing the interface, the ($\Delta\rho/\rho + 2\Delta V_S/V_S$) term is close to 0 and the R_2 has the same sign as R_0. Thus, the AVO can identify fluid transitions.

2.6.2 AVO for anisotropic case

Equation 2.30 is also the 3-term Shuey equation, only for the anisotropic case (Thomsen, 2002).

$$R_p\left(\theta_w\right) = R_0 + R_2 \sin^2 \theta_w + R_4 \sin^2 \theta_w \tan^2 \theta_w, \tag{2.30}$$

where R_p is the P-wave reflection coefficient and θ_w is the wavefront angle. The incidence angle is assumed to be equal to the wavefront angle, thus the incidence angle will be used for Equation 2.30. R_0, R_2 and R_4 are defined in Equation 2.31, 2.32 and 2.33.

$$R_0 = \frac{1}{2} \left[\frac{\Delta V_{P0}}{V_{P0}} + \frac{\Delta\rho}{\rho} \right], \tag{2.31}$$

$$R_2 = \frac{1}{2} \left[\frac{\Delta V_{P0}}{V_{P0}} - \frac{4V_{S0}^2}{V_{P0}^2} \left(\frac{\Delta\rho}{\rho} + \frac{2\Delta V_{S0}}{V_{S0}} \right) + \Delta\delta \right], \tag{2.32}$$

$$R_4 = \frac{1}{2} \left[\frac{\Delta V_{P0}}{V_{P0}} + \Delta\varepsilon \right], \tag{2.33}$$

where V_{P0} is the P-wave velocity averaged over an interface, V_{S0} is the S-wave velocity averaged over an interface and ρ is the density also averaged over an interface. ΔV_{P0}, ΔV_{S0} and $\Delta \rho$ are the changes over an interface in the P-wave velocity, the S-wave velocity and the density respectively. $\Delta \varepsilon$ and $\Delta \delta$ are the changes across an interface in the anisotropy parameters. The 0 added to the subscript means that the velocities are measured in a vertical direction. Equation 2.30 shows that the factor multiplying with $\Delta V_{P0}/V_{P0}$ is the same as for $\Delta \delta$. All the terms in the equation are of the same order as $\Delta \delta$ $(<< 1)$, thus the anisotropy should not be neglected.

Chapter 3

Methodology

Most of the work in this thesis consists of calculations, filtering of data and generating plots using Matlab. Landmark's two softwares OpenWorks and Compass have been used for exporting data. Well Seismic Fusion (WSF), which is a software within OpenWorks, has been utilized to acquire amplitudes for real seismic gathers. Some of the figures in this thesis have been made in DecisionSpace Desktop, also a software within OpenWorks.

3.1 Estimation of anisotropy parameters

To estimate the anisotropy parameters, Equation 2.12 in Section 2.4 is applied. For this equation, the phase velocity, V_p, and the angle of the wave vector relative to the x_3-axis, θ, are required. V_p is assumed to be the velocity calculated from the P-wave sonic log, and θ is the inclination angle of the wellbore. Thus the P-wave sonic log and the inclination angle log are needed in order to estimate the anisotropy parameters.

Firstly, an overview of all the wells on Troll West with both a P-wave sonic log (LFP_DT log) and an inclination angle log available was established. Well lists in OpenWorks were examined carefully and 35 wells, which meet the criteria, were found. Microsoft Excel was used as an aid to organize and to get an overview of the data needed. A feature in OpenWorks, called Well Data Export, was utilized for exporting the P-wave sonic logs, while Compass was used for exporting the inclination angle logs. Since the purpose of this thesis is to study how anisotropy is affecting an AVO analysis, the logs

were exported in intervals for the reservoir and the cap rock. The exporting was done for each interval for each well.

Table 3.1 shows an overview of all the 35 wells used in this work, with their respective reservoir intervals and the average inclination angle for each well within the reservoir interval. This table shows that the Sognefjord Fm. is the reservoir formation in all the wells used in this work. The depths of the reservoir in each well are varying as well as the thicknesses. It also shows that most of the wells have an inclination angle of $<4\,°$, which is approximately vertical. Only nine wells are deviated, with a maximum average inclination angle around $64\,°$.

Table 3.2 shows an overview of all the wells, with their respective cap rock intervals and the average inclination angle for each well within the cap rock interval. This table shows that the cap rock varies between the Draupne Fm., the Shetland Gp. and the Lista Fm. The Draupne Fm. is the cap rock in 25 wells, and the Shetland Gp. and the Lista Fm. are the cap rocks in eight and two wells respectively. It shows that of the nine deviated wells, six of the wells have the Draupne Fm., two of the wells have the Shetland Gp. and only one well has the Lista Fm. as the cap rock. The maximum average inclination angle within the cap rock interval is approximately $61\,°$.

Figure 3.1 shows where the 35 wells in this study are situated on the Troll Field.

To estimate the anisotropy parameters, the velocity calculated from the sonic log was plotted versus the inclination angle. The velocity was plotted in the unit km/s and the inclination as $\sin(inc)^2$. To convert from the slowness from the sonic log [μs/ft] to the velocity used in the plot [km/s], a conversion factor of velocity $= (3.048 \cdot 10^2) /$slowness is used.

From the data set, a polynomial function of second order was fitted to the data, giving the coefficients in Equation 2.13 in Section 2.4, which are given by Equation 2.14, 2.15 and 2.16. Matlab's built-in function, polyfit, was used to obtain the coefficients. As mentioned in Section 2.4, coefficients B and C should be negative for sandstones, thus the curve from the second order polynomial function will show a decrease in velocity with inclination angle. The opposite will be true for shales, where the curve will show an

Well	Reservoir formation	Reservoir interval, meters MD	Mean inclination angle, °
NO 31/2-1	Sognefjord	1440.20-1594.50	0.82
NO 31/2-10	Sognefjord	1600.31-1798.41	1.19
NO 31/2-11	Sognefjord	1557.97-1678.10	0.57
NO 31/2-12	Sognefjord	1364.88-1540.58	0.80
NO 31/2-13 S	Sognefjord	1727.6-1932.05	44.31
NO 31/2-14	Sognefjord	1533.10-1684.6	0.89
NO 31/2-15	Sognefjord	1482.28-1635.56	3.49
NO 31/2-17 A	Sognefjord	1689.98-1894.68	42.61
NO 31/2-18	Sognefjord	1518.83-1686.95	0.58
NO 31/2-18 A	Sognefjord	1519.23-1704.37	23.15
NO 31/2-3	Sognefjord	1384.30-1554.29	0.98
NO 31/2-4 R	Sognefjord	1366.94-1519.84	1.00
NO 31/2-5	Sognefjord	1536.02-1693.19	2.12
NO 31/2-6	Sognefjord	1491.80-1672.37	1.08
NO 31/2-7	Sognefjord	1545.40-1660	0.45
NO 31/2-9	Sognefjord	1548.90-1708.50	2.11
NO 31/2-B-3 H	Sognefjord	1784.23-2040.45	54.61
NO 31/2-D-10 H	Sognefjord	1496.62-1649.30	3.23
NO 31/2-D-9	Sognefjord	1537.50-1702.11	1.04
NO 31/2-E-6 H	Sognefjord	1730.41-2057.46	62.40
NO 31/2-F-6 H	Sognefjord	1869.98-2094.99	48.80
NO 31/2-G-4 H	Sognefjord	1617.5-1882.0	55.24
NO 31/2-L-41	Sognefjord	1485.90-1647.41	1.29
NO 31/2-M-41	Sognefjord	1489.99-1658.50	1.00
NO 31/2-M-42	Sognefjord	1576.60-1733	1.95
NO 31/3-1	Sognefjord	1352.30-1511.61	0.52
NO 31/3-2	Sognefjord	1567.01-1724.80	0.56
NO 31/3-3	Sognefjord	1747.09-1931.50	2.05
NO 31/3-S-41	Sognefjord	1503.40-1656	0.56
NO 31/5-2	Sognefjord	1519.27-1673.91	0.27
NO 31/5-3	Sognefjord	1555.10-1717.10	1.74
NO 31/5-4 S	Sognefjord	1619.43-1874.94	53.67
NO 31/5-5	Sognefjord	1572.40-1721.50	0.32
NO 31/5-H-5 H	Sognefjord	1730.87-2069.35	63.92
NO 31/5-J-41	Sognefjord	1540.62-1707.23	0.64

Table 3.1: An overview of all the wells with the reservoir intervals and the mean inclination angles within the reservoir interval.

Well	Cap rock	Cap rock interval, meters MD	Mean inclination angle, °
NO 31/2-1	Draupne Fm.	1415.07-1440.20	0.60
NO 31/2-10	Draupne Fm.	1564.05-1600.31	1.39
NO 31/2-11	Draupne Fm.	1554.05-1557.97	0.50
NO 31/2-12	Shetland Gp.	1357.45-1364.88	0.96
NO 31/2-13 S	Lista Fm.	1576.30-1727.60	49.96
NO 31/2-14	Draupne Fm.	1532.00-1533.10	0.50
NO 31/2-15	Shetland Gp.	1455.35-1482.28	3.42
NO 31/2-17 A	Draupne Fm.	1681.50-1689.98	42.53
NO 31/2-18	Shetland Gp.	1496.91-1518.83	0.41
NO 31/2-18 A	Shetland Gp.	1497.07-1519.23	8.75
NO 31/2-3	Shetland Gp.	1374.99-1384.30	0.75
NO 31/2-4 R	Shetland Gp.	1357.88-1366.94	0.20
NO 31/2-5	Lista Fm.	1427.76-1536.02	0.83
NO 31/2-6	Draupne Fm.	1482.48-1491.80	1.24
NO 31/2-7	Draupne Fm.	1535.06-1545.40	0.12
NO 31/2-9	Draupne Fm.	1545.03-1548.90	2.01
NO 31/2-B-3 H	Shetland Gp.	1777.78-1784.23	59.39
NO 31/2-D-10 H	Draupne Fm.	1483.32-1496.62	3.23
NO 31/2-D-9	Draupne Fm.	1531.92-1537.50	1.19
NO 31/2-E-6 H	Draupne Fm.	1709.59-1730.41	60.89
NO 31/2-F-6 H	Draupne Fm.	1848.57-1869.98	49.60
NO 31/2-G-4 H	Draupne Fm.	1601.36-1617.50	52.57
NO 31/2-L-41	Draupne Fm.	1425.63-1485.90	1.34
NO 31/2-M-41	Shetland Gp.	1481.79-1489.99	0.91
NO 31/2-M-42	Draupne Fm.	1554.15-1576.60	2.00
NO 31/3-1	Draupne Fm.	1320.51-1352.30	0.33
NO 31/3-2	Draupne Fm.	1540.85-1567.01	0.51
NO 31/3-3	Draupne Fm.	1632.32-1747.09	2.47
NO 31/3-S-41	Draupne Fm.	1457.76-1503.40	1.00
NO 31/5-2	Draupne Fm.	1474.47-1519.27	0.49
NO 31/5-3	Draupne Fm.	1547.10-1555.10	1.86
NO 31/5-4 S	Draupne Fm.	1566.84-1619.43	52.15
NO 31/5-5	Draupne Fm.	1563.59-1572.40	0.23
NO 31/5-H-5 H	Draupne Fm.	1716.00-1730.87	60.90
NO 31/5-J-41	Draupne Fm.	1438.24-1540.62	0.31

Table 3.2: An overview of all the wells with the cap rock intervals and the mean inclination angles within the cap rock interval.
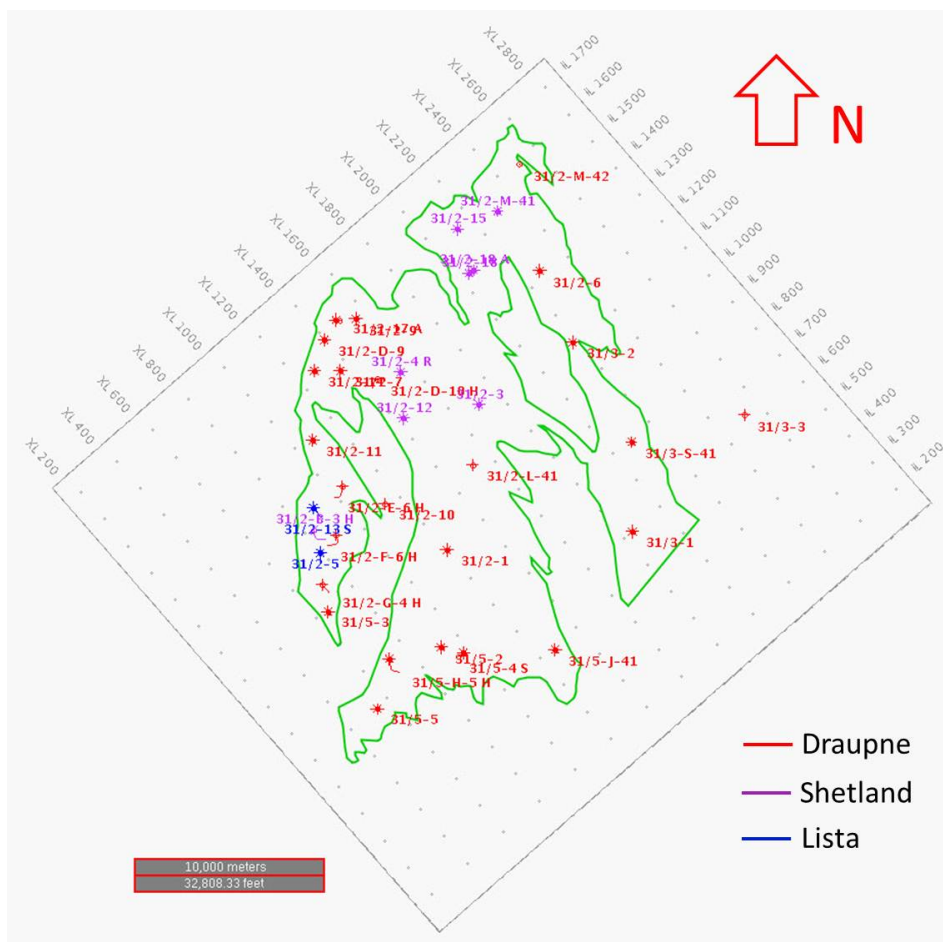
Figure 3.1: The outline of the seismic survey showing the 35 wells used in this work. The green polygon shows the outline of the reservoir. The wells are color coded in which formation is the cap rock. (Figure generated in DecisionSpace Desktop).

increase in velocity with inclination angle.

Next, Equation 2.17 and 2.18 were applied to calculate the anisotropy parameters. The anisotropy parameters were estimated for the reservoir and the three different cap rocks. The plots and the values for the anisotropy parameters for the reservoir and each of the cap rocks are shown in Section 4.1. An example of a Matlab script for calculating the anisotropy parameters is shown in Appendix A.1.

3.2 Filtering of the data

From the plot of the reservoir in Section 4.1, a large variation in the data set was noticed, thus filtering of the data was decided to be performed. The large variation in the data set is also reflected in the value of the standard deviation of the velocity (see Table 4.1).

3.2.1 Porosity filtering

A filtering on porosity was applied first. Porosity logs (PHIT) were exported for the reservoir interval (LFP_PHIT for well 31/3-1 and 31/3-3 and PHIE for well 31/5-H-5 H). The PHIT logs are total porosity calculated from the density (RHOB) logs, and the PHIE log is effective porosity, which is usually smaller than total porosity. The PHIE logs are the same as the PHIT logs, only the porosity is set to 0 where the calcite flag is 1. The PHIT logs are calculated using Equation 3.1. This has not been done in this work.

$$\rho_b = (1 - \phi)\,\rho_{ma} + \phi\rho_{fl}, \tag{3.1}$$

where ρ_b is the bulk density of the rock, ϕ is the porosity, ρ_{ma} is the density of the rock matrix and ρ_{fl} is the density of the fluids in the formation. This can be rewritten as Equation 3.2.

$$\phi = \frac{\rho_b - \rho_{ma}}{\rho_{fl} - \rho_{ma}}, \tag{3.2}$$

where the values from the RHOB logs will be used for ρ_b, and ρ_{ma} and ρ_{fl} are known. Normally $\rho_{ma} = 2.65$ g/cm^3 for sandstone and $\rho_{fl} \approx 1$ g/cm^3 for water, usually a little higher for brine (salt water).

The porosity filtering started at 15 % and went up to 40 %, with a 5 % interval. Next, the filtering was done with a 1 % interval, starting at 20 % (20 %, 21 %, 22 %,...,40 %).

After filtering on porosity and obtaining the second order polynomial fitted curve for each filter, a plot with the curves for five filters (15-20 %, 20-25 %, 25-30 %, 30-35 % and 35-40 %) was generated. This was done to see how the different curves relate to each other and vary with inclination angle.

It is expected that the lower porosity filters correspond to higher velocities and vice versa. This plot would also show if the velocity decreases with inclination angle (for sandstone). If this is true, the plot would show that no further filtering is required. If the shape of the curves varies a lot and the velocity is not decreasing with inclination angle, this either implies that more filtering on other parameters is necessary or that too much data have been removed after filtering and thus the filter interval should not be used further. Hence, this plot could give an indication of the necessity of filtering. The plot showing the curves for the different filters is shown in Section 4.2.

3.2.2 Acoustic impedance filtering

After different porosity filters were executed and data points were removed, there were still some abnormally high velocity values. Porosity and velocity are strongly related, because the velocity increases with depth and porosity decreases with depth (Avseth et al., 2005) (due to increased pressure of the overburden). Thus the abnormally high velocity values were expected to be removed when filtering on porosity had been applied. Due to these high velocity values still being present after filtering on porosity, filtering on acoustic impedance (AI) was of interest. The formula for AI is shown in Equation 3.3.

$$AI = V_P \cdot \rho_b, \tag{3.3}$$

where AI is the acoustic impedance, V_P is the P-wave velocity (calculated from the sonic log, with the unit km/s) and ρ_b is the bulk density (from the density log, with the unit g/cm^3). This shows that the velocity and the density are needed. Due to this, the density logs (LFP_RHOB) were exported. The filtering was done for values from 4-8 km/s · g/cm^3, with intervals of 1, 2 and 3 km/s · g/cm^3, adding up to 10 different filters. The porosity filters and the AI filters were also combined. A filtering on AI is indirectly a filtering on lithology, because the high density values can be related to calcite layers in between or in the sandstones in the reservoir. From the logs, it was observed that the high density values correspond to high velocity values. Since the clay content in the reservoir is close to zero, no V_{cl} log has been generated, thus filtering on AI was an important aspect of filtering on lithology.

3.2.3   Depth filtering

Since the different porosity filters did not correspond well with which velocity values were removed, a porosity versus depth plot was generated. The reason was to see if the expected trend where the porosity decreases with depth is present for this reservoir. If a clear trend is not present, this indicates that the porosity and depth are not closely related and it would therefore be necessary to filter on depth as well as the porosity. The resulting plot is shown in Section 4.2. Seen from this plot and Table 3.1, where it can be seen that the depth of the reservoir varies a lot, it was necessary to filter on depth. No additional logs were required to be exported, since the depth is present in all the logs. The depth filtering was done for values from 1600-1800 meters MD (measured depth), with intervals of 50 meters.

Subsequently, the depth was filtered with intervals of 20 meters, from 1600 m MD to 1800 m MD. Filtering was also applied with intervals of 100 and 200 meters, especially when including the porosity filters, the AI filters and both. When the depth filter was included, porosity filters were applied with intervals of 2 % as well.

In the end, seven different types of filters had been generated; porosity, AI, depth, porosity & AI, porosity & depth, AI & depth and porosity & AI & depth, with a total of 270 different filters. Appendix C.1 shows a table of the different filters for the reservoir with values for ε and δ. A lot of trial and error with different filters was necessary to try and get robust results that were comparable with Richard Tøndel's result. All the filtering described so far, were performed for the reservoir interval. In Section 4.2, plots and values for some of the filters are shown.

3.2.4   Filtering of the data for the Draupne Fm.

Filtering was also performed for the Draupne Fm. Since the Shetland Gp. and the Lista Fm. are not representative in the data set (only eight and two wells respectively), filtering was found to be unnecessary for these formations. The cap rock was only filtered for depth and acoustic impedance, due to the fact that there is no porosity log for the cap rock on the Troll Field. It is assumed that the porosity is zero since the cap rock is tight and sealing (no hydrocarbons can escape), and is therefore not calculated from

the density log. The depth filtering was done from 1450-1750 meters MD, with intervals of 50, 100 and 200 meters. The AI filtering was done for the same range and intervals as the reservoir. These filters were also combined, adding to a total of 62 different filters for the Draupne Fm. Appendix C.2 shows a table of the different filters for the Draupne Fm. with values for ε and δ.

The filtering was necessary to have comparable data and trustworthy results. For all the filters and the non-filtered data, the number of points, the mean and the standard deviation of the velocity were calculated using built-in functions (length, mean and std) in Matlab. Particularly important was looking at the standard deviation of the velocity for comparison of the non-filtered data and the filtered data. This is important because lower values of standard deviation indicate less uncertainty in the values being measured.

In advance of the filtering of the data, histograms were generated for porosity (only the reservoir), acoustic impedance and depth for both the reservoir and the Draupne Fm. to look at the distribution of the different parameters. This was done to look at the ranges for each parameter and thereby use reasonable ranges when filtering. In addition, histograms for depth were generated having vertical and horizontal wells separately to be certain that the filtering on depth would include both horizontal and vertical wells. The plots for all the histograms are shown in Appendix D.1 for the reservoir and Appendix D.2 for the Draupne Fm. Explanations for the different ranges chosen for the different parameters are included.

3.3 Calculating the standard deviation of ε

To calculate the standard deviation of ε, more coding in Matlab was required. The mean values and the standard deviations of the vertical and the horizontal P-wave velocity are needed to perform the calculations (see Equation 2.25). This was only done for the non-filtered case and selected filters for both the reservoir and the Draupne Fm.

To calculate the mean and the standard deviation of the vertical and the horizontal P-wave velocity, the vertical and the horizontal wells had to be separated into two scripts and then the built-in Matlab functions, mean and

std, were applied to automatically calculate the mean and the standard deviation of each. All the wells that were close to vertical were used for the vertical case. Since no wells in this data set are exactly horizontal, an approximation was done using wells with the largest inclination angle (about 64°, 0.8 in the plot).

For the horizontal case for the reservoir, well 31/2-E-6 H (average inclination angle of 62.40) and 31/5-H-5 H (average inclination angle of 63.92) were used for all the filters shown in Chapter 4, except for Filter III, where 31/5-H-5 H was removed after filtering. For this filter, only the well 31/2-E-6 H was used.

For the horizontal case for the Draupne Fm., wells 31/2-E-6 H (average inclination angle of 60.89) and 31/5-H-5 H (average inclination angle of 60.90) were also used for the non-filtered and the filtered data, except for Filter VI, where the wells 31/2-G-4 H and 31/5-4 S were used instead. For this filter, the wells 31/2-E-6 H and 31/5-H-5 H were removed after filtering. The average inclination angle for well 31/2-G-4 H is 52.57 and for well 31/5-4 S, the average inclination angle is 52.15 (see Table 3.2). The values for the standard deviation of the ε are shown in Section 4.4.

3.4   The AVO analysis

Computing AVO was done for well 31/2-L-41 in Matlab. This well was chosen because it was used in the specialization project "Seismic interpretation of an alternative top 4-series on the Troll Field" by Hilde Haktorson (Haktorson, 2011), and it was there noticed that the S-wave sonic log had a high response at the interface between the Draupne Fm. and the Sognefjord Fm.

The AVO analysis was done for an isotropic and an anisotropic case. The formulas used for computing the reflection coefficient versus the incidence angle are shown in Subsection 2.6.1 for the isotropic case, and in Subsection 2.6.2 for the anisotropic case. These formulas are approximate solutions for how the reflection coefficient of the P-wave vary with incidence angle (3-term Shuey equation). Seen from Equation 2.26 (2.27, 2.28, 2.29), the P-wave velocity, the S-wave velocity and the density are needed for both the cap rock and the reservoir. Seen from Equation 2.30 (2.31, 2.32, 2.33), the anisotropy parameters, δ and ε, estimated for the cap rock and the reservoir

	Cap rock, Draupne Fm.	Reservoir, Sogne-fjord Fm.
P-wave slowness [μs/ft]	150	150
P-wave velocity [m/s]	2033.3	2033.3
S-wave slowness [μs/ft]	350	230
S-wave velocity [m/s]	871.4	1326.1
Density [kg/m^3]	2125	1875

Table 3.3: The input values for the P-wave velocity, the S-wave velocity and the density in the AVO analysis.

are needed as well. The anisotropy parameters used are shown in Section 4.5.

The input values for the P-wave velocities, the S-wave velocities and the densities are taken from Haktorson (2011) and shown in Table 3.3. Table 3.3 shows that the P-wave velocity is constant across the interface, while the S-wave velocity has a strong increase in velocity across the interface. The density decreases across the interface. These values were read from the same logs as used in this work (in addition to LFP_DTS) for an interval of about 10 meters above and below the top of Sognefjord, in Syntool, a software in OpenWorks. The plot generated is shown in Section 4.5.

A Matlab function called Zoeppritz was used to find the exact solution for the isotropic case. Given the P-wave velocity, the S-wave velocity, the density for both the layers (the same values as in Table 3.3) and the incidence angle as inputs, the amplitude value (at that specific incidence angle) was returned. This was done repeatedly for incidence angles of $1 - 50°$ with an increment of $1°$. The amplitude values versus the incidence angles were plotted in the same plot as the isotropic and the anisotropic cases for comparison. This plot is shown in Section 4.5.

Next, seismic prestack gathers were included in the AVO analysis. A software in OpenWorks called Well Seismic Fusion (WSF) was used to examine the gathers close to well 31/2-L-41. Three gathers, Gather 1, Gather 2 and Gather 3, were displayed as amplitude versus offset. All the gathers are at in-line 1032, but at different crosslines. Gather 1, Gather 2 and Gather 3 are

at crossline 1520, 1521 and 1522, respectively. Figure 3.2 shows the three
prestack gathers as amplitude versus offset, while Figure 3.3 shows the loca-
tion of the three gathers.

Figure 3.2: The prestack gathers close to well 31/2-L-41 as amplitude versus
offset. The dashed green line is the top of the Sognefjord Fm. (the boundary
between the reservoir and the Draupne Fm.).
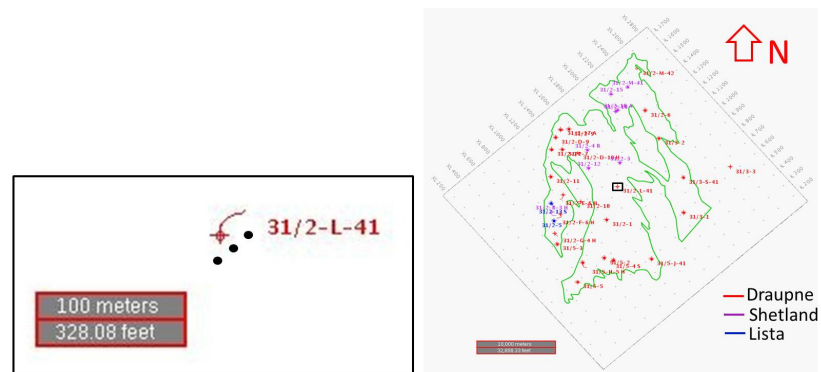
Figure 3.3: The location of the gathers close to the well. Gather 1, Gather 2
and Gather 3 are shown as black dots, where Gather 1 is the most southern
dot, Gather 2 is the middle dot and Gather 3 is the most northern dot.

To compare the seismic gathers with the AVO plots already generated, con-
version from offset to incidence angle was desired. This was done automat-
ically in WSF, using a velocity model. Figure 3.4 shows the three prestack
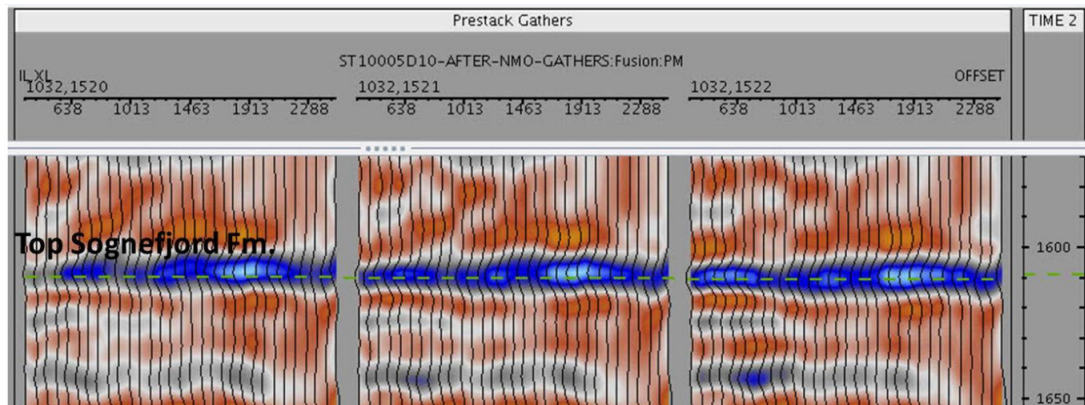gathers as amplitude versus incidence angle.

Figure 3.4: The prestack gathers close to well 31/2-L-41 as amplitude versus incidence angle. The dashed green line is the top of the Sognefjord Fm. (the boundary between the reservoir and the Draupne Fm.).
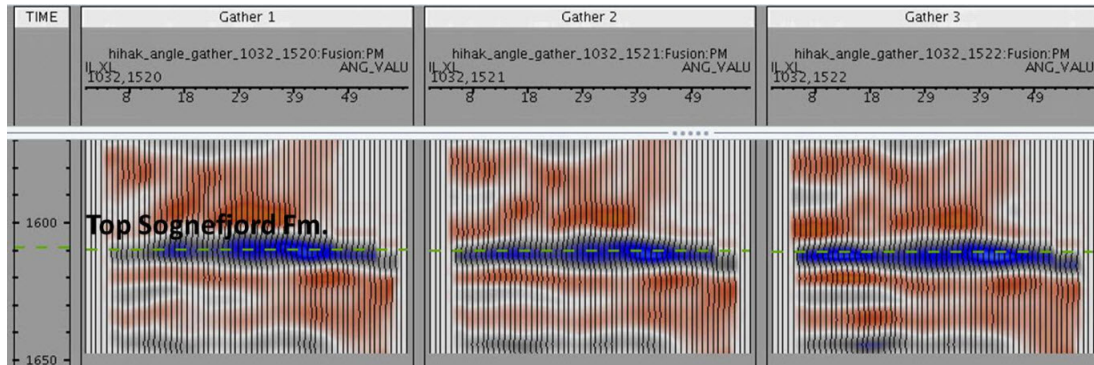
For these three gathers, an amplitude versus incidence angle plot was generated in WSF. The amplitudes were extracted from around the top Sognefjord horizon, at a time window of 1604–1616 ms. Figure 3.5 shows the amplitude versus incidence angle plot. It shows that the amplitude values range from around -3000 to around -10,000. Figure 4.23 in page 76 shows that the reflection coefficient in the AVO plots range from -0.5 to 0. Hence, in order to compare the gathers with the model (the isotropic and the anisotropic case), the amplitude values from the gathers were required to be scaled. Only incidence angle values up to $40\,^\circ$ were scaled. This was done because a quick calculation using a maximum offset of 2400 m, an average velocity down to the reservoir of 1800 m/s (taken from the velocity model) and a two-way travel time (TWT) of 1.6 s, shows that the maximum incidence angle is around $40\,^\circ$ (see equations in Appendix B).

Initially, the amplitude values would be scaled with the reflection coefficients at zero offset, since the amplitudes are expected to be the same at normal incidence. However, seen from Figure 4.23 in page 76, the reflection coefficients at zero offset for the models are close to zero (the amplitudes are weak). Thus, to get a signal when scaling the amplitude values, the values were decided to be scaled with reflection coefficient values at far offset. At far offset, the isotropic and the anisotropic cases differ. Since the gathers will only give an indication of the variation in amplitude and the slope of the curve, which model is chosen for scaling is inessential. The amplitude value at $40\,^\circ$ was set to the reflection coefficient value for the isotropic case,
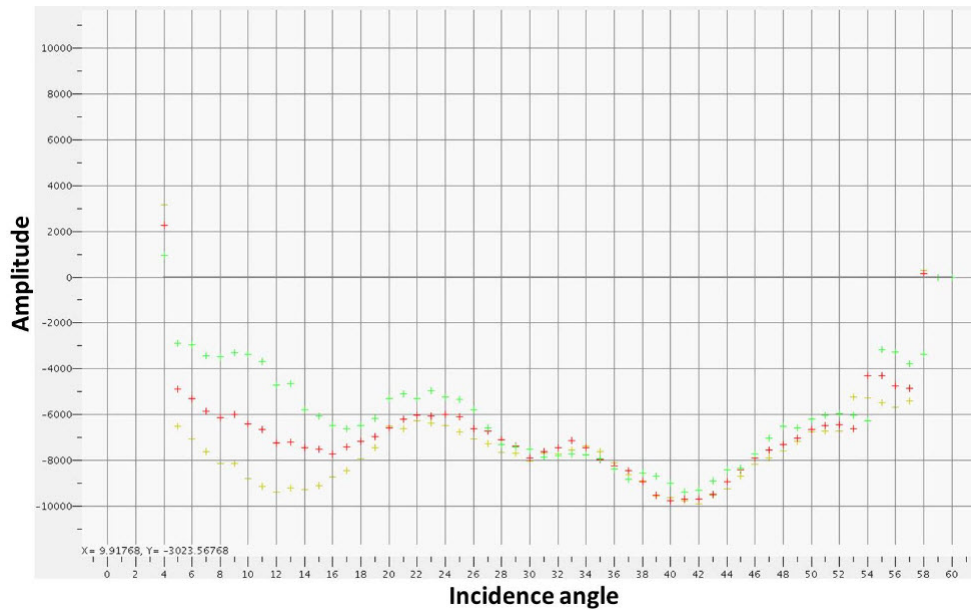
Figure 3.5: An AVO plot of the three gathers. The green points are data from Gather 1, the red points are data from Gather 2 and the yellow points are data from Gather 3.

which is -0.23. From the amplitude values at $40\,^\circ$, the scaling factors for all the gathers were found. For Gather 1, all the amplitude values were divided by the scaling factor 39,287. For Gather 2 and Gather 3, the scaling factors were found to be 42,591 and 41,991, respectively. The scaled values were then included in the plot for the AVO analysis. A Matlab script for generating the AVO plot including the values from the seismic gathers is shown in Appendix A.2. The plot generated from this script is shown in Section 4.5.

Chapter 4

Results

4.1 The anisotropy parameters

The plots showing the velocity versus the inclination angle for the reservoir, the Draupne Fm., the Shetland Gp. and the Lista Fm. are shown in Figure 4.1, 4.3, 4.5 and 4.7, respectively (see page 44, 46, 48, and 50). Each well has a specific color code shown in the legends. From the figures, a drastically decrease in number of wells from the reservoir (35 wells) and the Draupne Fm. (25 wells) to the Shetland Gp. (8 wells) and the Lista Fm. (2 wells) can be seen. This is in accordance with Table 3.2.

Figure 4.2, 4.4, 4.6 and 4.8 show the same plots with all the wells for each formation (not color coded) including the fitted curve for the second order polynomial function. The fewer wells (data at fewer angles) and the more variation in velocity, the higher uncertainty of the fitted polynomial curve. Since the anisotropy parameters are calculated from the fitted curve, higher uncertainty of the fitted curve leads to higher uncertainty of the anisotropy parameters, thus make them less reliable.

Figure 4.1: The velocity values versus inclination angle from the wells in the reservoir. The data points have not been filtered.

Figure 4.2: The velocity values versus inclination angle from the wells in the reservoir. The data points have not been filtered. The blue curve is the second order polynomial fitted curve.

Figure 4.3: The velocity values versus inclination angle from the wells in the Draupne Fm. The data points have not been filtered.

Figure 4.4: The velocity values versus inclination angle from the wells in the Draupne Fm. The data points have not been filtered. The blue curve is the second order polynomial fitted curve.
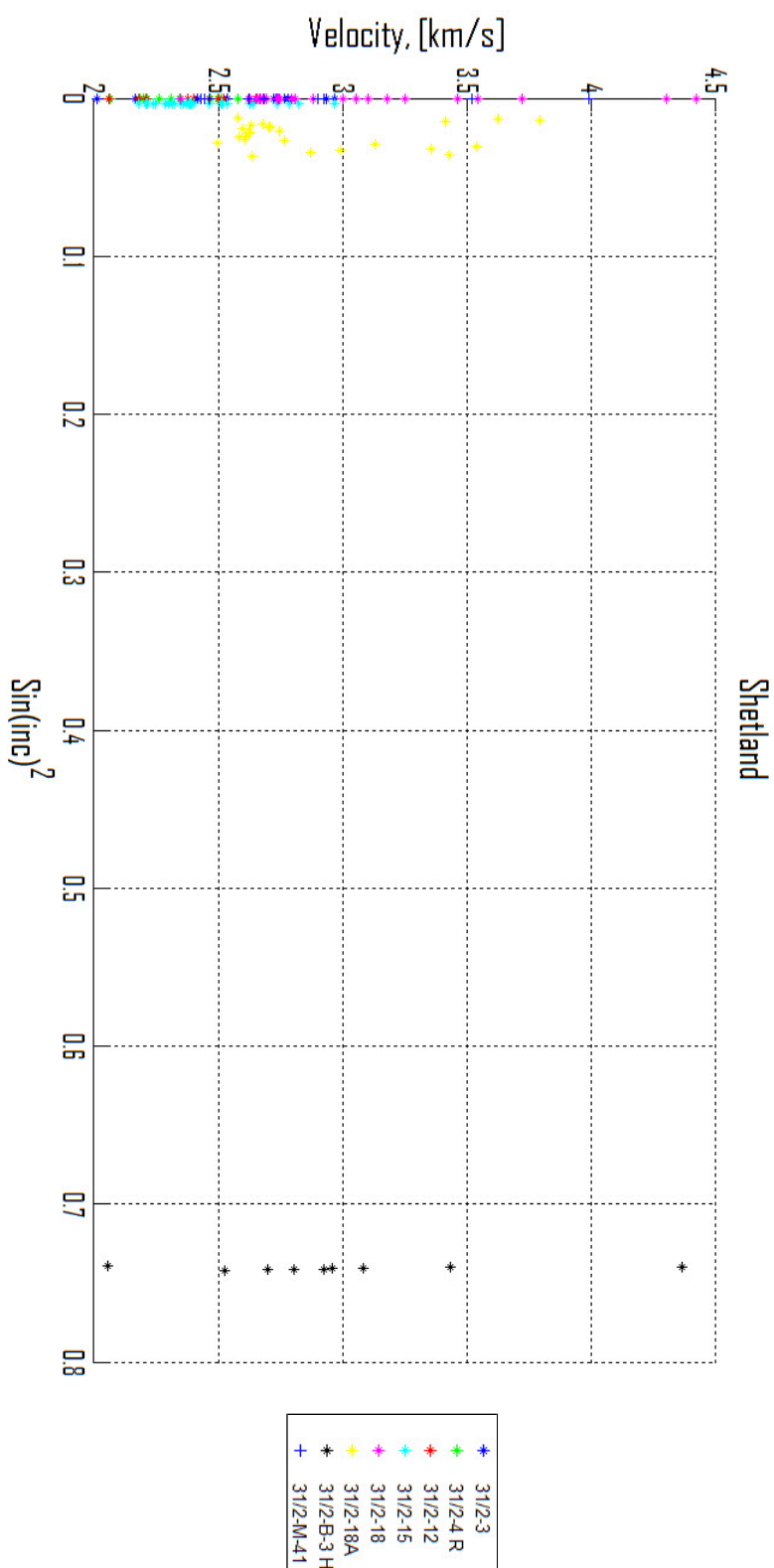
Figure 4.5: The velocity values versus inclination angle from the wells in the Shetland Gp. The data points have not been filtered.

Figure 4.6: The velocity values versus inclination angle from the wells in the Shetland Gp. The data points have not been filtered. The blue curve is the second order polynomial fitted curve.
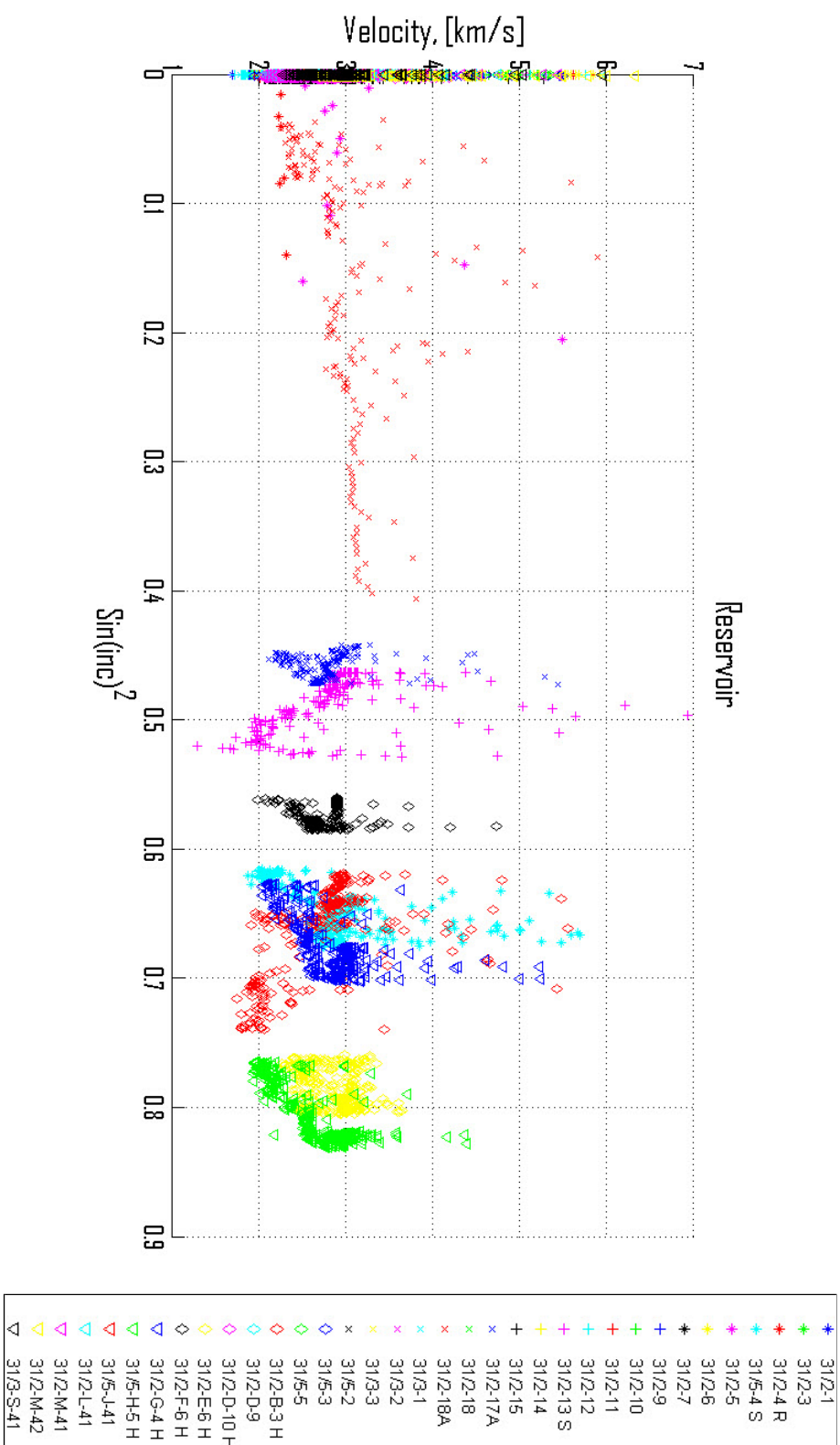
Figure 4.7: The velocity values versus inclination angle from the wells in the Lista Fm. The data points have not been filtered.
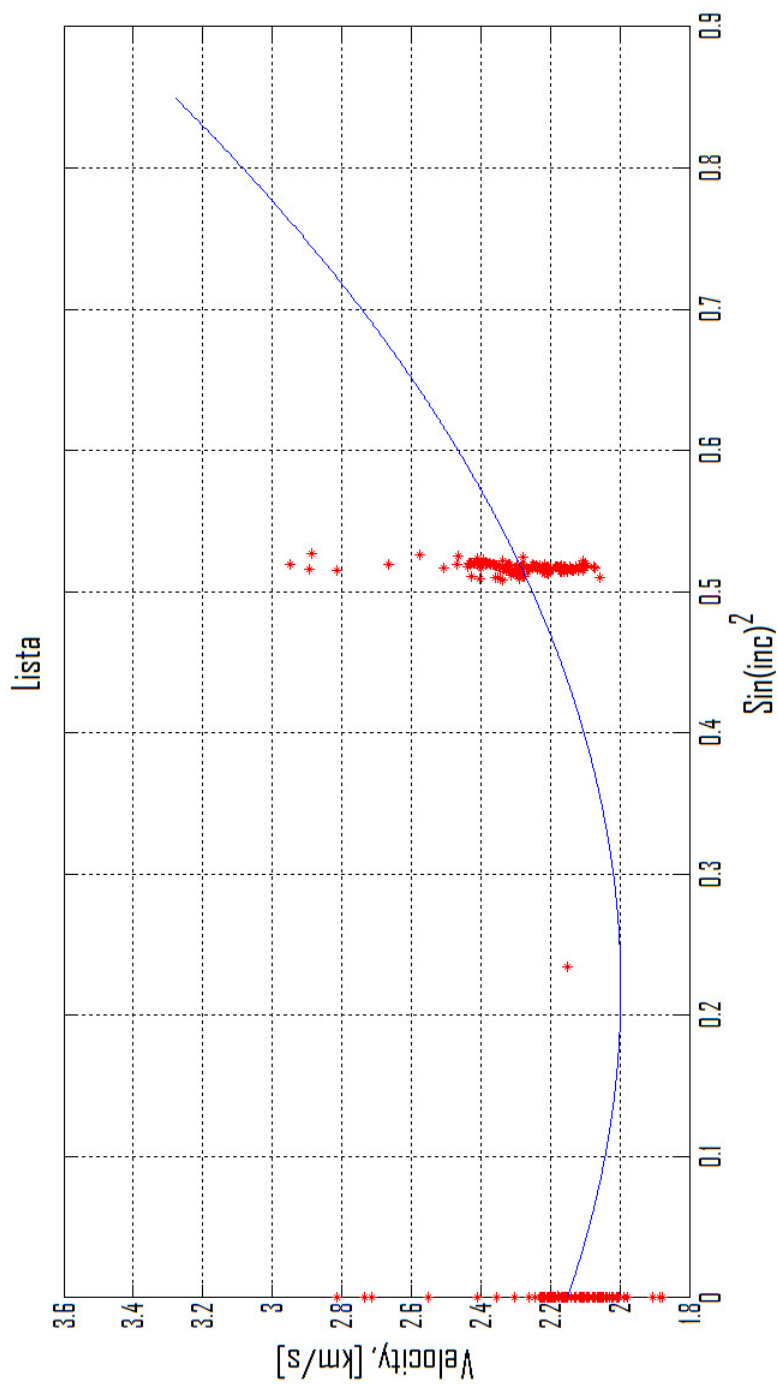
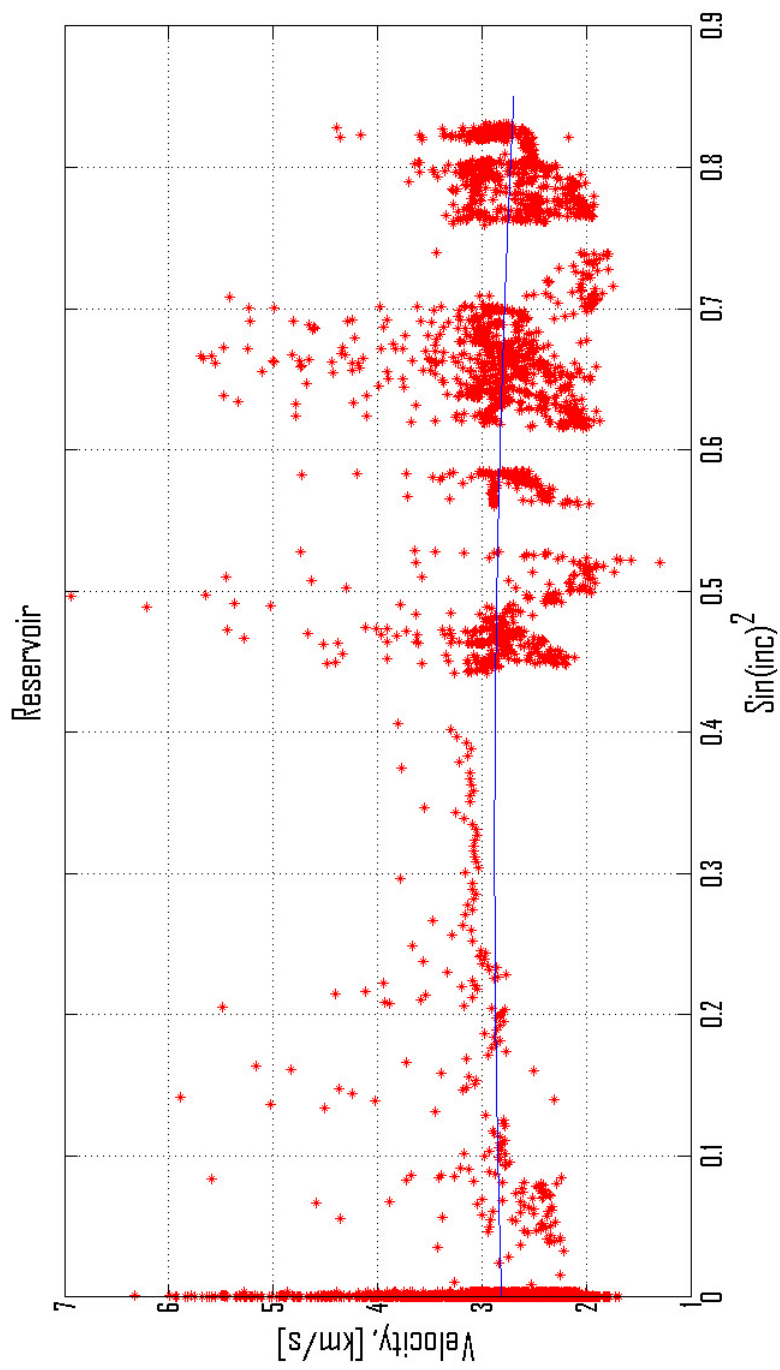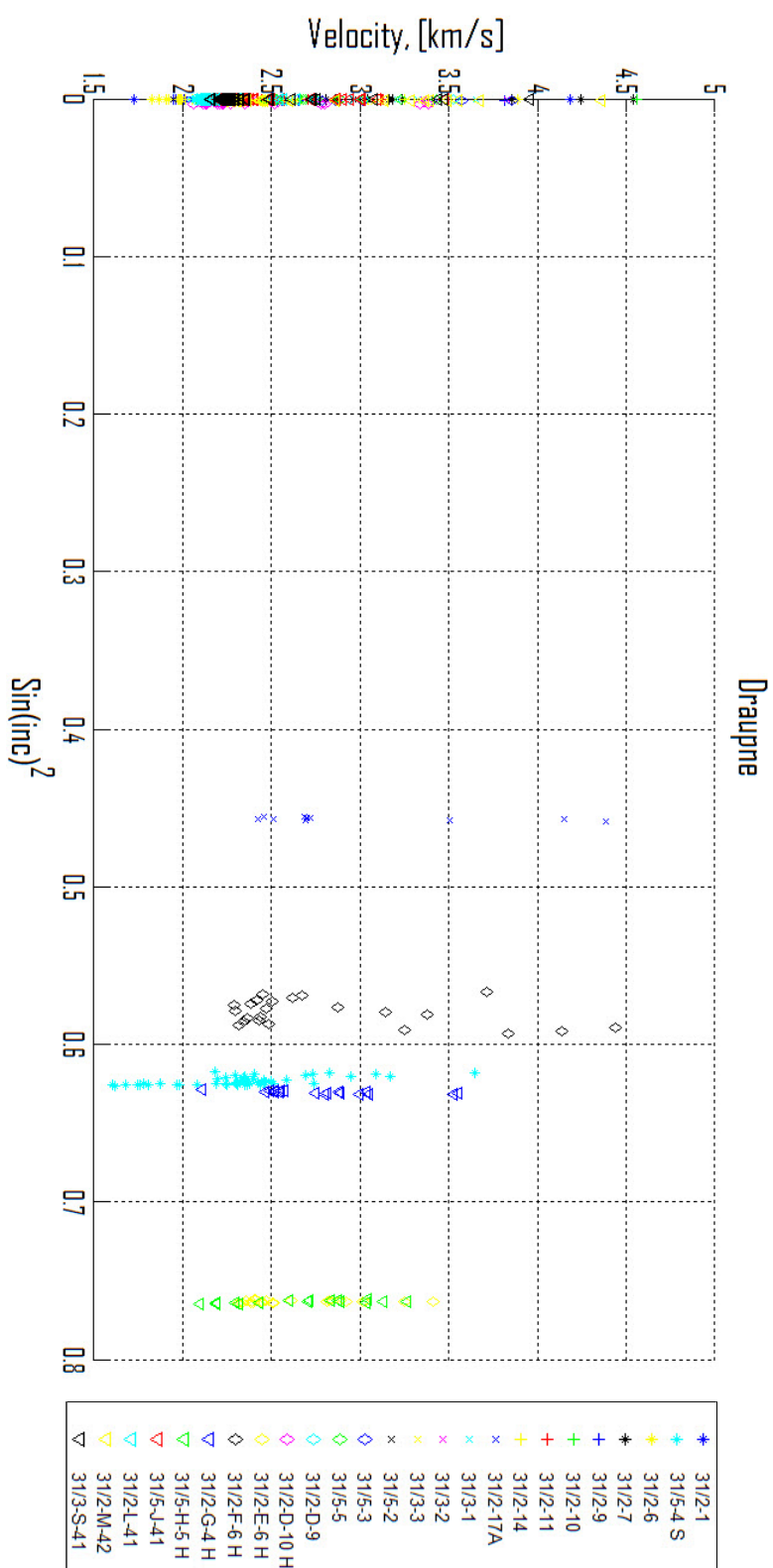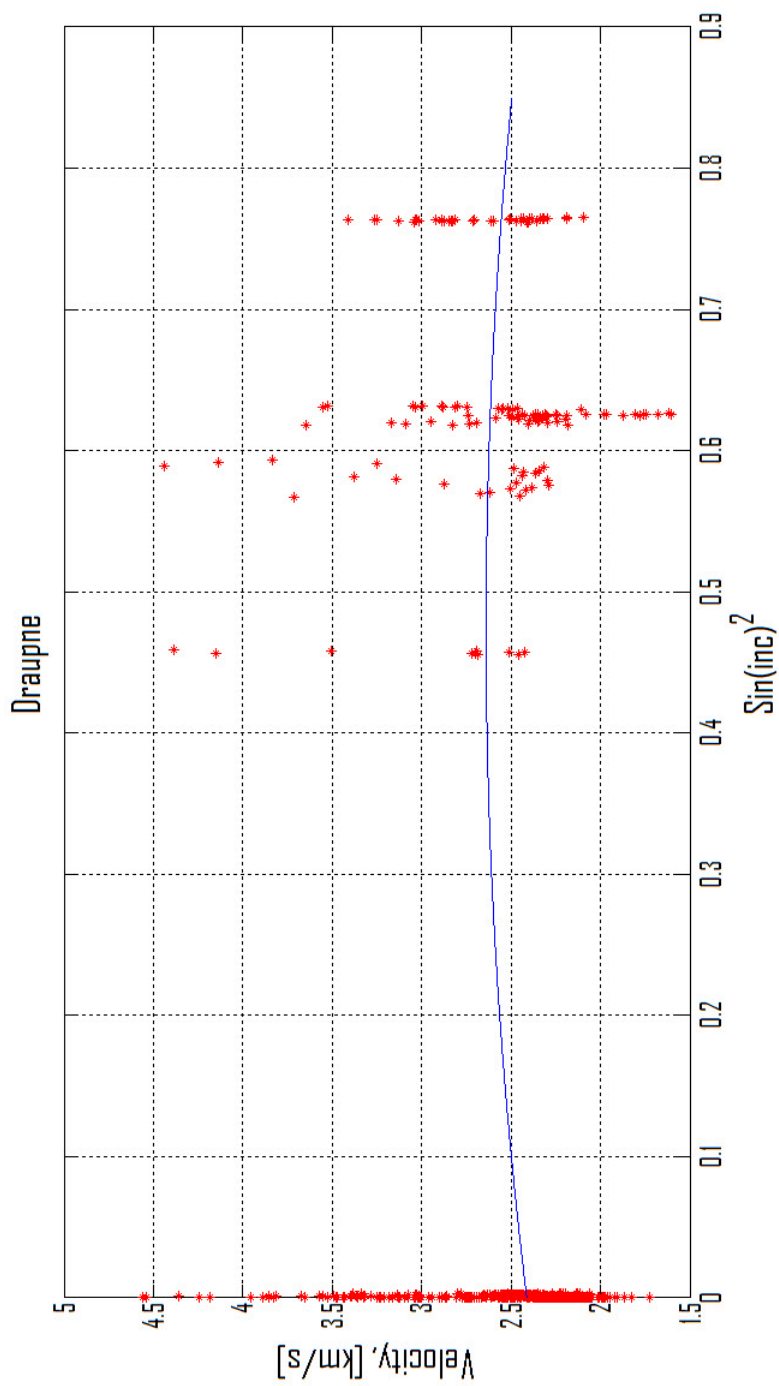Figure 4.8: The velocity values versus inclination angle from the wells in the Lista Fm. The data points have not been filtered. The blue curve is the second order polynomial fitted curve.
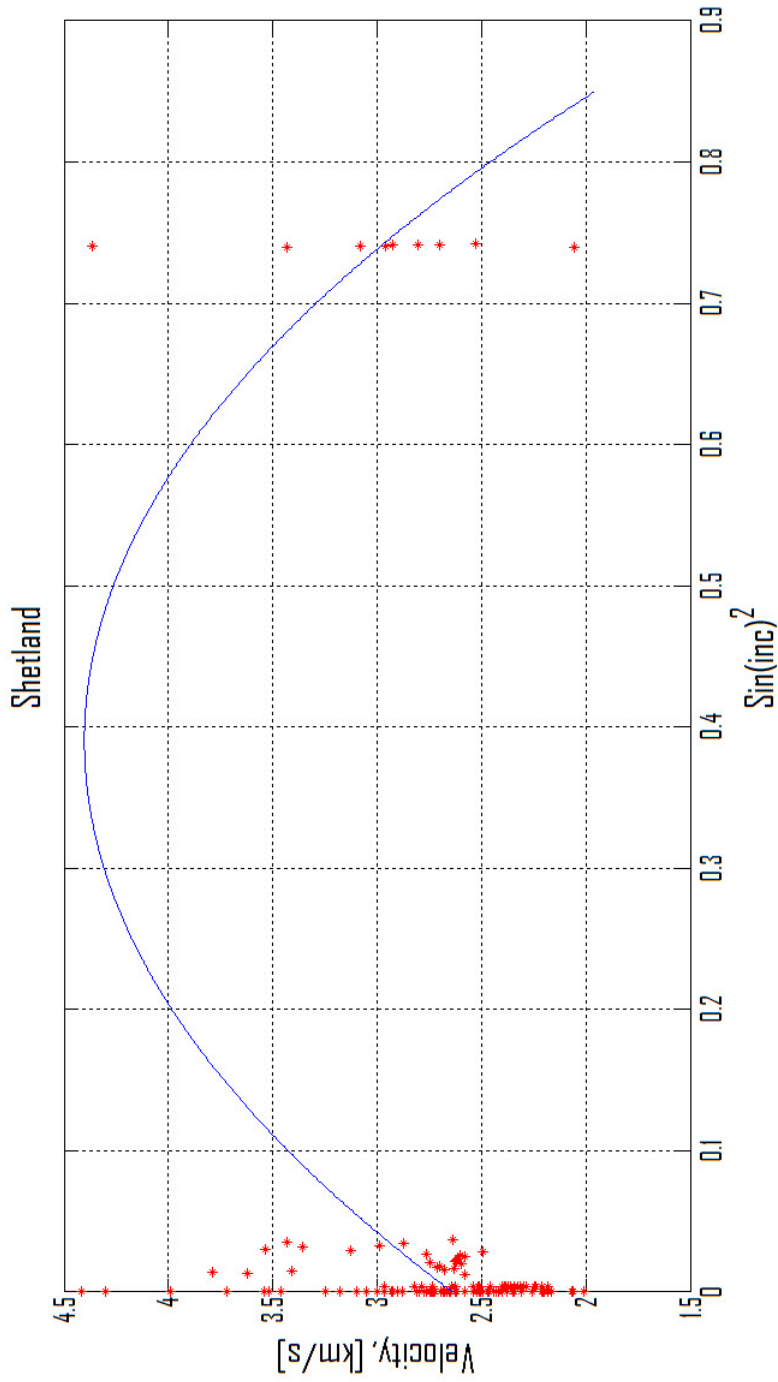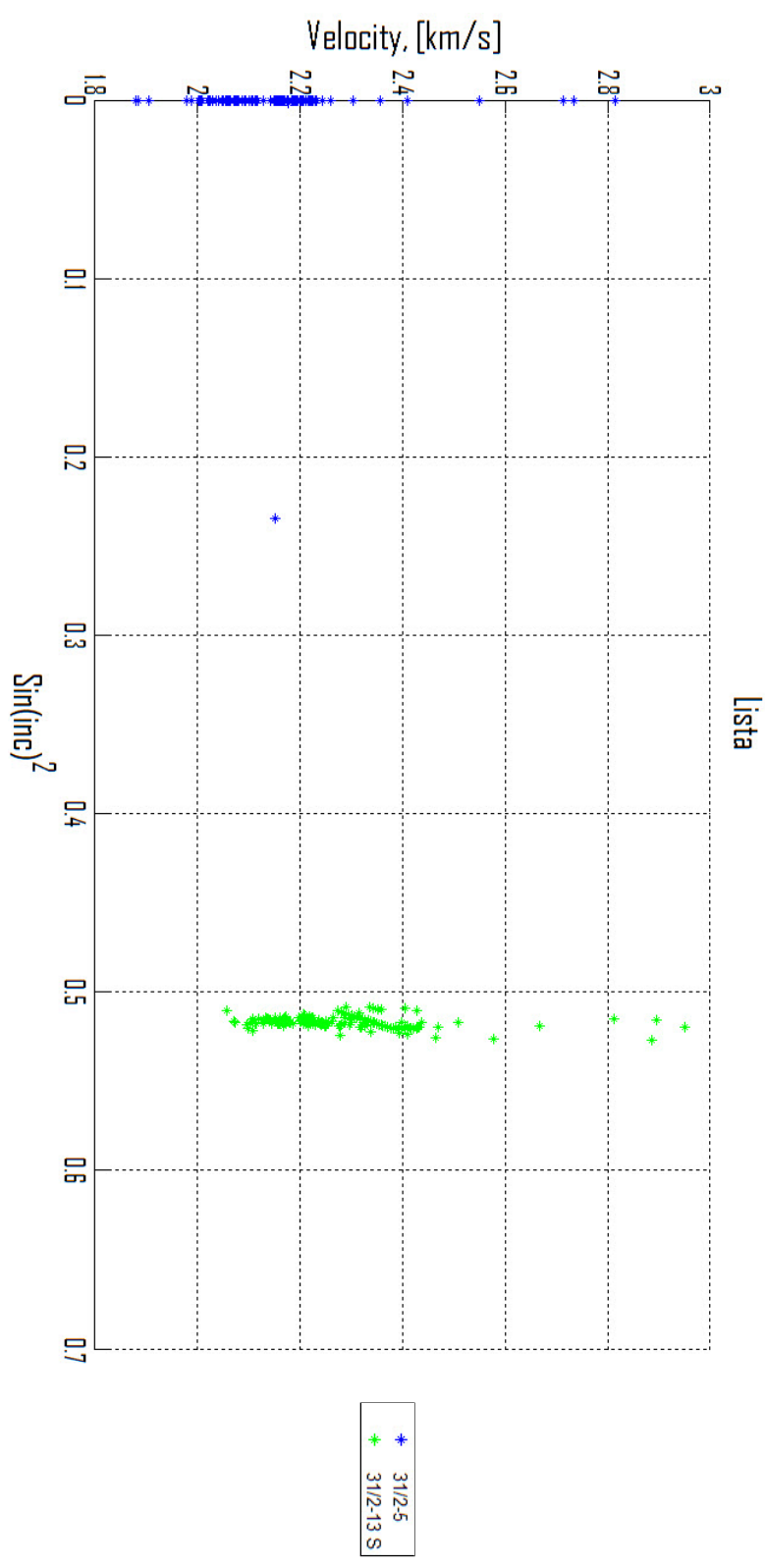
From Figure 4.1, a large variation in the data can be seen, with velocity values up to 7 km/s. This large variation makes the results less reliable, thus filtering is required. The x-axis ($\sin(inc)^2$) ranges from 0 to 0.84. The range should go up to 1 ($90\,^\circ$), in order to get the exact horizontal velocity. Thus with this data set, only an approximate horizontal velocity is obtained.

Figure 4.3, 4.5 and 4.7 show a large variation in the velocities too, but the maximum velocity value is lower than for the reservoir, only around 3-4.5 km/s. In Figure 4.3, the x-axis ranges from 0 to 0.77, and in Figure 4.5 and 4.7, the x-axis ranges from 0 to 0.74 and 0.53, respectively. Hence, for the cap rocks, the approximate horizontal velocity will be further from the exact value than for the reservoir. Since ε is dependent on the vertical and the horizontal P-wave velocity, this parameter is expected to have a higher uncertainty for the cap rocks than the reservoir. Figure 4.5 and 4.7 show that the Shetland Gp. and the Lista Fm. have few wells (data at few angles), and a large gap in angles from $0\,^\circ$ to $59\,^\circ$ and $47\,^\circ$ respectively is present. Hence the anisotropy parameters for these formations will be less reliable.

Figure 4.2 and 4.4 show that enough points are present to generate a stable fitted curve. For Figure 4.6 and 4.8, the fitted curves are unstable and have a high uncertainty, due to lack of wells and a large variation in velocity.

Table 4.1 shows the ε and the δ values for the reservoir and the three cap rocks. Seen in this table, the values for the anisotropy parameters for the Shetland Gp. and the Lista Fm. are much higher than the values for the reservoir and the Draupne Fm. Also, the number of samples is decreasing as seen from the figures.

As mentioned, an assumption for using the formulas in Section 2.4, is that the anisotropy is weak, hence the parameters are $\ll 1$. The parameters are also expected to be negative for sandstone and positive for shale (Walsh et al., 2006). In the book written by Mavko et al. (2009), it is stated that $\varepsilon - \delta \geq 0$ and that δ is smaller in sands than in shales. According to these statements, the values for the Shetland Gp. and the Lista Fm. are outside the range of expected values, most likely due to lack of wells (angles). When comparing the preceding statements with Table 4.1, filtering was seen to be necessary. Although, the anisotropy parameters for the Shetland Gp. and the Lista Fm. were not according to expected values, filtering was not done for these formations because they are not representative in the data set.

Formation or Group	ε	δ	Number of samples	Mean of V_p	Stand. dev. of V_p
Reservoir	-0.084	0.148	6405	2.807	± 0.564
Draupne	-0.022	0.399	752	2.449	± 0.419
Shetland	-0.962	3.428	128	2.709	± 0.465
Lista	0.842	-0.654	264	2.227	± 0.158

Table 4.1: An overview of the anisotropy parameters for the different formations. The number of samples, the mean and the standard deviation of the velocity are also shown.

4.2 Filtering of the data

After looking through and sorting all the filters generated for the reservoir, a few filters were selected as the best. Table 4.2 shows the anisotropy parameters for the selected filters for the reservoir, including the result from the non-filtered data. The anisotropy parameters for the reservoir for the rest of the filters are listed in the table in Appendix C.1.

In Table 4.2, Filter I includes a depth filter on 1600-1800 meters MD, a porosity filter on 20-30 % and an AI filter on 5-6 km/s · g/cm³. Filter II and Filter III are the same, except the porosity filters are on 20-25 % and 25-30 %, respectively. Seen from the table, the results are more consistent with the

Filter	ε	δ	Number of samples	Mean of V_p	Stand. dev. of V_p
All data	-0.084	0.148	6405	2.807	± 0.564
Filter I	-0.081	-0.003	92	2.608	± 0.113
Filter II	-0.113	-0.137	21	2.588	± 0.094
Filter III	-0.076	-0.016	71	2.614	± 0.117

Table 4.2: An overview of the results for the anisotropy parameters for some of the filters applied for the reservoir. The number of samples, the mean and the standard deviation of the velocity are also shown.

statements in Section 4.1 now than before filtering. The standard deviation of the velocity, which is the variation from the mean value, is as expected decreasing from the non-filtered case to the filtered cases. The number of samples is also decreasing. Some of the numbers may even be too small (too many data points are removed after filtering to still be representative), especially for Filter II.

Figure 4.9, 4.11, and 4.13 show the velocity versus inclination angle plots for each of the filters in Table 4.2. From these figures, a large reduction in number of wells from the non-filtered case can be seen.

Figure 4.10, 4.12, and 4.14 show the same plots including the second order polynomial fitted curve.

Figure 4.9: The velocity values versus inclination angle from the wells in the reservoir. Filter I has been applied to the data points.

Figure 4.10: The velocity values versus inclination angle from the wells in the reservoir. Filter I has been applied to the data points. The blue curve is the second order polynomial fitted curve.
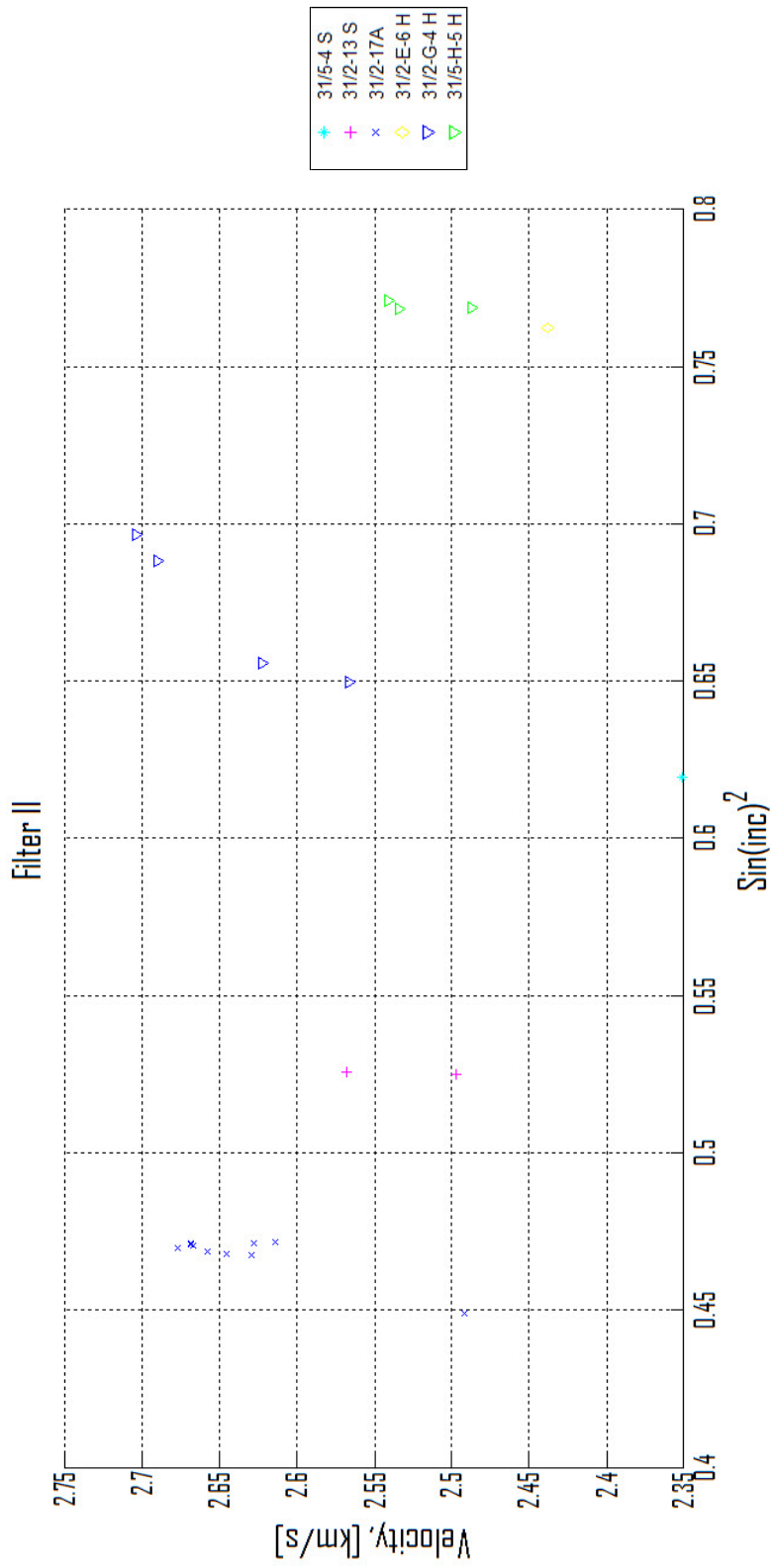
Figure 4.11: The velocity values versus inclination angle from the wells in the reservoir. Filter II has been applied to the data points.

Figure 4.12: The velocity values versus inclination angle from the wells in the reservoir. Filter II has been applied to the data points. The blue curve is the second order polynomial fitted curve.
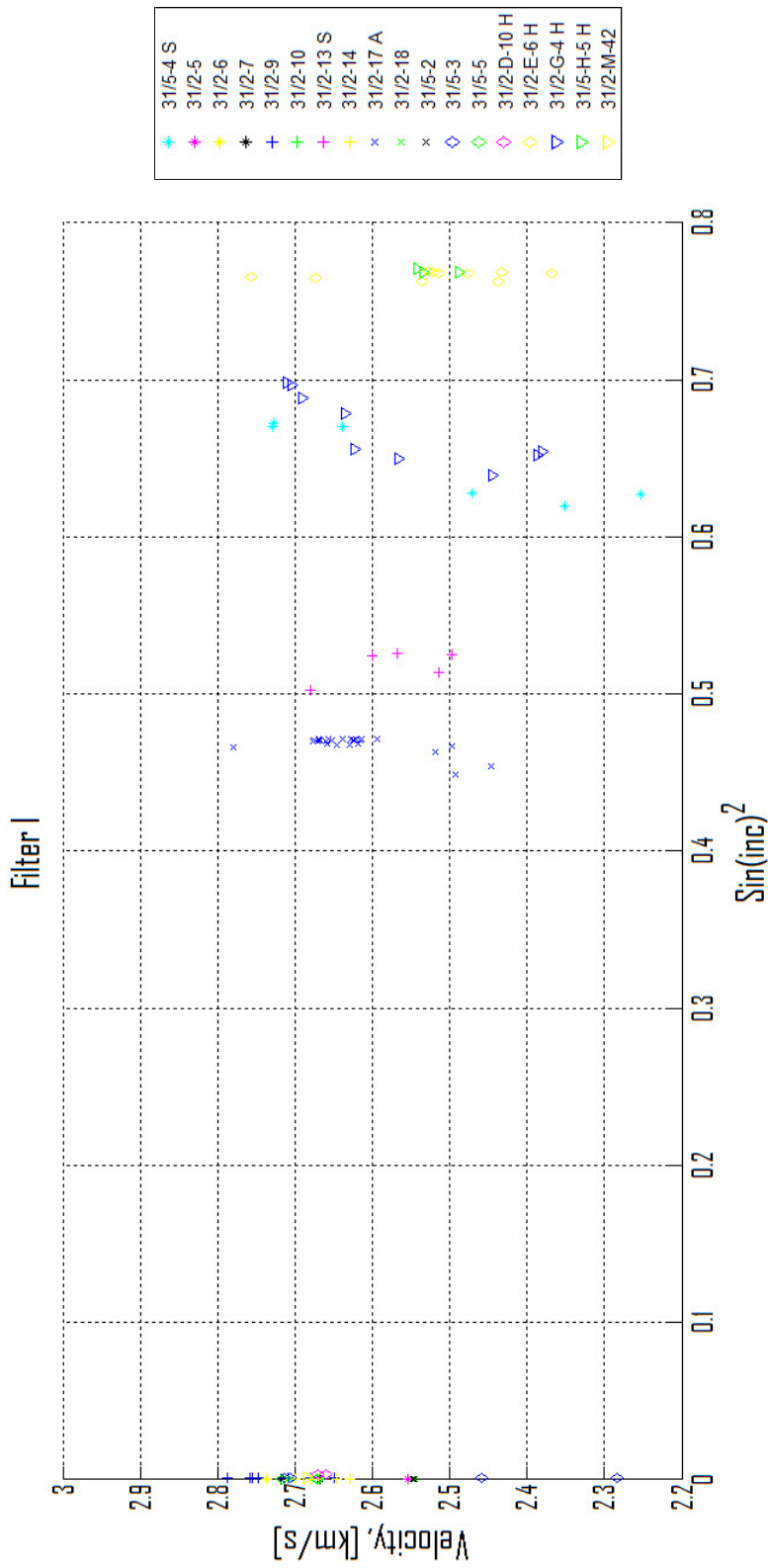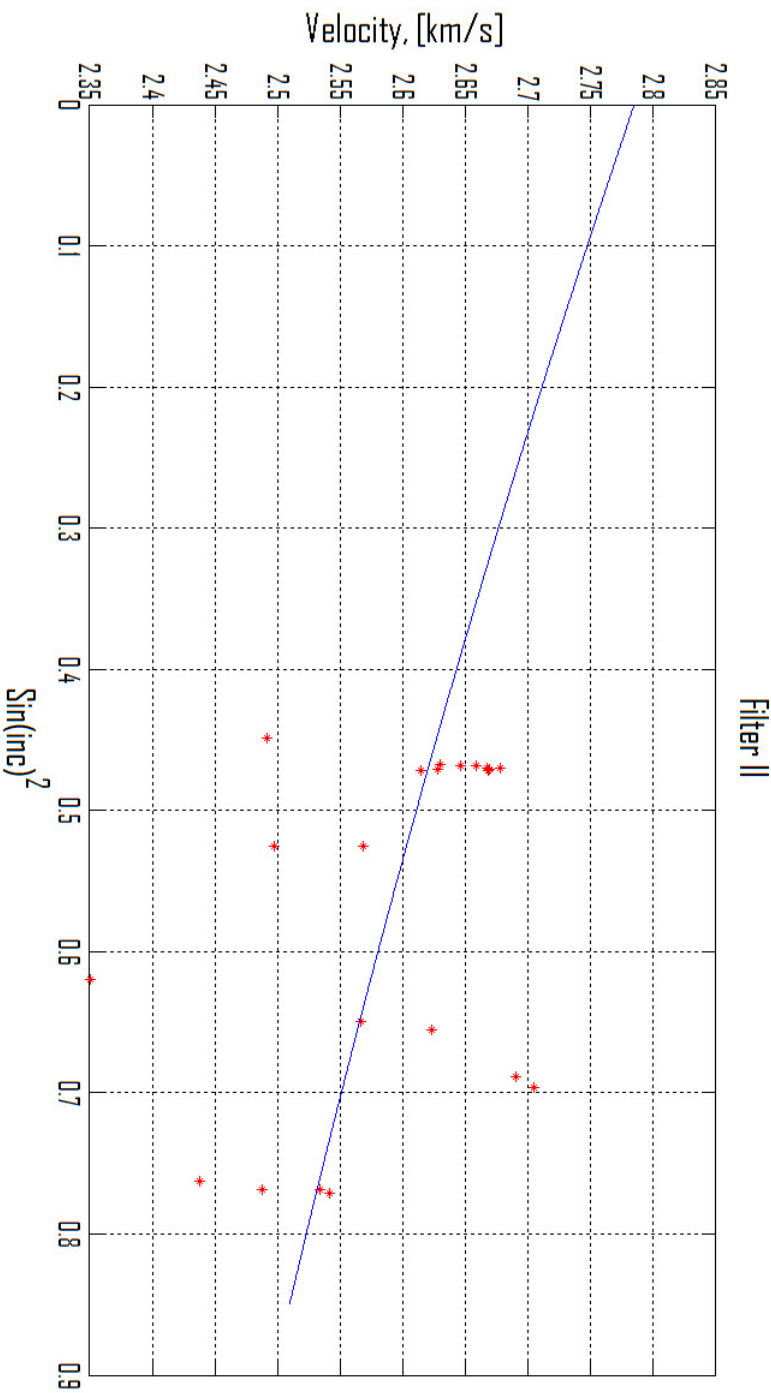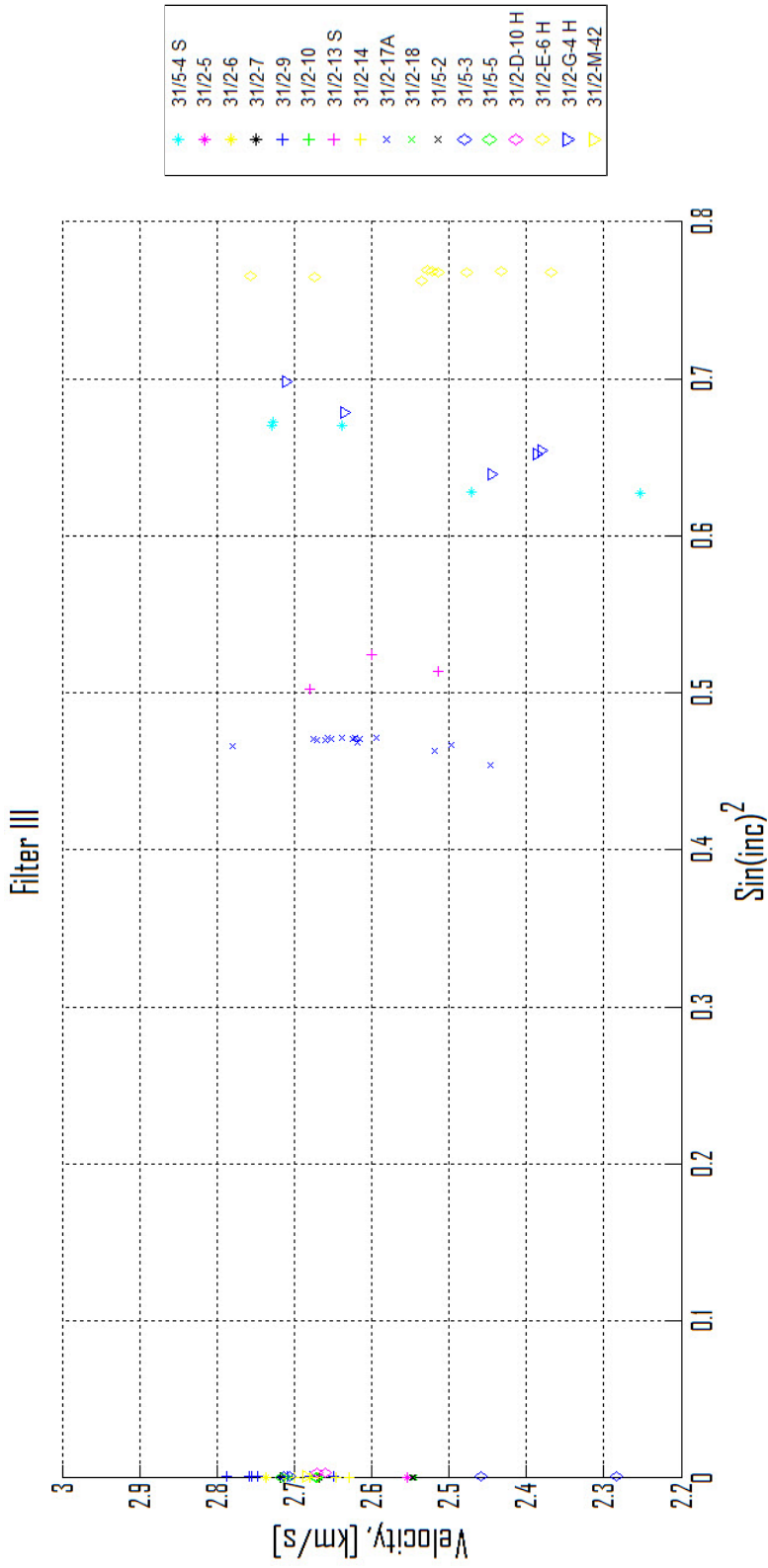
Figure 4.13: The velocity values versus inclination angle from the wells in the reservoir. Filter III has been applied to the data points.
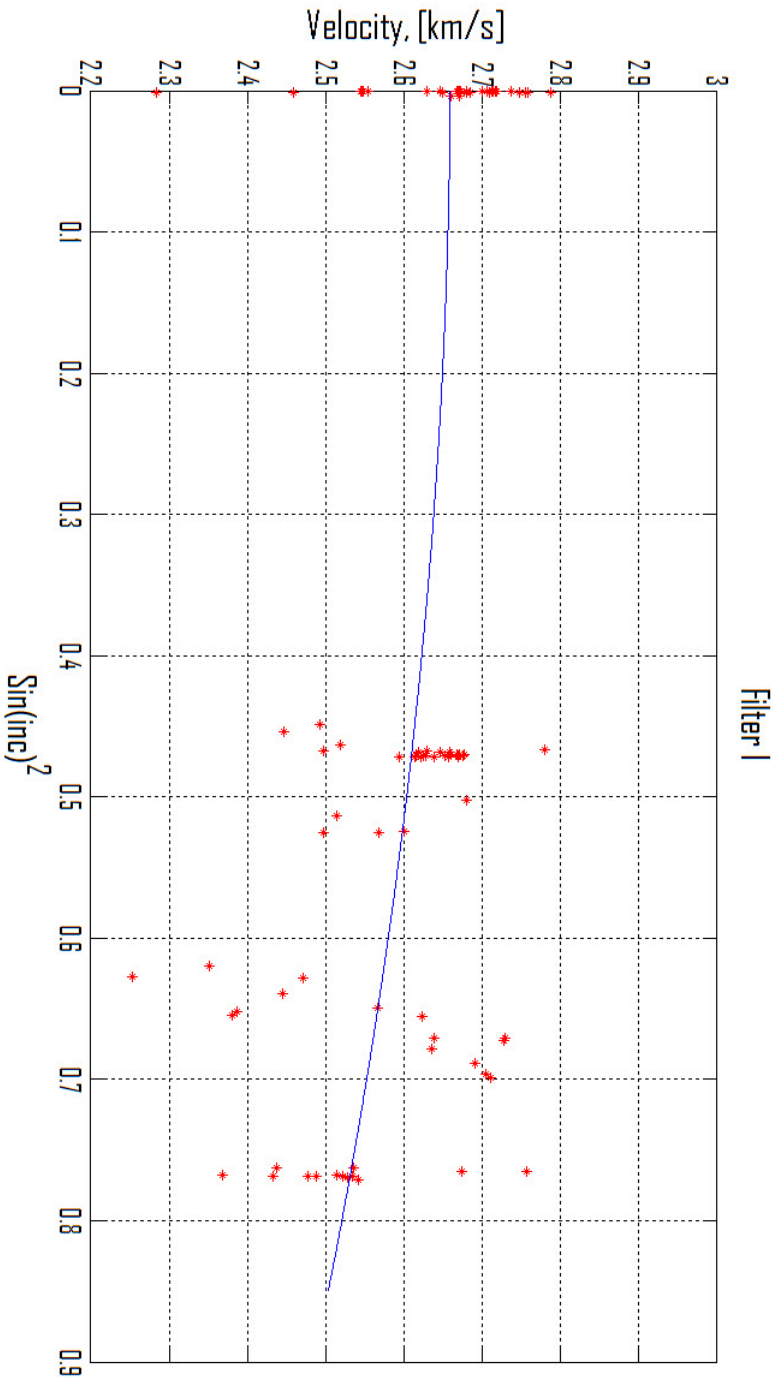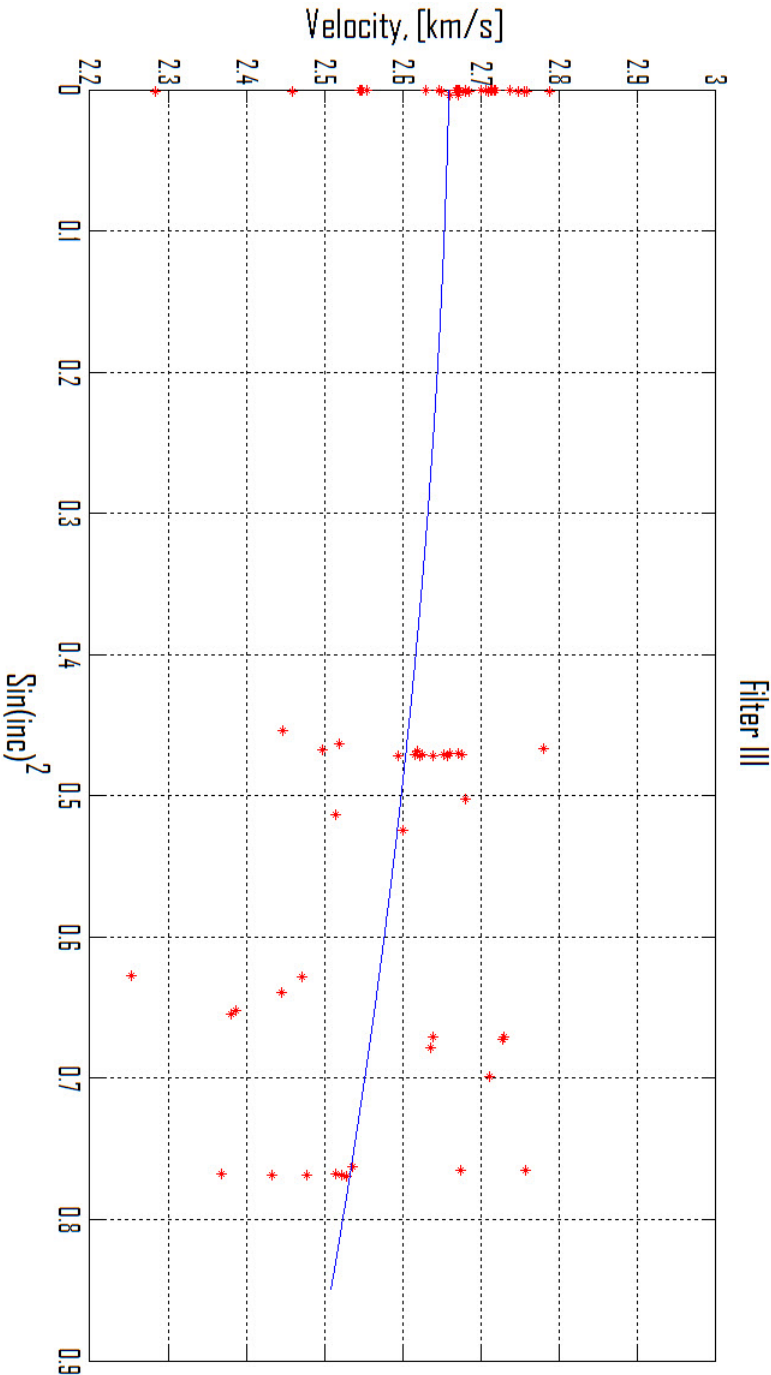
Figure 4.14: The velocity values versus inclination angle from the wells in the reservoir. Filter III has been applied to the data points. The blue curve is the second order polynomial fitted curve.

Figure 4.9, 4.11 and 4.13 show that the most deviated wells are still present after filtering. The vertical wells are also still present, except in Figure 4.11, where all the vertical wells are removed after Filter II has been applied. This would imply less reliable results, and larger values for the anisotropy parameters when applying Filter II than when applying the other filters can be seen in Table 4.2. Figure 4.9 and Figure 4.13 show that there are data from 18 and 17 wells, respectively, after filtering. Data from only 6 wells are present after filtering with Filter II (see Figure 4.11).

Figure 4.10 and 4.14 show that the fitted curves are stable, but since Filter II is lacking vertical wells, this fitted curve is not reliable (see Figure 4.12). All the figures show that the velocity is decreasing with inclination angle as expected for sandstones.

Figure 4.15 displays a plot with the fitted curves for five porosity filters. Seen from this figure, the data filtered on the lowest porosity values correspond with the higher velocity values. Only the curves from porosity filter 25-30 % and 30-35 % have the expected shape (see Chapter 5) and a slightly decrease in velocity with inclination angle. The plot shows that the porosity filter 15-20 % and 35-40 %, which have curves that are furthest from the expected curve, may be out of range and exclude too many data points or that more filtering on other parameters is required. The plot also gives an indication that filter I and III are better than Filter II.

A plot with all the porosity values for the reservoir versus the measured depth values of the wells are shown in Figure 4.16. Seen from this figure, the porosity varies a lot and does not have a very consistent decrease with depth. There is only a slight decrease of porosity with depth seen from the blue line in the figure. After generating this plot, it was decided to filter on depth too, since the porosity is not very dependent on depth.
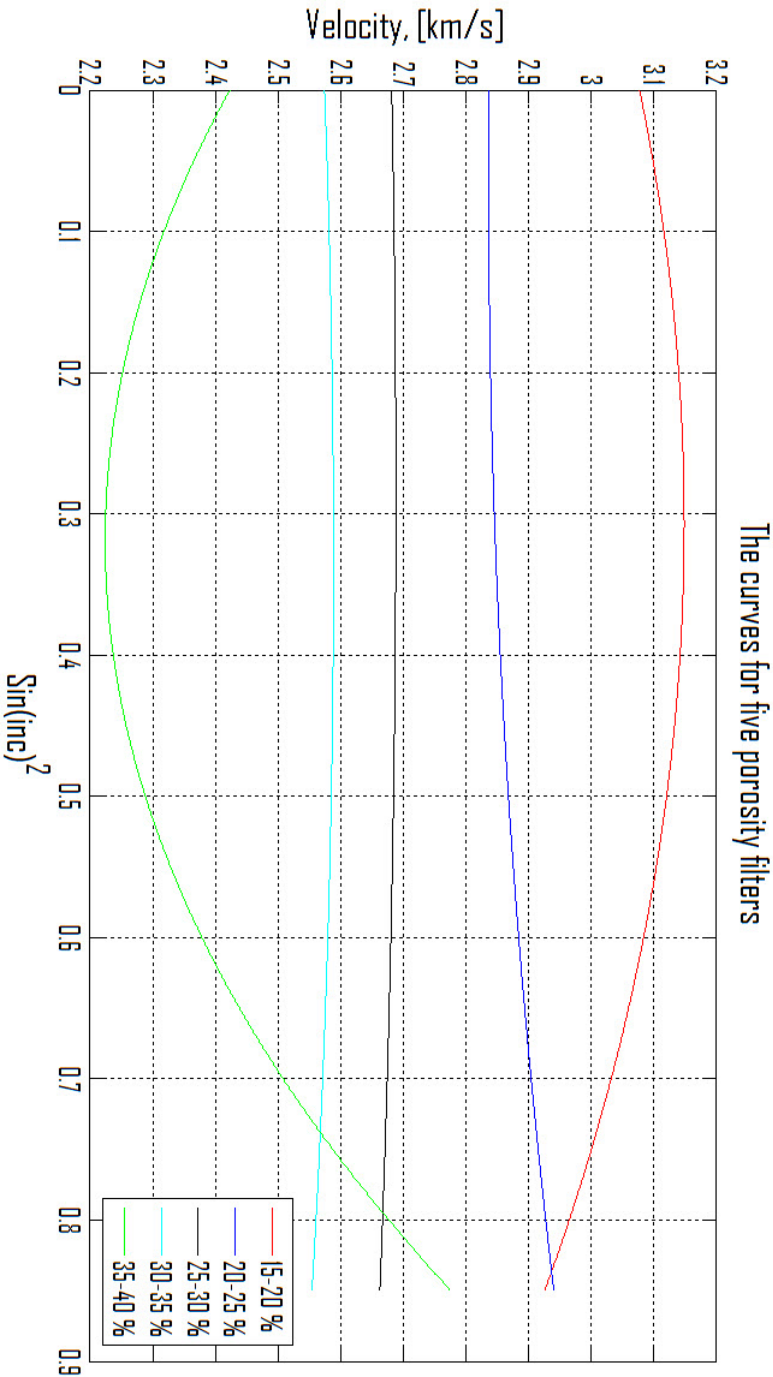
Figure 4.15: The curves for five porosity filters for the reservoir. The different colored lines indicate the different filters with 5 % interval.
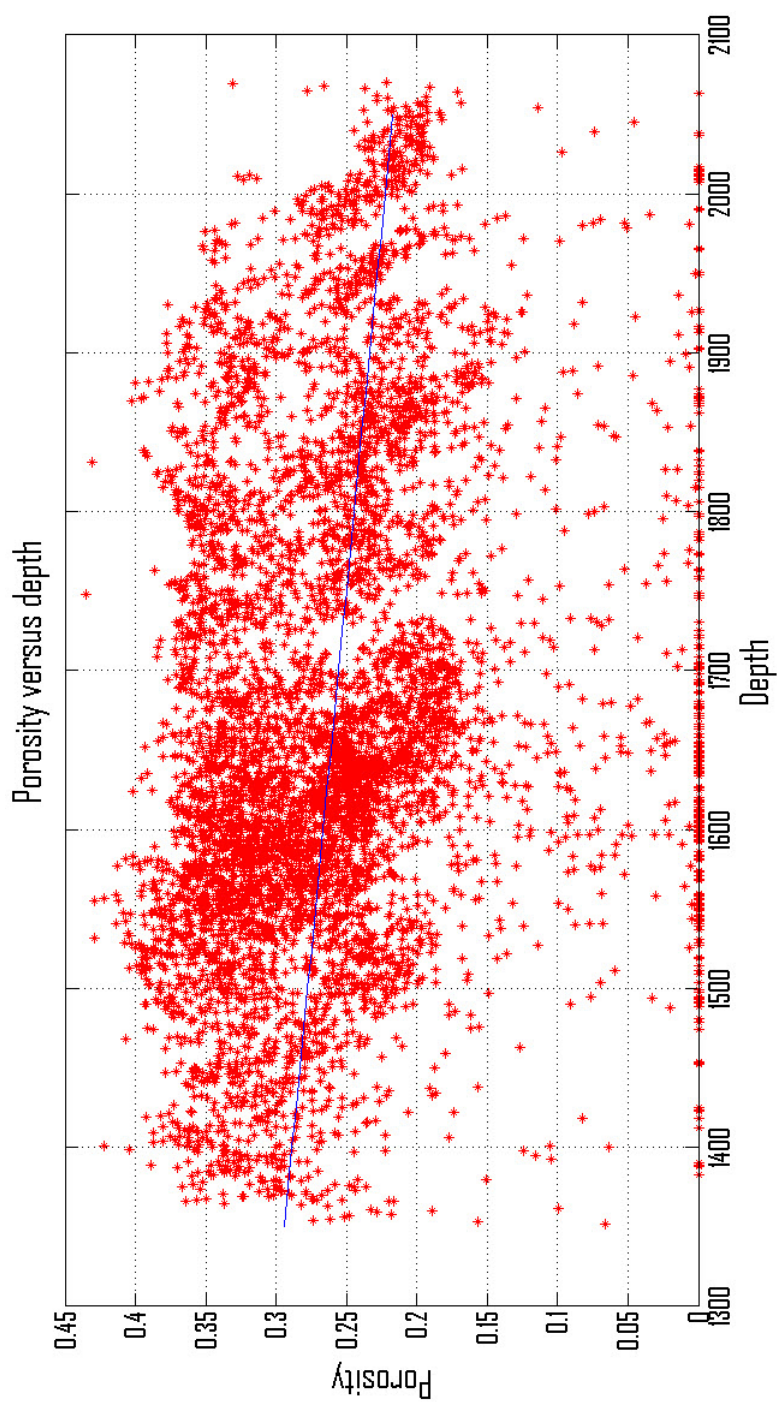
Figure 4.16: The porosity values versus measured depth of the wells in the reservoir interval. The blue curve is a first order polynomial fitted curve.

4.3 Filtering for the Draupne Fm.

Table 4.3 shows the anisotropy parameters for the selected filters for the Draupne Fm., including the result from the non-filtered data. The average values of the three selected filters for ε and δ are also shown. The anisotropy parameters for the Draupne Fm. for the rest of the filters are listed in the table in Appendix C.2. In Table 4.3, Filter IV is an AI filter on 5-8 km/s $\cdot$ g/cm^3 and Filter V is an AI filter on 4-8 km/s $\cdot$ g/cm^3. Filter VI is a filter including a depth filter on 1600-1700 meters MD and an AI filter on 5-7 km/s $\cdot$ g/cm^3. Seen from the table, the filters were not very good, so an average of the filters was calculated. This mean value has no values for "Number of samples", "Mean value of V_p" and "Standard deviation of V_p". Both the standard deviation and the number of samples are decreasing from the non-filtered case to the filtered cases as expected. For Filter V, the number of samples has not been reduced as much as for the other filters, thus this filter may be the best.

Figure 4.17, 4.19, and 4.21 show the velocity versus inclination angle plots for each of the filters in Table 4.3. From these figures, a large reduction in number of wells from the non-filtered case (see Figure 4.3) can be seen.

Figure 4.18, 4.20, and 4.22 show the same plots including the second order polynomial fitted curve.

Filter	ε	δ	Number of samples	Mean of V_p	Stand. dev. of V_p
All data	-0.022	0.399	752	2.449	± 0.419
Filter IV	0.086	0.019	381	2.554	± 0.274
Filter V	0.146	0.066	687	2.396	± 0.276
Filter VI	0.087	0.079	102	2.529	± 0.153
Mean value	0.106	0.055	—	—	—

Table 4.3: An overview of the results for the anisotropy parameters for some filters applied for the Draupne Fm. The number of samples, the mean and the standard deviation of the velocity are also shown.
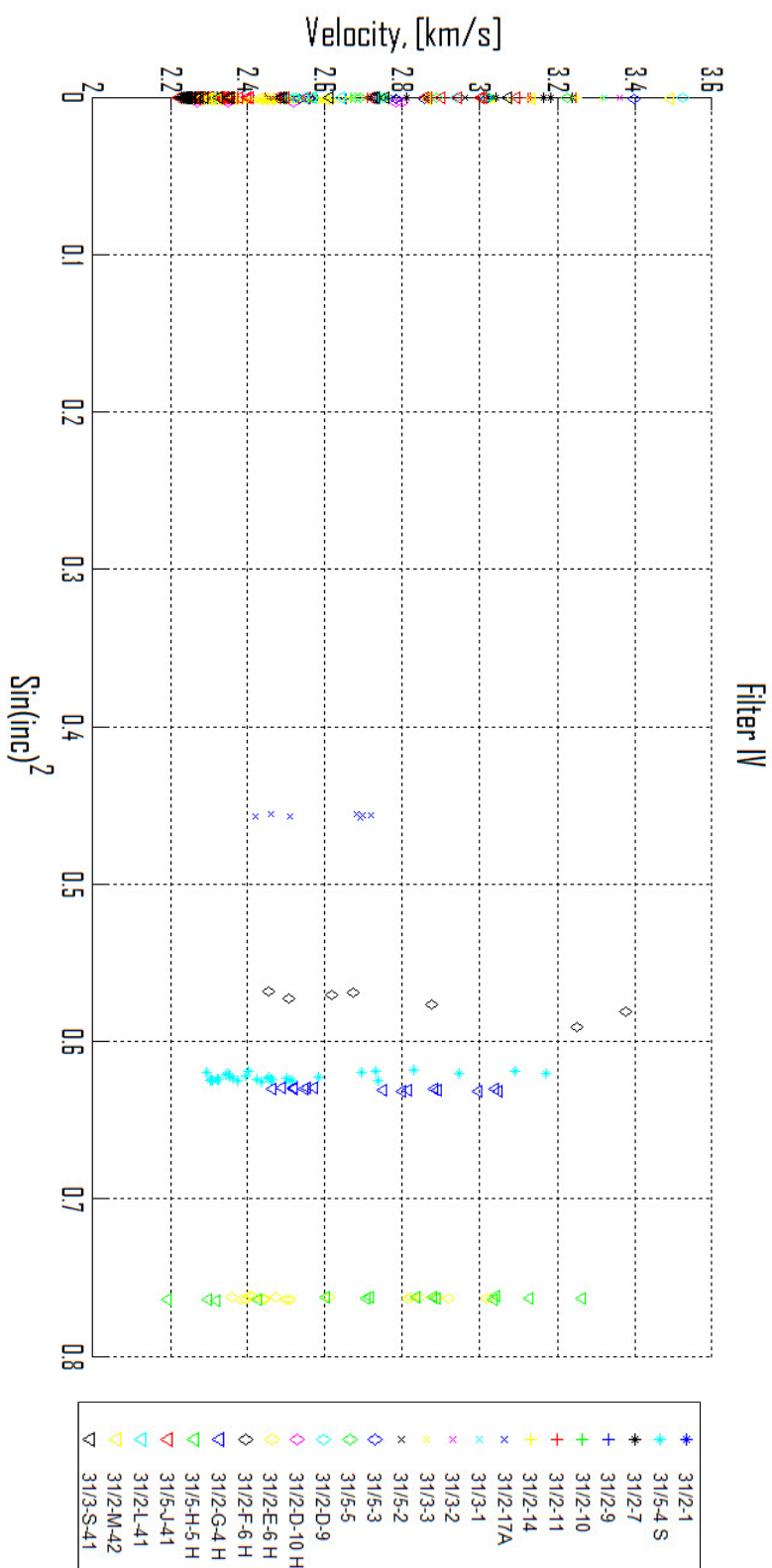
Figure 4.17: The velocity values versus inclination angle from the wells in the Draupne Fm. Filter IV has been applied to the data points.
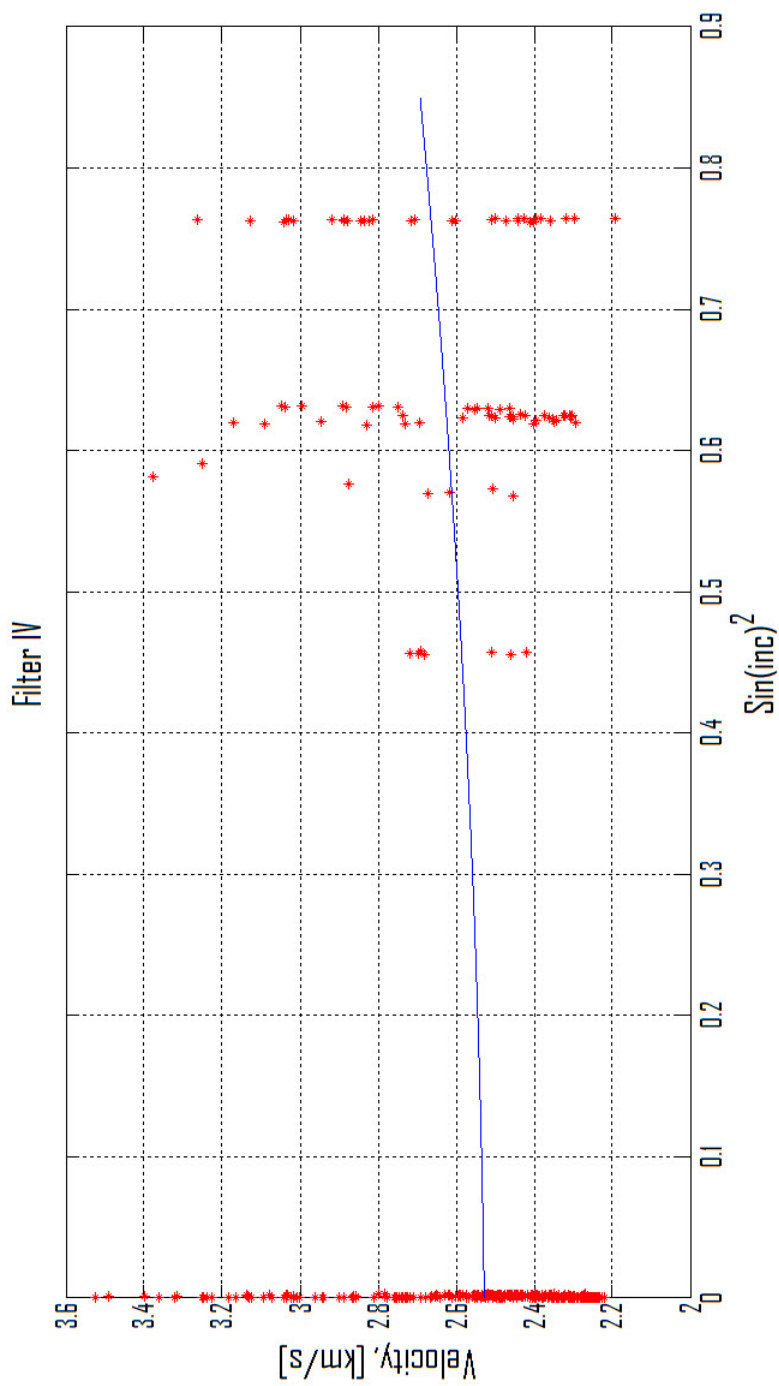
Figure 4.18: The velocity values versus inclination angle from the wells in the Draupne Fm. Filter IV has been applied to the data points. The blue curve is the second order polynomial fitted curve.
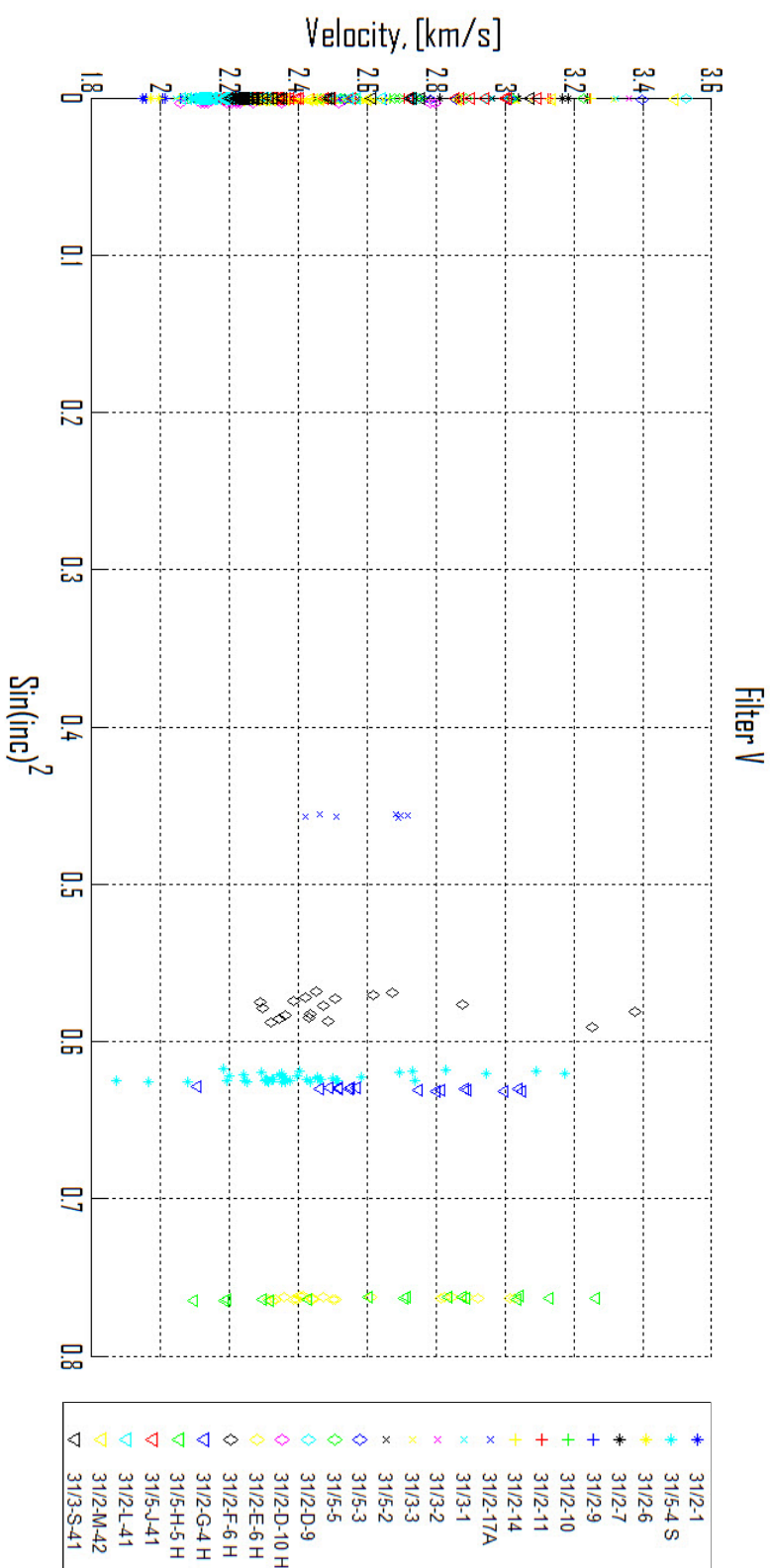
Figure 4.19: The velocity values versus inclination angle from the wells in the Draupne Fm. Filter V has been applied to the data points.
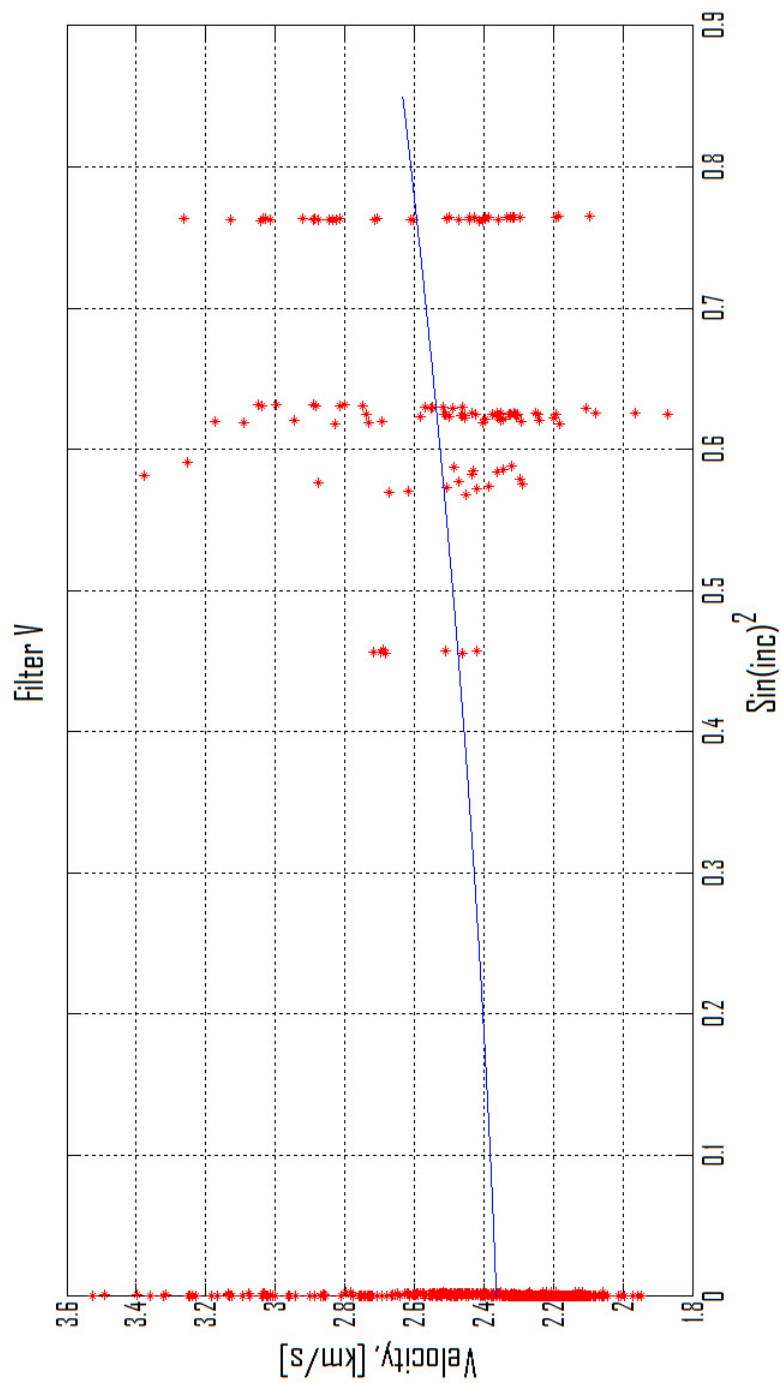
Figure 4.20: The velocity values versus inclination angle from the wells in the Draupne Fm. Filter V has been applied to the data points. The blue curve is the second order polynomial fitted curve.
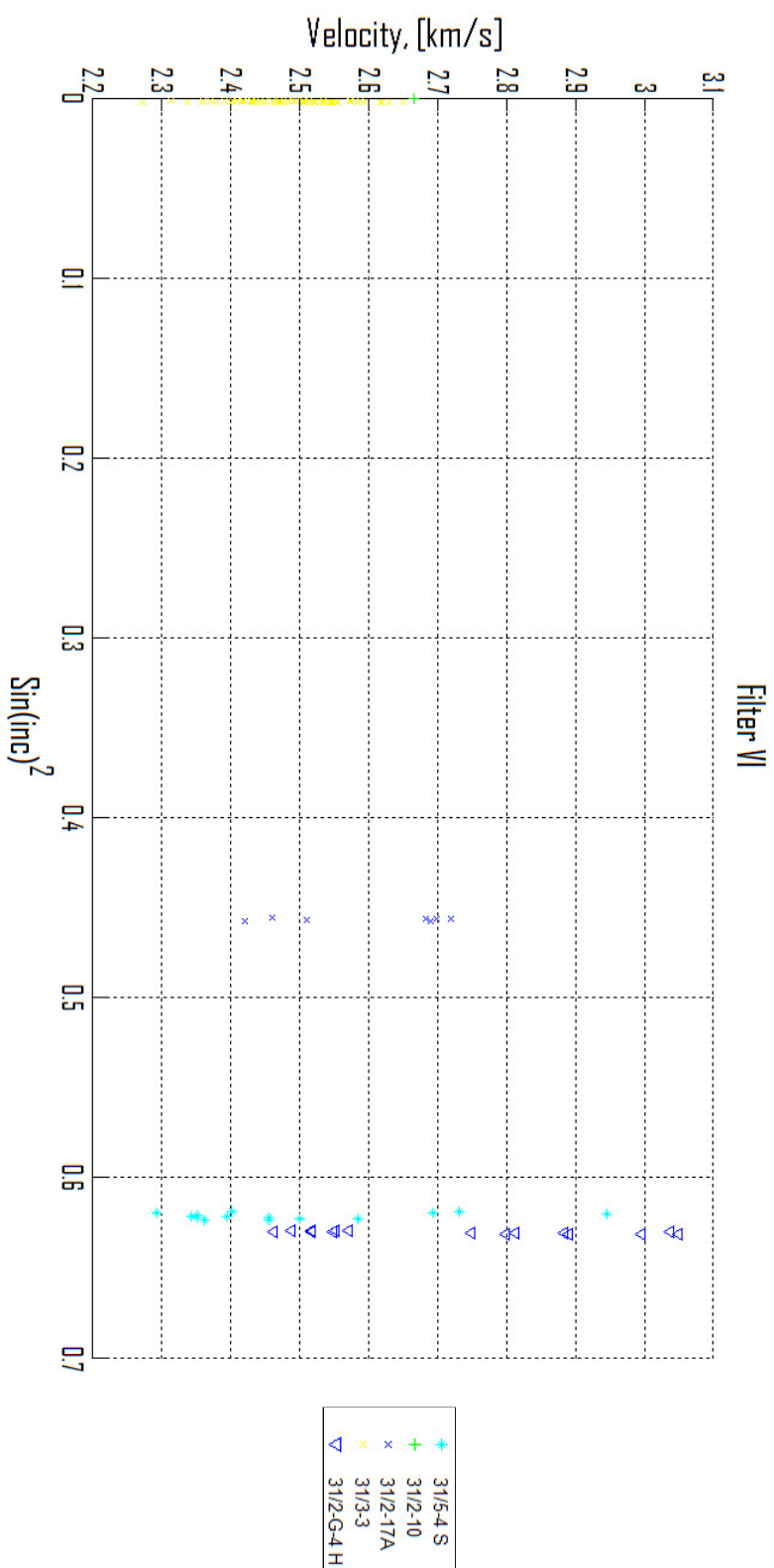
Figure 4.21: The velocity values versus inclination angle from the wells in the Draupne Fm. Filter VI has been applied to the data points.
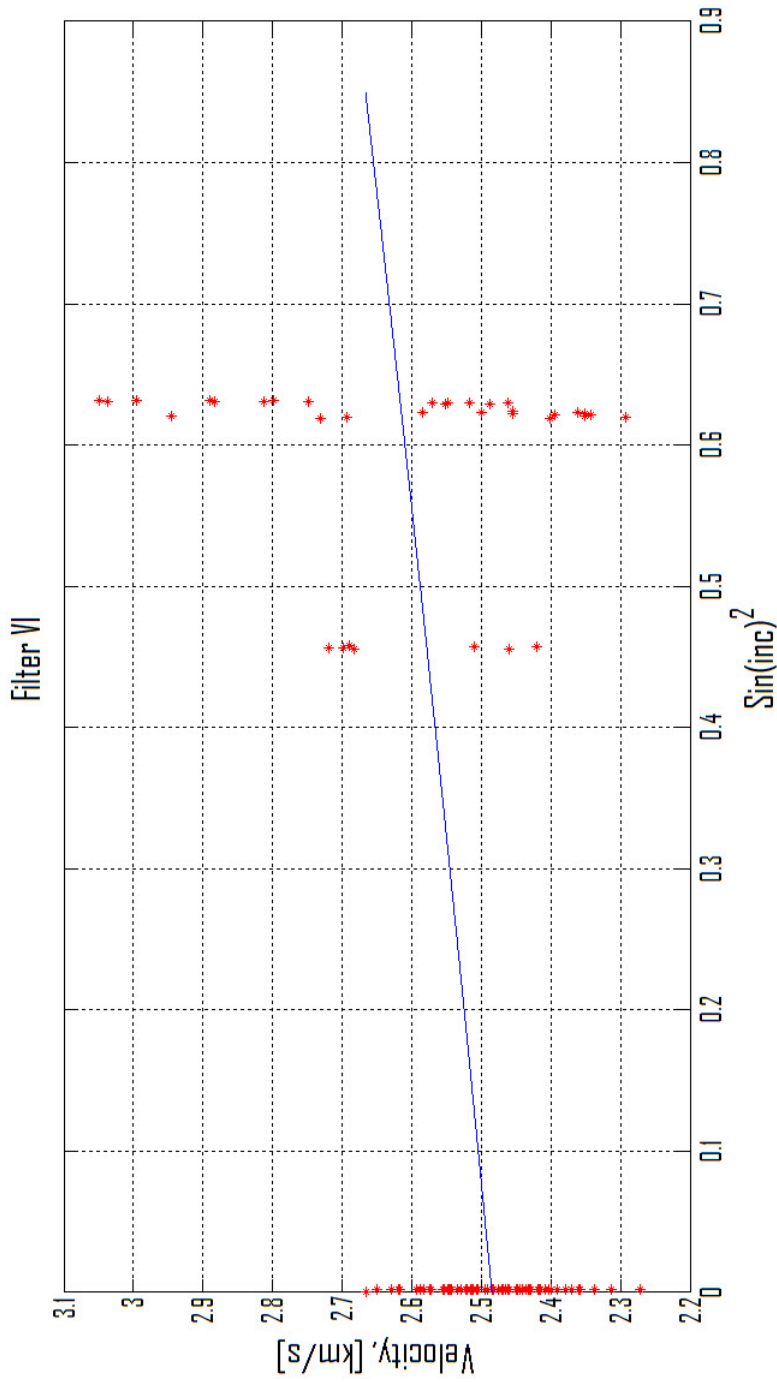
Figure 4.22: The velocity values versus inclination angle from the wells in the Draupne Fm. Filter VI has been applied to the data points. The blue curve is the second order polynomial fitted curve.

Figure 4.17 and 4.19 show that after applying the different filters for the Draupne Fm., the vertical and the most deviated wells are still present. When applying Filter VI (see Figure 4.21), the vertical wells are still present, but the most deviated wells are removed. There are still some deviated wells, with the largest angle at about 53°. Figure 4.17 and Figure 4.19 show that there are data from 24 and 25 wells, respectively, after filtering. In Figure 4.21 (Filter VI), there are only 5 wells left in the data after filtering.

For Figure 4.18, 4.20 and 4.22, the second order polynomial fitted curves look stable, even though the plot in Figure 4.22 is lacking data for more angles than the other filters. All the figures show that the velocity is increasing with inclination angle as expected for shales (Hornby et al., 2002).

4.4   Standard deviation of ε

Table 4.4 shows the standard deviation of ε for the reservoir, both the filters from Table 4.2 and the non-filtered case. The values for the mean and the standard deviation of the vertical and the horizontal P-wave velocity are also shown. Seen from the table, the standard deviation of ε for the filters are smaller, hence better, than for the non-filtered (All data) case. For Filter II, all the vertical wells were removed after filtering, thus no standard deviation could be calculated for this filter.

The values for ε and the standard deviation of ε for the filters and the non-filtered case for the reservoir are shown in Table 4.5. From this table, it

Filter	V_v (mean)	V_h (mean)	σ_{V_v} (Stand. dev.)	σ_{V_h} (Stand. dev.)	Stand. dev. of ε
All data	2.8087	2.7222	$\pm$ 0.570	$\pm$ 0.370	$\pm$ 0.229
Filter I	2.6583	2.5241	$\pm$ 0.098	$\pm$ 0.100	$\pm$ 0.049
Filter II	—	2.5001	—	$\pm$ 0.048	—
Filter III	2.6583	2.5347	$\pm$ 0.098	$\pm$ 0.118	$\pm$ 0.054

Table 4.4: The standard deviation of ε for the different filters and the non-filtered case for the reservoir.

Filter	ε	Stand. dev. of ε
All data	-0.084	$\pm$ 0.229
Filter I	-0.081	$\pm$ 0.049
Filter II	-0.113	—
Filter III	-0.076	$\pm$ 0.054

Table 4.5: ε and the standard deviation of ε for the different filters and the non-filtered case for the reservoir.

Filter	V_v (mean)	V_h (mean)	σ_{V_v} (Stand. dev.)	σ_{V_h} (Stand. dev.)	Stand. dev. of ε
All data	2.4120	2.6538	$\pm$ 0.387	$\pm$ 0.338	$\pm$ 0.248
Filter IV	2.5281	2.6746	$\pm$ 0.270	$\pm$ 0.286	$\pm$ 0.169
Filter V	2.3639	2.6173	$\pm$ 0.261	$\pm$ 0.306	$\pm$ 0.197
Filter VI	2.4849	2.6113	$\pm$ 0.081	$\pm$ 0.231	$\pm$ 0.104
Mean value	—	—	—	—	—

Table 4.6: The standard deviation of ε for the different filters and the non-filtered case for the Draupne Fm.

can easily be seen that anisotropy parameters gained after applying Filter I are the best values to choose for an AVO analysis, due to lowest standard deviation of ε (60 %).

Table 4.6 shows the standard deviation of ε for the Draupne Fm., both the filters from Table 4.3 and the non-filtered case. The values for the mean and the standard deviation of the vertical and the horizontal P-wave velocity are also shown. Seen from this table, the standard deviation of ε for the filters are also better than for the non-filtered (All data) case. But the value of the standard deviation is still very large.

The values for ε and the standard deviation of ε for the filters and the non-filtered case for the Draupne Fm. are shown in Table 4.7. Seen from this table, and comparing the value of the standard deviation of ε with the value

Filter	ε	Stand. dev. of ε
All data	-0.022	± 0.248
Filter IV	0.086	± 0.169
Filter V	0.146	± 0.197
Filter VI	0.087	± 0.104
Mean value	0.106	—

Table 4.7: ε and the standard deviation of ε for the different filters and the non-filtered case for the Draupne Fm.

of ε (for Filter IV), the standard deviation values are almost 100 % of the value itself. Filter IV has a particular large standard deviation compared to the value of ε, but none of the filters are very good, thus the mean values are the best values to choose for an AVO analysis.

4.5   The AVO analysis

As mentioned in Section 3.4, the AVO analysis was performed for the 31/2-L-41 well. For the anisotropic case, ε and δ are needed for the reservoir and the Draupne Fm., which is the cap rock in the well in question. For the reservoir, the values generated when applying Filter I was chosen. The values are -0.081 for ε and -0.003 for δ. Since the value for δ is less reliable due to the lack of deviated wells, the uncertainty of the δ-estimate is considered to be much higher than the uncertainty of the ε-estimate, thus δ was estimated in a different way. According to Li (2006), $\delta = 0.32\varepsilon$. This is an empirical relation. This new δ value, which is -0.026, was used in the AVO analysis instead. For the Draupne Fm., the average value from Filter IV, V and VI was chosen. The values are 0.106 for ε and 0.055 for δ. The values used in the AVO analysis are shown in Table 4.8.

Figure 4.23 shows the reflection coefficient versus the incidence angle for the isotropic and the anisotropic case. This figure shows that the reflection coefficients at zero incidence angle (the intercept, R_0) are negative and close to zero for both the isotropic and the anisotropic case. The gradients, R_2, are

	ε	δ
The reservoir	-0.081	-0.026
The Draupne Fm.	0.106	0.055

Table 4.8: The anisotropy parameters for the reservoir and the Draupne Fm. used in the AVO analysis.

also negative. Thus, the amplitude (absolute value of reflection coefficient) increases with incidence angle for both cases. The two curves are coincident at small angles, starting to deviate from each other at around $13 - 15\,°$. The fact that the curves overlay at zero offset can be seen from Equation 2.30, where the first term is the intercept, which does not contain any anisotropy parameters. These are only present in the second and the third term of the equation. Hence, the anisotropy is only affecting the amplitudes at large offsets. Seen from Figure 4.23, the increase in amplitude from the isotropic case to the anisotropic case is 33 % at $50\,°$ and 22 % at $40\,°$. At $20\,°$ it is about 9 %. At far offset, this increase in amplitude is evident.

Figure 4.24 shows the same as Figure 4.23, including the exact solution from the Zoeppritz's equations, which is for the isotropic case. This figure shows that the curve from the Zoeppritz's equations is very close to the approximate solution (the isotropic curve). The amplitudes are still increasing with incidence angle. The difference from the exact isotropic to the anisotropic case is somewhat larger than for the approximate isotropic case.

Figure 4.25 shows the same as Figure 4.24, including amplitude values from three gathers. This figure shows that the amplitude of all the three gathers vary with incidence angle. For Gather 1, a general increase can be seen. Gather 2 and 3 do not show a clear increase in amplitude with incidence angle. Looking at the slope of the gathers qualitatively, it may be closer to the isotropic case than the anisotropic case, but this is difficult to say certainly.
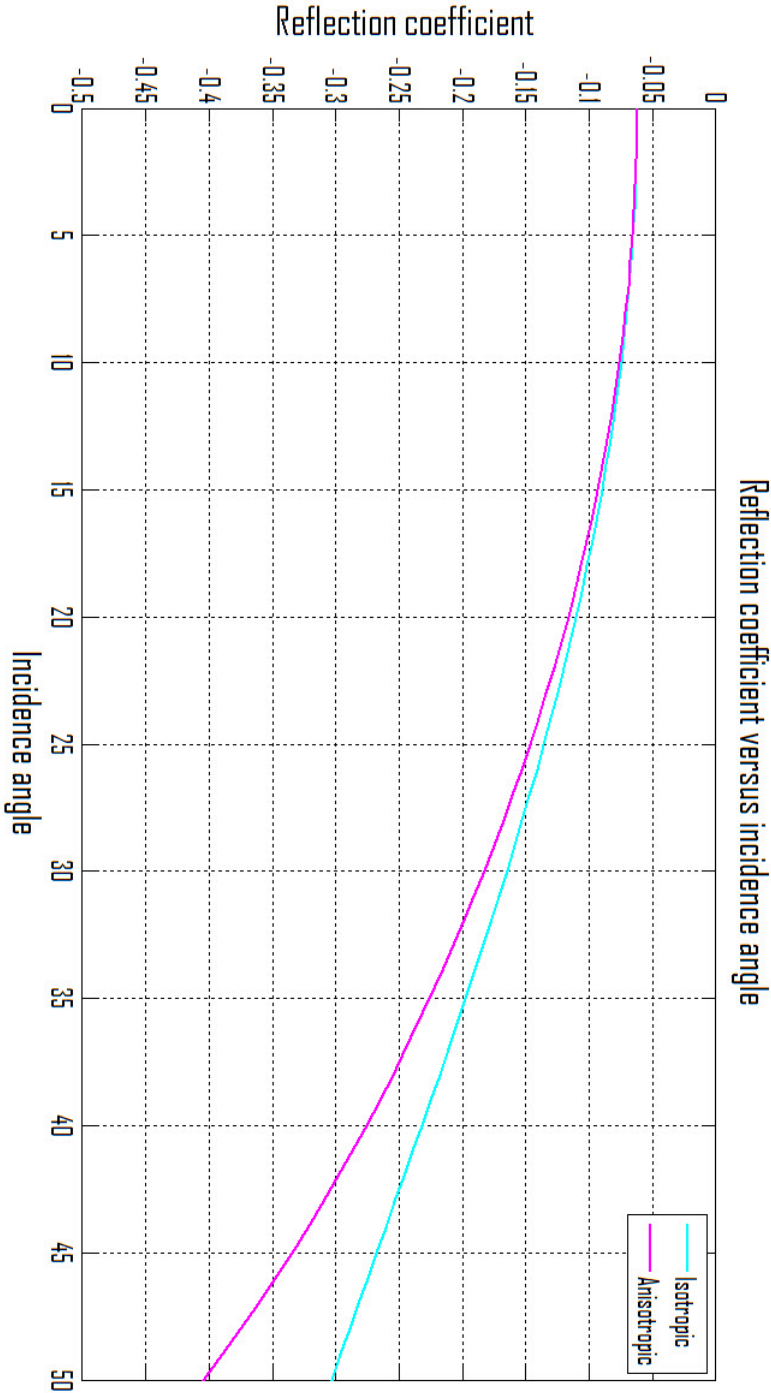
Figure 4.23: An AVO plot for the isotropic and the anisotropic case for well 31/2-L-41. The reflection coefficient is unitless and the incidence angle is in degrees.
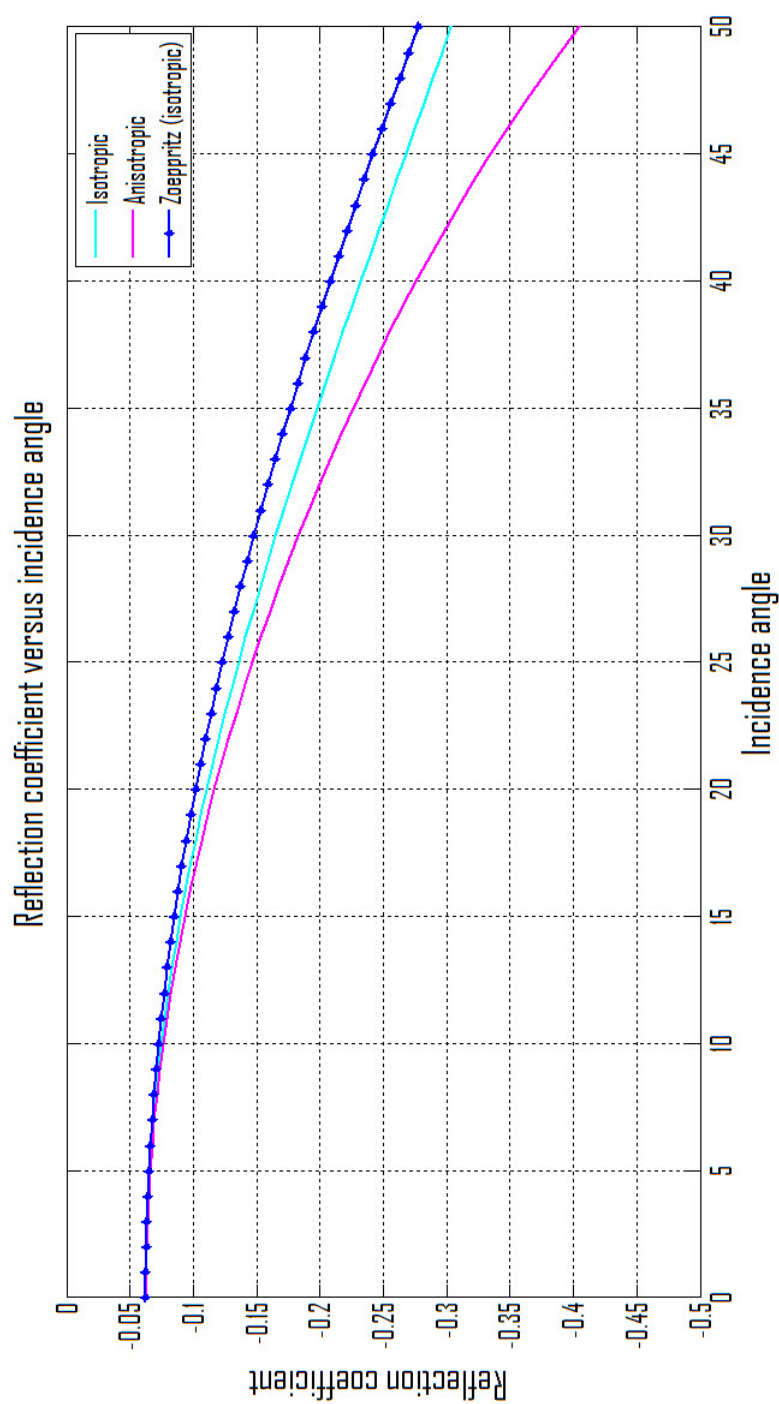
Figure 4.24: An AVO plot for the isotropic and the anisotropic case for well 31/2-L-41, including the curve for the exact solution for the isotropic case (Zoeppritz's equations). The reflection coefficient is unitless and the incidence angle is in degrees.
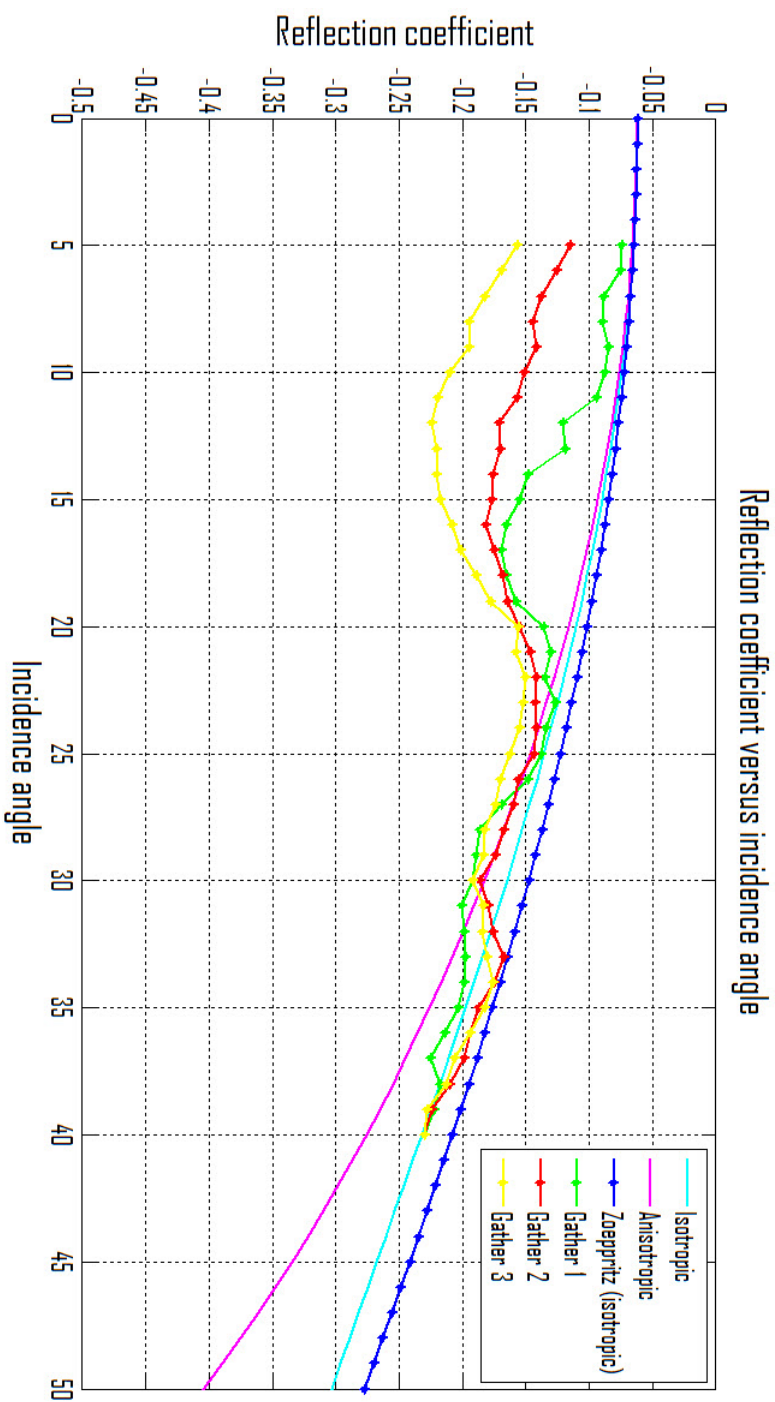
Figure 4.25: An AVO plot for the isotropic and the anisotropic case for well 31/2-L-41, including the curve for the exact solution for the isotropic case (Zoeppritz's equations). The three gathers are also shown. The reflection coefficient is unitless and the incidence angle is in degrees.

Chapter 5

Discussion of results

The anisotropy parameters for the Troll West Field found in this work, were estimated using an approximate equation (see Equation 2.10). For this equation, weak anisotropy ($<< 1$) is assumed. Since Richard Tøndel's result of $\varepsilon = -0.08$, which is $<< 1$, applies to the Troll Field, this assumption is valid.

The values from the P-wave sonic logs and the inclination angle logs were plotted, fitted to a second order polynomial function and compared with Equation 2.10. This is an equation for the phase velocity of the P-wave. Thus, the velocity values measured from the P-wave sonic log are assumed to be the phase velocity, which is the rate at which the phase of a wave propagates in space. This assumption may be wrong and the velocities from the sonic log may as well be the group velocity, which is defined as the velocity with which the overall shape of the wave's amplitude propagates in space. It is hard to know if the sonic log measures the phase or the group velocity, but the difference should not be too large, so the assumption should be valid. Although the assumptions may be wrong, the results for the anisotropy parameters are just estimates, and will be adequate for this purpose.

In Equation 2.10, the angle of the wave vector relative to the x_3-axis, θ, is also required. If the layer (in this case the reservoir) is horizontal, the x_3-axis is the vertical axis and the angle of the wave vector is the same as the inclination angle of the wellbore. If the reservoir layer is dipping, the x_3-axis is perpendicular to the reservoir and the angle of the wave vector will be the effective dip, which is the angle at which the wellbore enters the reservoir relative to the x_3-axis. Thus, the effective dip is a combination of the dip of

the reservoir and the inclination angle of the wellbore. Presuming that the deviation of the well is downdip, the effective dip is the inclination angle of the well added to the dip of the reservoir. Presuming that the deviation of the well is updip, the effective dip is the inclination angle of the well subtracted from the dip of the reservoir. Since the dip of the reservoir layer was not accounted for in this work, this could lead to errors in the estimation of the anisotropy parameters. However, the average dip of the Sognefjord Fm. is around $2-3\,°$, thus disregarding this dip should not lead to large errors in the estimation.

When drilling a well, large cavities can develop, creating cavings around the wellbore. This setting would cause the logging tools to measure values that are not correct in-situ values. However, the logs used in this study are corrected for such errors. Figure 4.1 shows large velocity values of 4000 m/s, up to 7000 m/s. Since the reservoir on the Troll Field is shallow, around 1400 m, it is questionable whether these velocities are true velocities. These large velocity values are most likely due to errors in the logging process, especially the values between 6000 m/s and 7000 m/s. The values could be caused by short cycle skipping in the sonic logging, where the signal in the near receiver comes from a cycle too late, resulting in an abnormally low sonic log value (high velocity). Comparing the sonic logs and the density logs, these high velocity values correspond well with high density values. The high density values are most likely due to calcite layers within the reservoir sandstone. The bulk modulus of calcite is large compared to the bulk modulus of quartz (75 GPa compared to 38 GPa) (Berge, 1998), leading to a larger velocity value. Thus, this indicates that the large velocity values measured could be true velocities. Still, there is no reason to conclude that the calcite layers would account for the large velocity values alone. Thus, incorrect values from the logs due to effects from drilling or logging may be another source of errors in the estimation.

To estimate ε, only the vertical ($0\,°$ inclination angle) and the horizontal ($90\,°$ inclination angle) P-wave velocities are required. Thus, a first order polynomial function would be sufficient to estimate this parameter. This can be seen from Equation 2.12, when inserting $\delta = 0$. However, to estimate δ, a second order polynomial function is needed because δ occurs both in the second and the third term of Equation 2.12. Thus, points between $0\,°$ and $90\,°$ are needed as well. This means that deviated wells must be included in the analysis, and the inclination angle of the wellbores should vary and cover the whole range from $0\,°$ to $90\,°$. The more points in this range of inclination

angle, the less uncertainty in the polynomial function. Few deviated wells compared to the number of vertical wells were found in this work (74 % of the total number of wells in this study are vertical wells), and the maximum inclination angle in the reservoir is only 67 ° (seen from Figure 4.1). To measure the exact horizontal velocity, an angle of 90 ° is needed, thus the horizontal velocity will be approximate. This leads to an uncertainty in ε. The lack of deviated wells indicates that there is a high uncertainty in the estimation of δ as well. This should be considered when analyzing the results.

The anisotropy parameters are expected to be positive for shale and negative for sandstone, also ε must be greater than δ (Mavko et al., 2009). These facts can be used to visualize the expected curve from the polynomial function, using Equation 2.12 and 2.13. The sign of the C coefficient (in Equation 2.13) indicates if the vertex of the curve is a highest point or a lowest point. If C is positive, the vertex will be a lowest point, and if C is negative, the vertex will be a highest point. The sign of the B coefficient indicates if the axis of symmetry is on the negative or the positive x-axis, depending on the sign of the C coefficient. Presuming the C coefficient is positive, the axis of symmetry is on the negative x-axis if B is positive and on the positive x-axis if B is negative. The opposite will be true if C is negative. The A coefficient, which is the intercept, is always positive and does not affect ε and δ.

Since both B and C coefficients can be positive and negative, four cases are inspected. Case 1 is for negative B and C, case 2 is for positive B and C, case 3 is for positive B and negative C and case 4 is for negative B and positive C. Equation 2.14, 2.15 and 2.16 are inspected. For case 1, ε and δ will be negative and $|\varepsilon| > |\delta|$. For case 2, ε and δ will be positive and $\varepsilon > \delta$. For case 3, δ is positive and ε can be both positive and negative as long as $\varepsilon < \delta$. Since ε should be larger than δ, the results from this case should not be considered valid. For case 4, δ is negative and ε can be both positive and negative as long as $\varepsilon > -\delta$. Since the anisotropy parameters should have the same sign for the same formation, this is only valid if ε is negative. Thus the absolute value of ε will be less than the absolute value of δ and thus not meet the criteria of $\varepsilon > \delta$. From this, only case 1 and case 2 should be considered further.

Case 1, where the anisotropy parameters are negative, is valid for the reservoir. For this case, the B and C coefficients are negative, thus the velocity will decrease with inclination angle. Case 2, where the anisotropy parameters are positive, is valid for the shale. For this case, the B and C coefficients are

positive, thus the velocity will increase with inclination angle. Only results from second order polynomial functions where the B and C coefficients have the same sign should be considered valid.

Figure 4.2 shows a curve with a negative C and a positive B, thus the results from this plot do not show negative anisotropy parameters and $\varepsilon < \delta$, which is verified from Table 4.1. Figure 4.10, 4.12, and 4.14 shows the curves for the filtered data. For all the filters, the curves show a decrease in velocity with inclination angle (B and C are negative). Figure 4.12, which shows Filter II, should not be considered valid since the filter is lacking data from vertical wells. Hence, Filter I and III fulfill the requirements, which can be seen from Table 4.2.

Figure 4.4 also shows a curve with a negative C and a positive B. Seen from Table 4.1, the anisotropy parameters are not positive as expected and $\varepsilon < \delta$. Figure 4.18, 4.20, and 4.22 shows the curves for the filtered data for the Draupne Fm. The curves show an increase in velocity with inclination angle (B and C are positive). This agrees well with the results in Table 4.3. Consequently, the filters exert better results. This shows that filtering was necessary, yet the filtering may remove too many data points, consequently the result will not be representative, as seen for Filter II in Table 4.2.

Since no filtering on fluids in the reservoir was applied, the data points are a mix of brine, oil and gas. If fluid filters had been applied, the data points could have been "cleaner", and the results could have been altered. However, the vertical and the horizontal P-wave velocity, which constitute the formula for ε, are equally affected by the fluids. Thus, the fluid effects are assumed to be "isotropic" and the result for ε should not change drastically. The effect on δ is harder to comprehend, hence filtering for fluids should be done to establish the difference.

Due to compaction (mechanical and chemical), porosity decreases with depth (Avseth et al., 2005). This is not evident in Figure 4.16, which shows a plot of the porosity versus depth for the reservoir interval. This independence between porosity and depth may be due to the fact that the porosity log is calculated from the density log, which is affected by the calcite layers in between and in the sandstones in the reservoir. Another reason for this may be that the reservoir is at a shallow depth, where the porosities may not change much with depth as seen from Figure 5.1. In addition, the plot is only for

the reservoir interval. Generating this plot for a larger interval could show a more definite decrease in porosity with depth.
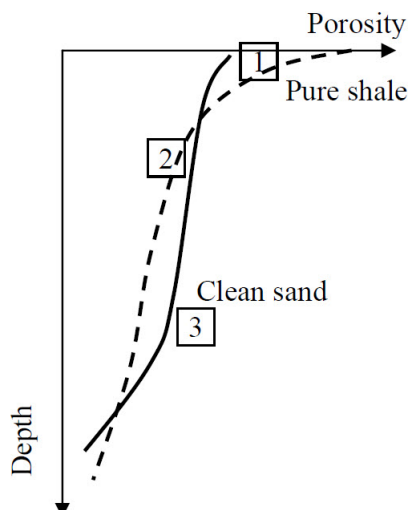
Figure 5.1: The porosity versus depth for a clean sand and a pure shale. For the sand, the porosities show a small decrease at shallow depths, while the larger decrease is evident first at larger depths (Avseth et al., 2005).

For the AVO analysis, Equation 2.30 shows that the wavefront angle, θ_w, is required. In this case, the incidence angle (ray angle) was applied and assumed to be equal to the wavefront angle. If this assumption is wrong, this could lead to an error in the AVO analysis. However, seen from Equation 5.1, the leading term is 1, thus the error in using ray angle instead of wavefront angle is small (Thomsen, 2002).

$$\tan \theta_w = \frac{\tan \theta_r}{1 + 2\delta + 4\eta \sin^2 \theta_r}, \qquad (5.1)$$

where θ_w is the wavefront angle, θ_r is the ray angle, δ is one of the anisotropy parameters previously defined and η is the far-offset anisotropy parameter.

The model for the isotropic and the anisotropic case show a large amplitude increase as a function of incidence angle. For the isotropic case, the amplitude at $50°$ is almost 5 times as large as the amplitude at zero offset, while the increase in amplitude is around 6 times for the anisotropic case. This increase is much larger than for the seismic gathers, thus the AVO effect on the gathers

appear to be small in comparison. A source of error for the large amplitude increase for the model, is that the input values (P-wave velocity, S-wave velocity and density) may not be very accurate (or even wrong) since these values are manually read off logs and not exported automatically. In this study, only three gathers around one well have been examined. Thus, more wells and more gathers could give a different result.

Chapter 6

Conclusions

The anisotropy parameters for the reservoir were found to be -0.081 $\pm$ 0.049 for ε and -0.003 for δ. The uncertainty of the δ-estimate was considered to be much higher than the uncertainty of the ε-estimate. Therefore an empirical relation ($\delta = 0.32\varepsilon$), was used in the AVO modeling study. This calculates δ to be -0.026.

The anisotropy parameters for the Draupne Fm. were found to be 0.106 for ε and 0.055 for δ. An average of the results from three filters was evaluated to be more correct than the values from the filters separately. Thus, no standard deviation has been found for the ε-estimate for the Draupne Fm.

The values found for the anisotropy parameters should not be considered definite. A large uncertainty (60 %) in the estimation of ε is present, even after filtering. The uncertainty in the estimation of δ is expected to be large as well, due to lack of deviated wells in the study. To be able to estimate this parameter with less uncertainty, more wells with inclination angles between $27 - 40\,^\circ$ are required. If these parameters were to be applied in other studies, caution must be taken and awareness of the sources of errors and the assumptions that are the basis for the equations are important.

When applying the anisotropy parameters in the AVO analysis, a difference between the isotropic and the anisotropic case could be observed at large angles. A difference of 33 % at $50\,^\circ$ is evident. This indicates that the anisotropy is an important factor in the AVO analysis.

When including the amplitude values from seismic gathers in the analysis, no conclusive statements could be established. It is difficult to conclude that the amplitudes from the gathers are closest to the isotropic or the anisotropic case. By looking at the slope qualitatively, the amplitude from the gathers may be closer to the isotropic case, but this may be due to the fact that the amplitudes were scaled to the isotropic case. A scaling to the anisotropic case might have given a different result. In addition, only three gathers around one well were studied, thus no definite conclusion for the anisotropy in real seismic gathers can be established.

Chapter 7

Further work

For further work, filtering for fluids in the reservoir could be done to see if the estimation of the anisotropy parameters would change much. For the AVO analysis, more seismic gathers could be included to get a better representation of the variation of the amplitudes with incidence angle. The AVO analysis could also be done for other wells showing an AVO effect. It would be interesting to see if the difference in amplitude between the isotropic and the anisotropic case would remain the same or if it would decrease or increase considerably when considering other wells. The amplitude values from the seismic gathers could also be scaled with the anisotropic case to see if this would change the result.

Bibliography

P. Avseth, T. Mukerji, and G. Mavko. *Quantitative Seismic Interpretation.* Cambridge University Press, 2005.

P. A. Berge. Pore compressibility in rocks. *Biot Conference on Poromechanics*, September, 1998.

L. Bolle. Troll field: Norway's giant offshore gas field. *M 54: Giant Oil and Gas Fields of the Decade 1978-1988*, 28, 1992.

T. Dreyer, M. Whitaker, J. Dexter, H. Flesche, and E. Larsen. From spit system to tide-dominated delta: integrated reservoir model of the upper jurassic sognefjord formation on the troll west field. *Petroleum Geology Conference*, 6, 2005.

K. Gibbons, T. Hellem, A. Kjemperud, S. D. Nio, and K. Vebenstad. Sequence architecture, facies development and carbonate-cemented horizons in the troll field reservoir, offshore norway. *Geological Society, London, Special Publications*, 69, 1993.

H. Haktorson. Seismic interpretation of an alternative top 4-series on the troll field. 2011.

F. J. Hilterman. Seismic amplitude interpretation. 2001.

B. E. Hornby, J. M. Howie, and D. W. Ince. Anisotropy correction for deviated-well sonic logs: Application to seismic well tie. *Geophysics*, 68, 2002.

S. Leiknes and I. Osvoll. Success factors in troll geosteering. *Offshore Technology Conference*, 17110, 2005.

Y. Li. An empirical method for estimation of anisotropic parameters in clastic rocks. *The Leading Edge*, June, 2006.

Y. Li and S. Pickford. Anisotropic well logs and their applications in seismic analysis. *SEG Int'l Exposition and 72nd Annual Meeting*, 2002.

T. Madsen and M. Abtahi. Handling the oil zone on troll. *Offshore Technology Conference*, 17109, 2005.

G. Mavko, T. Mukerji, and J. Dvorkin. *The Rock Physics Handbook*. Cambridge University Press, 2009.

J. Kr. Mikkelsen, T. Norheim, and S. I. Sagatun. The troll story. *Offshore Technology Conference*, 17108, 2005.

M. A. Slawinski. Tutorial on seismic waves in linearly elastic, anisotropic and nonuniform continua. *CSEG Recorder*, January, 2002.

L. Thomsen. Weak elastic anisotropy. *Geophysics*, 51, 1986.

L. Thomsen. *Understanding Seismic Anisotropy in Exploration and Exploitation*. Society of Exploration Geophysicists and European Association of Geoscientists & Engineers, 2002.

R. Tøndel. Vp anisotropy from the troll field. *Internal Statoil report*, 2005.

J. Walsh, B Sinha, and A. Donald. Formation anisotropy parameters using borehole sonic data. *SPWLA 74th Annual Logging Symposium*, June, 2006.

J. Walsh, B. Sinha, T. Plona, D. Miller, D. Bentley, and M. Ammerman. Derivation of anisotropy parameters in a shale using borehole sonic data. *SEG San Antonio Annual Meeting*, pages 323–327, 2007.

Appendix A

Matlab scripts

A.1 Anisotropy parameters

The following script shows an example of the estimation of the anisotropy parameters for the reservoir. In this example, a filter including depth 1600-1800 m MD, porosity 20-30 % and AI 5-6 km/s $\cdot$ g/cm^3 has been applied. For estimation of the anisotropy parameters for the cap rocks (except the Draupne Fm.), the scripts are similar, only the filtering is excluded and the input logs have been replaced. The scripts are the same for the other filters, only the numbers have been replaced. For the filters for The Draupne Fm., the input logs have been replaced too.

```matlab
clear all

sonicfiles={'sonic1.txt','sonic3.txt','sonic4R.txt',...
      'sonic4S.txt','sonic5.txt','sonic6.txt',...
      'sonic7.txt','sonic9.txt','sonic10.txt',...
      'sonic11.txt','sonic12.txt','sonic13S.txt',...
      'sonic14.txt','sonic15.txt','sonic17A.txt',...
      'sonic18.txt','sonic18A.txt','sonic31.txt',...
      'sonic32.txt','sonic33.txt','sonic52.txt',...
      'sonic53.txt','sonic55.txt','sonicB3H.txt',...
      'sonicD9.txt','sonicD10H.txt','sonicE6H.txt',...
      'sonicF6H.txt','sonicG4H.txt','sonicH5H.txt',...
      'sonicJ41.txt','sonicL41.txt','sonicM41.txt',...
      'sonicM42.txt','sonicS41.txt'};

incfiles={'inc1.txt','inc3.txt','inc4R.txt','inc4S.txt',...
      'inc5.txt','inc6.txt','inc7.txt','inc9.txt',...
```

```matlab
        'inc10.txt','inc11.txt','inc12.txt','inc13S.txt',...
        'inc14.txt','inc15.txt','inc17A.txt','inc18.txt',...
        'inc18A.txt','inc31.txt','inc32.txt','inc33.txt',...
        'inc52.txt','inc53.txt','inc55.txt','incB3H.txt',...
        'incD9.txt','incD10H.txt','incE6H.txt','incF6H.txt',...
        'incG4H.txt','incH5H.txt','incJ41.txt','incL41.txt',...
        'incM41.txt','incM42.txt','incS41.txt'};

porfiles={'phit1.txt','phit3.txt','phit4R.txt','phit4S.txt',...
        'phit5.txt','phit6.txt','phit7.txt','phit9.txt',...
        'phit10.txt','phit11.txt','phit12.txt','phit13S.txt',...
        'phit14.txt','phit15.txt','phit17A.txt','phit18.txt',...
        'phit18A.txt','philfp31.txt','phit32.txt','philfp33.txt',...
        'phit52.txt','phit53.txt','phit55.txt','phitB3H.txt',...
        'phitD9.txt','phitD10H.txt','phitE6H.txt','phitF6H.txt',...
        'phitG4H.txt','phieH5H.txt','phitJ41.txt','phitL41.txt',...
        'phitM41.txt','phitM42.txt','phitS41.txt'};

rhofiles={'rhob1.txt','rhob3.txt','rhob4R.txt','rhob4S.txt',...
        'rhob5.txt','rhob6.txt','rhob7.txt','rhob9.txt',...
        'rhob10.txt','rhob11.txt','rhob12.txt','rhob13S.txt',...
        'rhob14.txt','rhob15.txt','rhob17A.txt','rhob18.txt',...
        'rhob18A.txt','rhob31.txt','rhob32.txt','rhob33.txt',...
        'rhob52.txt','rhob53.txt','rhob55.txt','rhobB3H.txt',...
        'rhobD9.txt','rhobD10H.txt','rhobE6H.txt','rhobF6H.txt',...
        'rhobG4H.txt','rhobH5H.txt','rhobJ41.txt','rhobL41.txt',...
        'rhobM41.txt','rhobM42.txt','rhobS41.txt'};

symbol={'b*','g*','r*','c*','m*','y*','k*','b+','g+','r+',...
        'c+','m+','y+','k+','bx','gx','rx','cx','mx','yx',...
        'kx','bd','gd','rd','cd','md','yd','kd','bv','gv',...
        'rv','cv','mv','yv','kv'};

figure
hold on
velAll=zeros(1);
xAll=zeros(1);
for i=1:length(sonicfiles)
    data1=load(sonicfiles{i});
    dt=data1(:,2);
    % sonic log in column 2 in sonicfiles
    dtNan=find(dt==-999.25);
    dt(dtNan) = NaN;
    vel=(1./dt).*10^6.*0.3048./1000;
    % convert sonic to velocity in km/s

    data2=load(incfiles{i});
    inc=data2(:,2);
    % inclination log in column 2 in incfiles
```

```matlab
incNan=find(inc==-999.25);
inc(incNan) = NaN;
inc_rad=inc.*(pi/180);
% convert inclination in degrees to radians
x=(sin(inc_rad)).^2; % make a variable x

data3=load(porfiles{i});
por=data3(:,2);
% porosity log in column 2 in porfiles
porNan=find(por==-999.25);
por(porNan) = NaN;

data4=load(rhofiles{i});
rho=data4(:,2);
% density log in column 2 in rhofiles
rhoNan=find(rho==-999.25);
rho(rhoNan) = NaN;

z=data1(:,1);
% depth log in column 1 in sonicfiles
zNan=find(z==-999.25);
z(zNan) = NaN;

n=isnan(vel);
% check for NaN in velocity, no NaN in x, n=1 for NaN

AI=vel.*rho; % acoustic impedance

index=find(n==0 & z>=1600 & z<=1800 & por>=0.2000 & por<=0.3000...
& AI>=5 & AI<=6);
vel_new=vel(index);
x_new=x(index);

plot(x_new,vel_new,symbol{i})
title('Reservoir filtered; depth 1600-1800 m MD, por 20-30%, AI 5-6')
xlabel('Sin(inc)^2')
ylabel('Velocity, [km/s]')
legend('31/5-4 S','31/2-5','31/2-6','31/2-7','31/2-9',...
'31/2-10','31/2-13 S','31/2-14','31/2-17 A','31/2-18',...
'31/5-2','31/5-3','31/5-5','31/2-D-10 H','31/2-E-6 H',...
    '31/2-G-4 H','31/5-H-5 H','31/2-M-42')

velLen=length(vel_new);
if i == 1 % for the first iteration..
    start_vel = 1; % the start is 1
end
stop_vel = start_vel + velLen - 1;
% stop is length of velocity added to the start,
% but -1 since it starts at 1
```

```matlab
    velAll(start_vel:stop_vel) = vel_new;
    % puts the velocity values from the first file and adds the
    % velocity values from the next files after each iteration
    start_vel = stop_vel + 1;
    % sets a new start ready for the next iteration which is the
    % next index after the end of the previous file

    xLen = length(x_new);
    if i == 1
        start_x = 1;
    end
    stop_x = start_x + xLen - 1;
    xAll(start_x:stop_x) = x_new;
    start_x = stop_x + 1;
end

P = polyfit(xAll,velAll,2)
% fits the points to polynomial function 2nd order

x2=0:0.001:0.85;

y=2.6589e+000-(8.4910e-003.*x2)-(205.7347e-003.*x2.^2);
% function from polyfit

Mean_value=mean(velAll)

Standard_deviation=std(velAll)

Number_of_samples=length(xAll)

hold on
figure
plot(xAll,velAll,'r*',x2,y)
title('Reservoir filtered; depth 1600-1800 m MD, por 20-30%, AI 5-6')
xlabel('Sin(inc)^2')
ylabel('Velocity, [km/s]')

A=2.6589e+000;
B=-8.4910e-003;
C=-205.7347e-003;
% coefficients from polyfit, A+Bx+Cx^2=0,
% Polyfit gives the coefficients in descending order,
% so C, B, A

alfa=A;
delta=B./alfa
epsilon=(C./alfa) + delta
% calculations of delta and epsilon
```

A.2   AVO

The following script is showing the coding for generating amplitude (reflection coefficient) versus incidence angle (AVA) plot for the isotropic case, the anisotropic case, the solution from the exact Zoeppritz's equations and the real seismic gathers.

```matlab
% 10 meters above and below top reservoir,
% suffix 1 is above and suffix 2 is below,
% isotropic
slowp1_iso=150;
slowp2_iso=150;
slows1_iso=350;
slows2_iso=230;
rhob1_iso=2.125;
rhob2_iso=1.875;

alpha1_iso=(1./slowp1_iso).*10.^6.*0.305;
alpha2_iso=(1./slowp2_iso).*10.^6.*0.305;
beta1_iso=(1./slows1_iso).*10.^6.*0.305;
beta2_iso=(1./slows2_iso).*10.^6.*0.305;
rho1_iso=rhob1_iso.*1000;
rho2_iso=rhob2_iso.*1000;

Dalpha_iso=alpha2_iso−alpha1_iso;
alpha_iso=0.5.*(alpha1_iso+alpha2_iso);
Dbeta_iso=beta2_iso−beta1_iso;
beta_iso=0.5.*(beta1_iso+beta2_iso);
Drho_iso=rho2_iso−rho1_iso;
rho_iso=0.5.*(rho1_iso+rho2_iso);

an=0:1:90;
anr=an.*(pi./180);

term1_iso=(1./2).*(Dalpha_iso./alpha_iso+Drho_iso./rho_iso);

m_iso=((Drho_iso./rho_iso)+(2.*Dbeta_iso./beta_iso));

term2_iso=((1./2).*(Dalpha_iso./alpha_iso)...
 − 2.*((beta_iso./alpha_iso).^2).*m_iso).*(sin(anr)).^2;

term3_iso=(1./2).*(Dalpha_iso./alpha_iso).*(sin(anr)).^2.*(tan(anr)).^2;

R_iso=term1_iso+term2_iso+term3_iso;

% 10 meters above and below top reservoir,
% suffix 1 is above and suffix 2 is below,
```

```matlab
% anisotropic
slowp1_ani=150;
slowp2_ani=150;
slows1_ani=350;
slows2_ani=230;
rhob1_ani=2.125;
rhob2_ani=1.875;

alpha1_ani=(1./slowp1_ani).*10.^6.*0.305;
alpha2_ani=(1./slowp2_ani).*10.^6.*0.305;
beta1_ani=(1./slows1_ani).*10.^6.*0.305;
beta2_ani=(1./slows2_ani).*10.^6.*0.305;
rho1_ani=rhob1_ani.*1000;
rho2_ani=rhob2_ani.*1000;

Dalpha_ani=alpha2_ani-alpha1_ani;
alpha_ani=0.5.*(alpha1_ani+alpha2_ani);
Dbeta_ani=beta2_ani-beta1_ani;
beta_ani=0.5.*(beta1_ani+beta2_ani);
Drho_ani=rho2_ani-rho1_ani;
rho_ani=0.5.*(rho1_ani+rho2_ani);

delta1=0.055; % for Draupne
delta2=-0.026; % for the reservoir, Sognefjord, delta=0.32*epsilon
Ddelta=delta2-delta1;
epsilon1=0.106; % for Draupne
epsilon2=-0.081; % for the reservoir, Sognefjord
Depsilon=epsilon2-epsilon1;

an=0:1:90;
anr=an.*(pi./180);

term1_ani=(1./2).*(Dalpha_ani./alpha_ani+Drho_ani./rho_ani);

m_ani=((Drho_ani./rho_ani)+(2.*Dbeta_ani./beta_ani));

term2_ani=((1./2).*(Dalpha_ani./alpha_ani)...
 - 2.*((beta_ani./alpha_ani).^2).*m_ani...
    + (1./2).*Ddelta).*(sin(anr)).^2;

term3_ani=(1./2).*((Dalpha_ani./alpha_ani)...
 + Depsilon).*(sin(anr)).^2.*(tan(anr)).^2;

R_ani=term1_ani+term2_ani+term3_ani;

A=[0.0625...
0.0626006...
0.0629023...
0.0634050...
```

```
0.0641081...
0.0650112...
0.0661136...
0.0674144...
0.0689126...
0.0706071...
0.0724966...
0.0745797...
0.0768547...
0.0793199...
0.0819734...
0.0848133...
0.0878373...
0.0910433...
0.0944286...
0.0979910...
0.1017275...
0.1056356...
0.1097121...
0.1139542...
0.1183587...
0.1229223...
0.1276416...
0.1325133...
0.1375338...
0.1426995...
0.1480066...
0.1534514...
0.1590299...
0.1647383...
0.1705725...
0.1765285...
0.1826021...
0.1887893...
0.1950858...
0.2014875...
0.2079900...
0.2145892...
0.2212808...
0.2280607...
0.2349245...
0.2418682...
0.2488876...
0.2559786...
0.2631374...
0.2703601...
0.2776430...
];
```

```
inci_angle=[0.0...
1.0...
2.0...
3.0...
4.0...
5.0...
6.0...
7.0...
8.0...
9.0...
10.0...
11.0...
12.0...
13.0...
14.0...
15.0...
16.0...
17.0...
18.0...
19.0...
20.0...
21.0...
22.0...
23.0...
24.0...
25.0...
26.0...
27.0...
28.0...
29.0...
30.0...
31.0...
32.0...
33.0...
34.0...
35.0...
36.0...
37.0...
38.0...
39.0...
40.0...
41.0...
42.0...
43.0...
44.0...
45.0...
46.0...
47.0...
48.0...
```

```
49.0...
50.0...
];

Amplitude_gather_1=[−0.074324923...   % inline 1032, crossline 1520
−0.07519035...
−0.088400841...
−0.089266268...
−0.084888225...
−0.08750996...
−0.094560646...
−0.120930722...
−0.119174413...
−0.148217131...
−0.155242364...
−0.165805666...
−0.169318282...
−0.165805666...
−0.157889553...
−0.135897521...
−0.130603143...
−0.13500664...
−0.127090527...
−0.134141213...
−0.137653829...
−0.148217131...
−0.169318282...
−0.186906817...
−0.189554006...
−0.192175741...
−0.200982736...
−0.199226428...
−0.19747012...
−0.198335547...
−0.203604471...
−0.214167773...
−0.225596503...
−0.21768039...
−0.222083887...
−0.23...
];

Amplitude_gather_2=[−0.114812168...   % inline 1032, crossline 1521
−0.125354226...
−0.138338097...
−0.144818293...
−0.141578195...
−0.151321968...
−0.1569804...
```

```
−0.170786035...
−0.169964271...
−0.175646182...
−0.177266231...
−0.182149857...
−0.174847897...
−0.168344222...
−0.16428236...
−0.155360351...
−0.146438342...
−0.141578195...
−0.143198244...
−0.141578195...
−0.144020008...
−0.156182115...
−0.159422213...
−0.167545937...
−0.174026133...
−0.18618824...
−0.179708044...
−0.175646182...
−0.167545937...
−0.174847897...
−0.187808289...
−0.194311964...
−0.199172111...
−0.209714169...
−0.224318089...
−0.23...
];

Amplitude_gather_3=[−0.156770553... % inline 1032, crossline 1522
−0.16910644...
−0.182275834...
−0.194611721...
−0.194611721...
−0.210257817...
−0.21930731...
−0.224236902...
−0.220117001...
−0.220950507...
−0.217664113...
−0.20861462...
−0.202018016...
−0.188848623...
−0.178155933...
−0.155937047...
−0.15841375...
−0.150173949...
```

```
−0.152650652...
−0.155127356...
−0.162533651...
−0.169939946...
−0.174036032...
−0.182275834...
−0.183919031...
−0.192158832...
−0.183919031...
−0.184752537...
−0.180632636...
−0.175703044...
−0.183109339...
−0.193802029...
−0.206137917...
−0.212710706...
−0.228356803...
−0.23...
];

angle_gather=[5.00...
6.00...
7.00...
8.00...
9.00...
10.00...
11.00...
12.00...
13.00...
14.00...
15.00...
16.00...
17.00...
18.00...
19.00...
20.00...
21.00...
22.00...
23.00...
24.00...
25.00...
26.00...
27.00...
28.00...
29.00...
30.00...
31.00...
32.00...
33.00...
```

```matlab
34.00...
35.00...
36.00...
37.00...
38.00...
39.00...
40.00...
];

figure
plot(an,R_iso,'c',an,R_ani,'m',inci_angle,-A,'b*',...
angle_gather,Amplitude_gather_1,'g*',...
angle_gather,Amplitude_gather_2,'r*',...
angle_gather,Amplitude_gather_3,'y*','LineWidth',2)
axis ([0 50 -0.50 0.00])
title('Reflection coefficient versus incidence angle');
legend('Isotropic','Anisotropic','Zoeppritz (isotropic)',...
'Gather 1','Gather 2','Gather 3')
xlabel('Incidence angle');
ylabel('Reflection coefficient');
```

Appendix B

From offset to incidence angle

The following equations show the derivation of how to convert from offset to incidence angle. Equation B.1 shows the relationship between the incidence angle and the offset.

$$\tan \theta = \frac{x}{2z}, \tag{B.1}$$

where θ is the incidence angle, x is the offset and z is the depth from the mean sea level (MSL) to the reservoir.

Equation B.2 shows the relationship between the distance, the velocity and the time.

$$z = \frac{V t_0}{2}, \tag{B.2}$$

where z is the distance (in this case depth), V is the average velocity and t_0 is the TWT at zero offset (normal incidence).

Inserting Equation B.2 into Equation B.1 gives Equation B.3.

$$\tan \theta = \frac{x}{V t_0}, \tag{B.3}$$

This equation can be applied when a constant velocity from the MSL to the reservoir is assumed. This formula was applied when calculating the maximum incidence angle.

Appendix C

ε and δ values for all the filters

C.1 The results for the reservoir

The table in the next seven pages shows the anisotropy parameters for the different filters for the reservoir. POR is porosity in %, AI is acoustic impedance in $km/s \cdot g/cm^3$ and depth is in MD.

Filter	ε	δ
POR 15-20%	-0.095	0.151
POR 20-25%	0.052	-0.009
POR 25-30%	-0.013	0.017
POR 30-35%	-0.017	0.033
POR 35-40%	0.292	-0.515
AI 4-6	0.031	-0.029
AI 4-7	0.012	0.025
AI 4-5	-0.089	0.005
AI 5-6	-0.015	0.013
AI 6-7	0.037	-0.073
AI 7-8	-0.030	0.003
AI 5-7	-0.013	-0.003
AI 5-8	-0.025	0.02
AI 6-8	0.017	-0.041
POR 15-20% & AI 5-7	-0.062	0.099
POR 15-20% & AI 5-8	-0.069	0.107
POR 15-20% & AI 4-6	0.068	-0.257
POR 20-25% & AI 4-6	-0.252	0.506
POR 20-25% & AI 5-7	0.075	-0.001
POR 20-25% & AI 6-8	0.07	-0.135
POR 20-25% & AI 5-8	0.084	-0.058
POR 25-30% & AI 5-8	0.023	-0.02
POR 25-30% & AI 4-6	-0.056	0.108
POR 25-30% & AI 5-7	0.023	-0.039
POR 25-30% & AI 6-8	-0.001	0.008
POR 30-35% & AI 4-6	0.054	-0.069
POR 30-35% & AI 6-8	-0.062	0.12
POR 30-35% & AI 5-7	-0.035	-0.171
POR 35-40% & AI 4-6	0.149	-0.275
POR 35-40% & AI 6-8	0.008	-0.157
POR 35-40% & AI 5-7	0.026	-0.295
POR 20-21%	0.012	0.015
POR 21-22%	0.036	-0.022
POR 22-23%	0.039	0.008
POR 23-24%	0.062	-0.041
POR 24-25%	0.075	-0.102
POR 25-26%	-0.027	0.000
POR 26-27%	0.008	-0.057
POR 27-28%	0.064	-0.102
POR 28-29%	-0.025	0.174
POR 29-30%	-0.116	0.087

Filter	ε	δ
POR 30-31%	-0.172	0.190
POR 31-32%	-0.011	0.027
POR 32-33%	0.008	-0.137
POR 33-34%	0.000	0.176
POR 34-35%	0.092	-0.094
POR 35-36%	0.221	-0.592
POR 36-37%	0.268	-0.359
POR 37-38%	0.329	-0.654
POR 38-39%	0.466	-0.985
POR 39-40%	0.493	-1.384
POR 20-21% & AI 4-6	-0.424	1.072
POR 20-21% & AI 5-8	0.061	0.018
POR 20-21% & AI 5-7	0.026	0.171
POR 20-21% & AI 6-8	0.046	-0.087
POR 21-22% & AI 5-8	0.05	0.028
POR 21-22% & AI 5-7	0.068	0.074
POR 21-22% & AI 4-6	0.515	-1.400
POR 22-23% & AI 5-8	0.062	-0.080
POR 22-23% & AI 5-7	0.051	0.002
POR 22-23% & AI 4-6	-0.082	0.114
POR 23-24% & AI 4-6	-0.236	0.405
POR 23-24% & AI 5-8	0.096	-0.098
POR 23-24% & AI 5-7	0.093	-0.082
POR 23-24% & AI 4-7	0.056	-0.004
POR 23-24% & AI 6-8	0.086	-0.169
POR 24-25% & AI 5-8	0.127	-0.134
POR 24-25% & AI 4-6	-0.359	0.701
POR 24-25% & AI 5-7	0.098	-0.071
POR 24-25% & AI 5-6	-0.073	0.334
POR 25-26% & AI 5-8	0.059	-0.067
POR 25-26% & AI 4-6	-0.229	0.448
POR 25-26% & AI 5-6	-0.006	0.216
POR 25-26% & AI 6-7	0.028	-0.034
POR 25-26% & AI 5-7	0.052	-0.068
POR 26-27% & AI 5-6	-0.010	0.148
POR 26-27% & AI 4-6	-0.170	0.255
POR 26-27% & AI 5-7	-0.030	0.038
POR 26-27% & AI 6-8	0.014	-0.024
POR 27-28% & AI 5-6	0.035	0.062
POR 27-28% & AI 6-7	-0.001	-0.040
POR 27-28% & AI 6-8	-0.033	0.022

Filter	ε	δ
POR 27-28% & AI 7-8	-0.016	-0.106
POR 27-28% & AI 4-6	0.120	-0.183
POR 28-29% & AI 5-6	0.000	0.024
POR 28-29% & AI 5-7	0.044	-0.142
POR 28-29% & AI 4-6	-0.005	0.033
POR 28-29% & AI 4-7	0.058	-0.131
POR 28-29% & AI 6-8	0.072	-0.074
POR 29-30% & AI 5-6	-0.040	0.019
POR 29-30% & AI 5-7	-0.032	-0.115
POR 29-30% & AI 6-7	-0.037	0.017
POR 29-30% & AI 6-8	-0.143	0.315
POR 29-30% & AI 7-8	-0.350	0.277
POR 29-30% & AI 5-8	-0.074	0.006
POR 30-31% & AI 5-7	-0.050	-0.156
POR 30-31% & AI 4-7	-0.040	0.021
POR 30-31% & AI 5-8	-0.075	-0.144
POR 30-31% & AI 6-8	-0.358	0.487
POR 31-32% & AI 5-7	-0.030	-0.099
POR 31-32% & AI 5-8	-0.047	-0.090
POR 31-32% & AI 6-8	-0.069	0.128
POR 31-32% & AI 4-7	0.057	-0.208
POR 32-33% & AI 5-7	-0.032	-0.213
POR 32-33% & AI 5-8	-0.038	-0.167
POR 32-33% & AI 6-8	-0.123	0.630
POR 32-33% & AI 4-7	0.062	-0.295
POR 32-33% & AI 6-7	0.005	0.016
POR 32-33% & AI 4-6	0.029	-0.102
POR 33-34% & AI 5-7	-0.018	-0.222
POR 33-34% & AI 5-8	-0.027	-0.218
POR 33-34% & AI 6-8	0.05	-0.067
POR 33-34% & AI 4-6	0.086	-0.133
POR 34-35% & AI 5-7	-0.034	-0.179
POR 34-35% & AI 5-8	-0.055	-0.146
POR 34-35% & AI 6-8	-0.397	0.834
POR 34-35% & AI 4-7	0.062	-0.140
POR 34-35% & AI 4-6	0.027	-0.030
POR 35-36% & AI 4-6	0.132	-0.258
POR 35-36% & AI 5-7	0.01	-0.253
POR 35-36% & AI 5-8	0.043	-0.31
POR 35-36% & AI 5-6	-0.053	-0.059
POR 36-37% & AI 5-8	0.013	-0.321

Filter	ε	δ
POR 36-37% & AI 5-7	0.047	-0.376
POR 36-37% & AI 4-6	0.177	-0.278
POR 36-37% & AI 5-6	-0.010	-0.210
POR 36-37% & AI 6-8	-0.135	0.107
POR 36-37% & AI 6-7	-0.051	-0.046
POR 37-38% & AI 5-7	0.135	-0.567
POR 37-38% & AI 4-6	0.119	-0.301
POR 37-38% & AI 6-8	0.083	-0.387
POR 37-38% & AI 5-6	-0.055	-0.119
POR 37-38% & AI 5-8	0.175	-0.714
POR 37-38% & AI 4-5	-0.021	-0.145
POR 38-39% & AI 5-7	0.413	-1.600
POR 38-39% & AI 4-6	0.292	-0.639
POR 38-39% & AI 5-6	0.413	-1.600
POR 38-39% & AI 4-7	0.292	-0.639
POR 39-40% & AI 5-7	5.043	-19.638
POR 39-40% & AI 4-6	0.318	-1.026
POR 39-40% & AI 5-6	-1.241	4.425
DEPTH 1530-1570	32.150	-1.267
DEPTH 1600-1650	-1.247	0.997
DEPTH 1650-1700	-0.629	0.257
DEPTH 1700-1750	-0.082	-0.394
DEPTH 1750-1800	-0.258	-0.148
DEPTH 1800-1850	-0.376	-0.070
DEPTH 1850-1900	-0.266	-0.263
DEPTH 1900-1950	-0.191	-0.481
DEPTH 1950-2000	2.456	7.271
DEPTH 1650-1700 & POR 25-26%	-14.815	24.221
DEPTH 1650-1700 & POR 29-30%	-0.585	-0.075
DEPTH 1650-1700 & AI 5-6	-0.257	0.149
DEPTH 1650-1700 & POR 29-30% & AI 5-6	19267	-36477
DEPTH 1700-1750 & POR 26-27%	0.162	-0.471
DEPTH 1700-1750 & POR 32-33%	-0.130	-0.456
DEPTH 1600-1650 & POR 24-25%	-0.617	0.066
DEPTH 1600-1650 & POR 27-28%	-1.069	0.447
DEPTH 1600-1650 & AI 5-6	-0.378	0.290
DEPTH 1600-1650 & AI 5-7	-0.395	0.215
DEPTH 1600-1650 & AI 6-8	-0.351	0.256
DEPTH 1800-1850 & AI 5-7	-0.153	-0.089
DEPTH 1800-1850 & POR 24-25%	-0.062	-0.229
DEPTH 1650-1700 & POR 20-25%	-0.482	0.300

Filter	ε	δ
DEPTH 1650-1700 & POR 25-30%	-0.418	-0.091
DEPTH 1750-1850	-0.321	-0.064
DEPTH 1750-1850 & POR 23-27%	-0.242	-0.087
DEPTH 1750-1850 & POR 23-27% & AI 4-6	-0.561	-1.978
DEPTH 1750-1850 & POR 23-27% & AI 5-8	0.117	-0.474
DEPTH 1600-1800	-0.271	-0.089
DEPTH 1600-1800 & POR 20-30%	-0.232	-0.006
DEPTH 1600-1800 & AI 5-7	-0.025	-0.220
DEPTH 1600-1800 & POR 20-30% & AI 5-7	-0.024	-0.137
DEPTH 1600-1800 & POR 20-30% & AI 5-6	-0.081	-0.003
DEPTH 1600-1800 & POR 20-25%	-0.189	-0.043
DEPTH 1600-1800 & POR 25-30%	-0.262	0.039
DEPTH 1600-1800 & POR 20-25% & AI 5-6	-0.113	-0.137
DEPTH 1600-1800 & POR 25-30% & AI 5-6	-0.076	-0.016
DEPTH 1600-1620 & POR 20-30% & AI 5-6	-9409	36
DEPTH 1620-1640 & POR 20-30% & AI 5-6	-268156	301
DEPTH 1640-1660 & POR 20-30% & AI 5-6	0.700	-1.553
DEPTH 1660-1680 & POR 20-30% & AI 5-6	1.118	-2.058
DEPTH 1680-1700 & POR 20-30% & AI 5-6	49293	-50.381
DEPTH 1700-1720 & POR 20-30% & AI 5-6	0.234	0.000
DEPTH 1720-1740 & POR 20-30% & AI 5-6	-2.264	-11.210
DEPTH 1740-1760 & POR 20-30% & AI 5-6	-2.440	-14.562
DEPTH 1760-1780 & POR 20-30% & AI 5-6	0.287	1.842
DEPTH 1780-1800 & POR 20-30% & AI 5-6	0.603	5.446
DEPTH 1600-1650 & POR 20-30% & AI 5-7	-0.470	0.245
DEPTH 1650-1700 & POR 20-30% & AI 5-7	-0.413	0.110
DEPTH 1700-1750 & POR 20-30% & AI 5-7	-0.079	-0.115
DEPTH 1750-1800 & POR 20-30% & AI 5-7	0.029	-0.382
DEPTH 1700-1750 & POR 20-30% & AI 5-6	-5.093	-25.889
DEPTH 1600-1700 & POR 20-30% & AI 5-7	-0.449	0.198
DEPTH 1700-1800 & POR 20-30% & AI 5-7	0.017	-0.314
DEPTH 1600-1800 & POR 20-22% & AI 5-7	0.113	-0.186
DEPTH 1600-1800 & POR 22-24% & AI 5-7	0.034	-0.184
DEPTH 1600-1800 & POR 24-26% & AI 5-7	-0.001	-0.195
DEPTH 1600-1800 & POR 26-28% & AI 5-7	-0.108	0.131
DEPTH 1600-1800 & POR 28-30% & AI 5-7	-0.023	-0.257
DEPTH 1600-1800 & POR 30-32% & AI 5-7	0.113	-0.544
DEPTH 1600-1800 & POR 32-34% & AI 5-7	0.104	-0.528
DEPTH 1600-1800 & POR 34-36% & AI 5-7	0.011	-0.289
DEPTH 1600-1800 & POR 36-38% & AI 5-7	0.234	-0.745
DEPTH 1600-1800 & POR 38-40% & AI 5-7	0.000	0.000

Filter	ε	δ
DEPTH 1600-1800 & POR 26-27% & AI 5-7	-0.091	0.084
DEPTH 1600-1800 & POR 27-28% & AI 5-7	-0.152	0.256
DEPTH 1600-1800 & POR 28-29% & AI 5-7	-0.123	-0.042
DEPTH 1600-1800 & POR 29-30% & AI 5-7	0.055	-0.417
DEPTH 1600-1800 & POR 20-21% & AI 5-7	0.043	-0.108
DEPTH 1600-1800 & POR 21-22% & AI 5-7	0.225	-0.340
DEPTH 1600-1800 & POR 22-23% & AI 5-7	-0.052	-0.081
DEPTH 1600-1800 & POR 23-24% & AI 5-7	0.097	-0.273
DEPTH 1600-1800 & POR 24-25% & AI 5-7	-0.018	-0.142
DEPTH 1600-1800 & POR 25-26% & AI 5-7	0.049	-0.303
DEPTH 1600-1800 & POR 20-22% & AI 5-6	NaN	NaN
DEPTH 1600-1800 & POR 22-24% & AI 5-6	-0.054	-0.427
DEPTH 1600-1800 & POR 24-26% & AI 5-6	-0.284	-1.081
DEPTH 1600-1800 & POR 26-28% & AI 5-6	-0.041	-0.058
DEPTH 1600-1800 & POR 28-30% & AI 5-6	-0.056	-0.053
DEPTH 1600-1800 & POR 20-25% & AI 5-7	0.025	-0.191
DEPTH 1600-1800 & POR 25-30% & AI 5-7	-0.054	-0.100
DEPTH 1600-1800 & POR 20-25% & AI 6-7	0.098	-0.179
DEPTH 1600-1800 & POR 25-30% & AI 6-7	-0.070	0.132
DEPTH 1600-1800 & POR 20-22% & AI 6-7	0.113	-0.186
DEPTH 1600-1800 & POR 22-24% & AI 6-7	0.105	-0.198
DEPTH 1600-1800 & POR 24-26% & AI 6-7	0.054	-0.075
DEPTH 1600-1800 & POR 26-28% & AI 6-7	-0.132	0.253
DEPTH 1600-1800 & POR 28-30% & AI 6-7	0.061	-0.233
DEPTH 1600-1800 & POR 20-22%	-0.199	0.047
DEPTH 1600-1800 & POR 22-24%	-0.156	0.022
DEPTH 1600-1800 & POR 24-26%	-0.263	0.002
DEPTH 1600-1800 & POR 26-28%	-0.362	0.105
DEPTH 1600-1800 & POR 28-30%	-0.197	-0.015
DEPTH 1600-1800 & AI 5-6	-0.053	-0.149
DEPTH 1600-1800 & AI 6-7	0.067	-0.141
DEPTH 1600-1800 & POR 20-30% & AI 6-7	0.030	-0.068
DEPTH 1600-1700	-0.843	0.537
DEPTH 1700-1800	-0.197	-0.218
DEPTH 1600-1620	-1.862	2.213
DEPTH 1620-1640	-0.760	0.180
DEPTH 1640-1660	-1.078	0.582
DEPTH 1660-1680	-0.739	0.356
DEPTH 1680-1700	-0.452	0.261
DEPTH 1700-1720	0.014	-0.426
DEPTH 1720-1740	-0.141	-0.246

Filter	ε	δ
DEPTH 1740-1760	-0.023	-0.673
DEPTH 1760-1780	-0.188	-0.080
DEPTH 1780-1800	-0.379	-0.021
DEPTH 1600-1800 & POR 20-21%	-0.336	0.161
DEPTH 1600-1800 & POR 21-22%	0.270	-0.564
DEPTH 1600-1800 & POR 22-23%	-0.261	0.125
DEPTH 1600-1800 & POR 23-24%	-0.073	-0.077
DEPTH 1600-1800 & POR 24-25%	-0.254	-0.041
DEPTH 1600-1800 & POR 25-26%	-0.279	0.063
DEPTH 1600-1800 & POR 26-27%	-0.389	0.204
DEPTH 1600-1800 & POR 27-28%	-0.303	-0.105
DEPTH 1600-1800 & POR 28-29%	-0.303	0.465
DEPTH 1600-1800 & POR 29-30%	-0.127	-0.322
DEPTH 1600-1700 & POR 20-30% & AI 5-6	0.831	-1.857
DEPTH 1700-1800 & POR 20-30% & AI 5-6	1.282	8.137
DEPTH 1600-1700 & POR 20-30% & AI 6-7	-0.282	0.140
DEPTH 1700-1800 & POR 20-30% & AI 6-7	0.081	-0.287
DEPTH 1600-1650 & POR 20-30% & AI 5-6	0.604	-1.460
DEPTH 1650-1700 & POR 20-30% & AI 5-6	0.959	-2.074
DEPTH 1750-1800 & POR 20-30% & AI 5-6	1.703	11.138
DEPTH 1600-1650 & POR 20-30% & AI 6-7	-0.307	0.188
DEPTH 1650-1700 & POR 20-30% & AI 6-7	3.127	-0.939
DEPTH 1700-1750 & POR 20-30% & AI 6-7	-0.191	0.282
DEPTH 1750-1800 & POR 20-30% & AI 6-7	0.136	-0.449

Table C.1: An overview of the anisotropy parameters, ε and δ, for the reservoir for all the filters.

C.2 The results for the Draupne Fm.

The table in the next two pages shows the anisotropy parameters for the different filters for the Draupne Fm.

Filter	ε	δ
DEPTH 1500-1700	-1.084	1.640
DEPTH 1500-1600	-39.742	65.711
DEPTH 1600-1700	-0.606	1.241
DEPTH 1450-1500	33274	-80.236
DEPTH 1500-1550	-149652	314
DEPTH 1550-1600	-54.843	89.399
DEPTH 1600-1650	4.495	-7.469
DEPTH 1650-1700	120.053	-101.229
DEPTH 1450-1750	0.045	0.123
DEPTH 1500-1750	0.020	-0.020
DEPTH 1550-1650	2.463	-4.244
AI 5-7	0.018	0.198
AI 5-6	-0.042	0.264
AI 5-8	0.086	0.019
AI 4-8	0.146	0.066
AI 6-8	0.010	0.015
AI 7-8	-0.092	0.068
AI 6-7	0.003	0.210
AI 4-5	-0.085	0.307
AI 4-6	-0.009	0.293
AI 4-7	0.061	0.231
DEPTH 1450-1750 & AI 5-7	0.044	0.120
DEPTH 1500-1700 & AI 5-7	-0.031	0.179
DEPTH 1550-1600 & AI 5-7	11.082	-18.599
DEPTH 1600-1650 & AI 5-7	5.997	-9.972
DEPTH 1650-1700 & AI 5-7	-21.843	18.720
DEPTH 1500-1600 & AI 5-7	-6.199	10.235
DEPTH 1600-1700 & AI 5-7	0.087	0.079
DEPTH 1500-1750 & AI 5-7	0.038	0.078
DEPTH 1550-1650 & AI 5-7	6.511	-10.843
DEPTH 1450-1750 & AI 5-6	-0.020	0.194
DEPTH 1500-1700 & AI 5-6	0.004	0.115
DEPTH 1600-1700 & AI 5-6	0.114	-0.063
DEPTH 1500-1750 & AI 5-6	-0.026	0.151
DEPTH 1450-1750 & AI 5-8	0.120	-0.083
DEPTH 1500-1700 & AI 5-8	0.021	-0.036
DEPTH 1600-1700 & AI 5-8	0.140	-0.006
DEPTH 1500-1750 & AI 5-8	0.109	-0.138
DEPTH 1450-1750 & AI 6-7	0.043	0.065
DEPTH 1500-1700 & AI 6-7	0.329	-0.338
DEPTH 1600-1700 & AI 6-7	0.392	-0.205

Filter	ε	δ
DEPTH 1500-1750 & AI 6-7	0.043	0.067
DEPTH 1450-1750 & AI 6-8	0.058	-0.163
DEPTH 1500-1700 & AI 6-8	0.374	-0.653
DEPTH 1600-1700 & AI 6-8	0.433	-0.483
DEPTH 1500-1750 & AI 6-8	0.053	-0.174
DEPTH 1450-1750 & AI 4-8	0.152	-0.019
DEPTH 1500-1700 & AI 4-8	-0.178	0.341
DEPTH 1600-1700 & AI 4-8	0.045	0.065
DEPTH 1500-1750 & AI 4-8	0.126	-0.130
DEPTH 1450-1750 & AI 4-6	0.001	0.211
DEPTH 1500-1700 & AI 4-6	-0.187	0.431
DEPTH 1600-1700 & AI 4-6	0.022	0.002
DEPTH 1500-1750 & AI 4-6	-0.014	0.129
DEPTH 1450-1750 & AI 4-7	0.063	0.167
DEPTH 1500-1700 & AI 4-7	-0.224	0.514
DEPTH 1600-1700 & AI 4-7	-0.007	0.149
DEPTH 1500-1750 & AI 4-7	0.047	0.075
DEPTH 1450-1750 & AI 4-5	0.103	-0.229
DEPTH 1500-1700 & AI 4-5	-0.066	0.007
DEPTH 1600-1700 & AI 4-5	-0.631	-3.227
DEPTH 1500-1750 & AI 4-5	0.089	-0.251

Table C.2: An overview of the anisotropy parameters, ε and δ, for the Draupne Fm. for all the filters.

Appendix D

Histograms

D.1 Histograms for the reservoir

Figure D.1 is a plot where the distribution of porosity values in the reservoir interval is shown. The plot shows that the porosity ranges from 0.00 to 0.44, with significantly more porosity values between 0.20 and 0.36, apart from the 0.00 porosity value. The range used when filtering on porosity is from 0.15 to 0.40, which is where most of the values lie.

Figure D.2 shows the distribution of acoustic impedance values in the reservoir interval. This figure shows that the acoustic impedance ranges from 2.5 to 18.5 $km/s \cdot g/cm^3$, with a break from 16.5 to 18.5 $km/s \cdot g/cm^3$. Most of the values lie between 4 and 8 $km/s \cdot g/cm^3$, so that is why this range has been used when filtering.

Figure D.3 is a plot showing the distribution of measured depth of the wells in the reservoir interval. This figure shows that the depth ranges from 1350 to 2100 meters MD. Most of the values lie between 1500 and 1700 meters, but a significant portion of the values also lie between 1750 and 1875 meters.

Figure D.4 shows the distribution of measured depth of the vertical wells in the reservoir interval. All the wells with inclination angles less than around 4° are taken into account in this plot. This plot shows that the depth ranges from 1350 to 1925 meters MD, but most of the values lie between 1525 and 1675 meters.

Figure D.5 shows the distribution of measured depth of the deviated wells in the reservoir interval. All the wells with inclination angle larger than around 40° are taken into account in this plot. This figure shows that the depth ranges from 1625 to 2100 meters MD. Most of the values lie between 1750 and 1900 meters. Comparing Figure D.4 and Figure D.5 shows that the deviated wells generally lie deeper in the reservoir than the vertical wells. This shows the importance of making these plots, because it is crucial to make sure that the depth filtering includes both vertical and horizontal wells. From Figure D.3, D.4 and D.5 it can be seen that 1600-1800 meters is a reasonable range for the depth filtering.
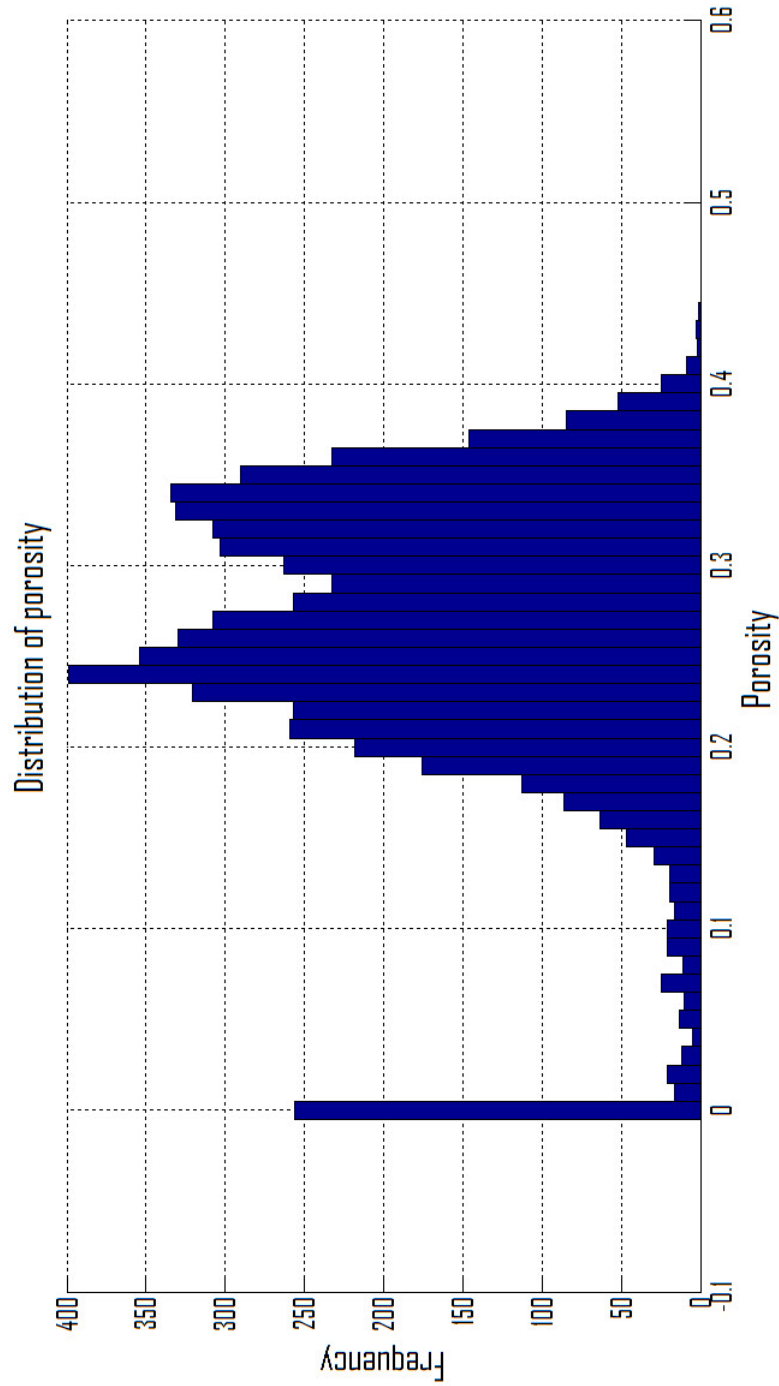
Figure D.1: A histogram showing the distribution of porosity values in the reservoir interval.
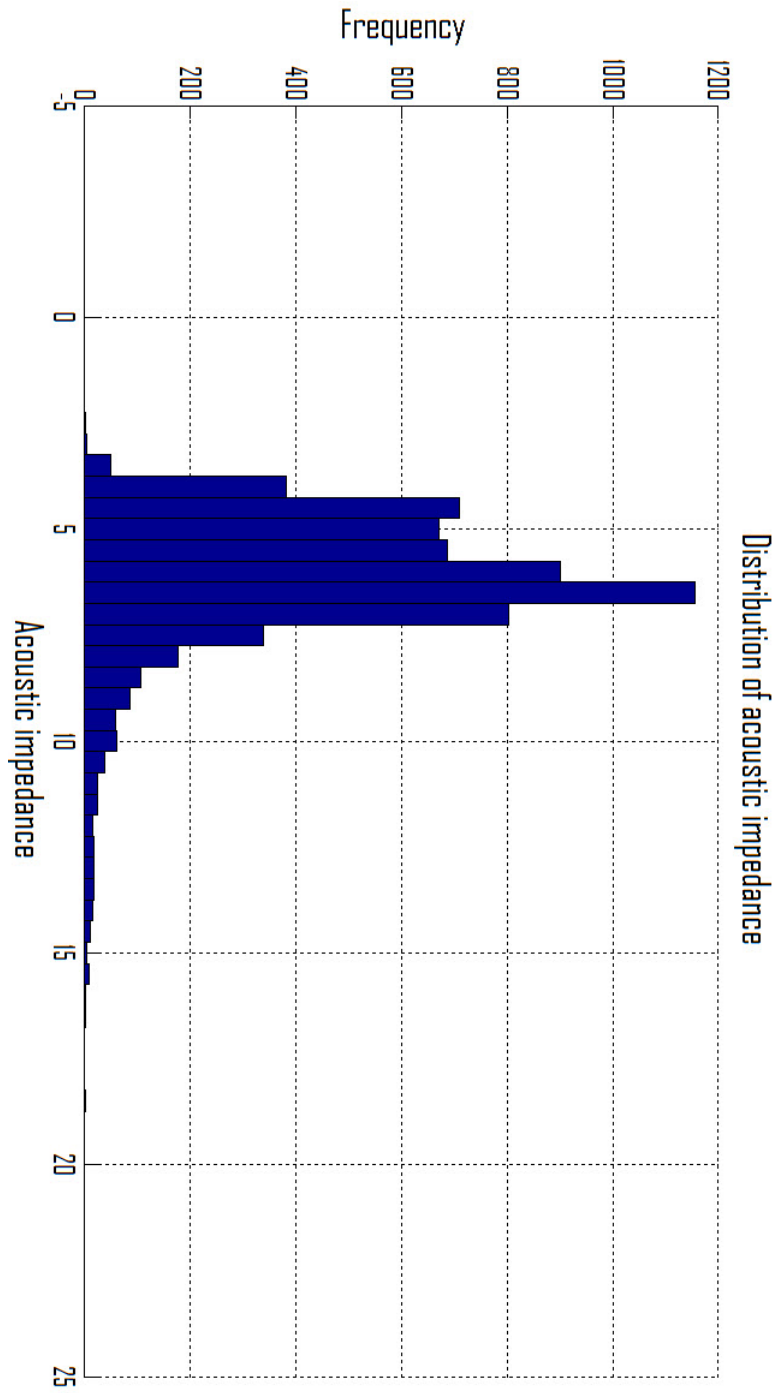
Figure D.2: A histogram showing the distribution of acoustic impedance values in the reservoir interval.
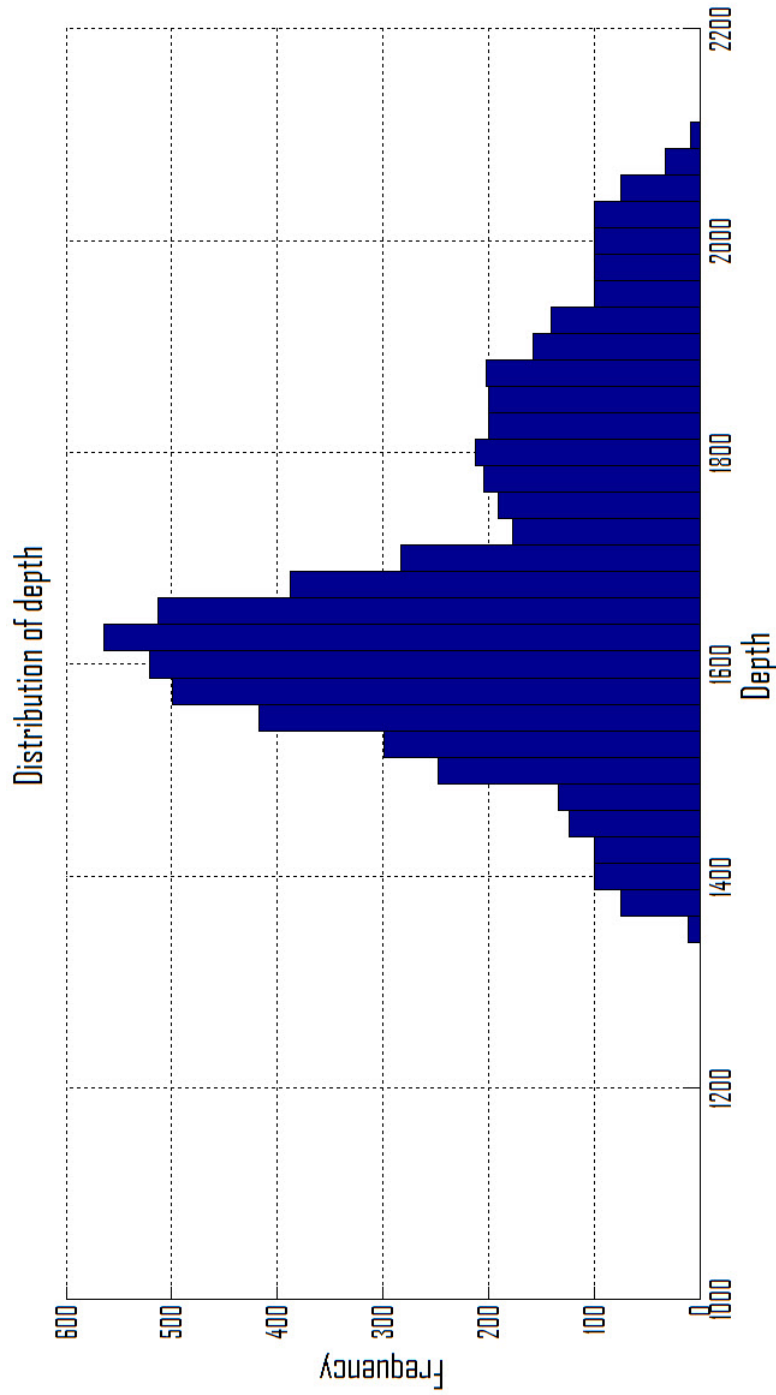
Figure D.3: A histogram showing the distribution of measured depth of the wells in the reservoir interval.
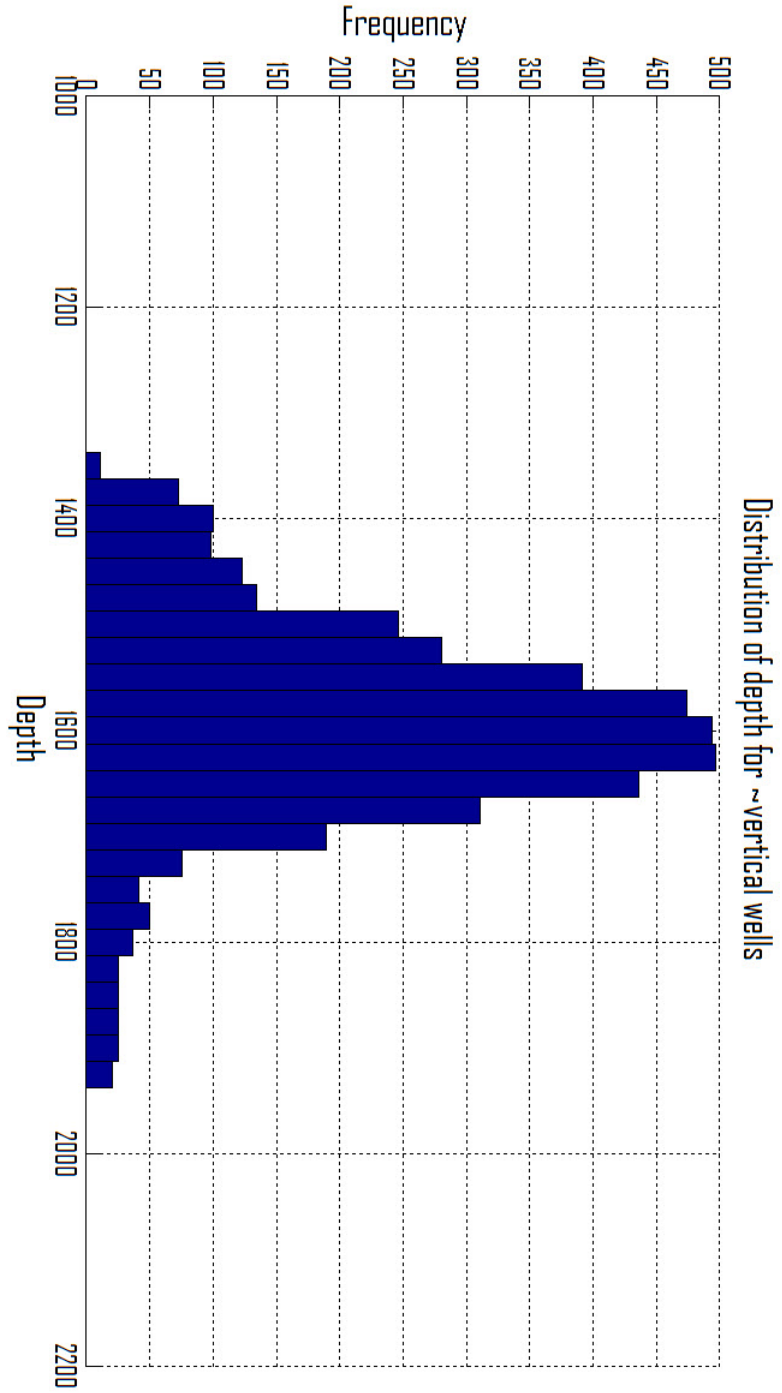
Figure D.4: A histogram showing the distribution of measured depth of the vertical wells in the reservoir interval.
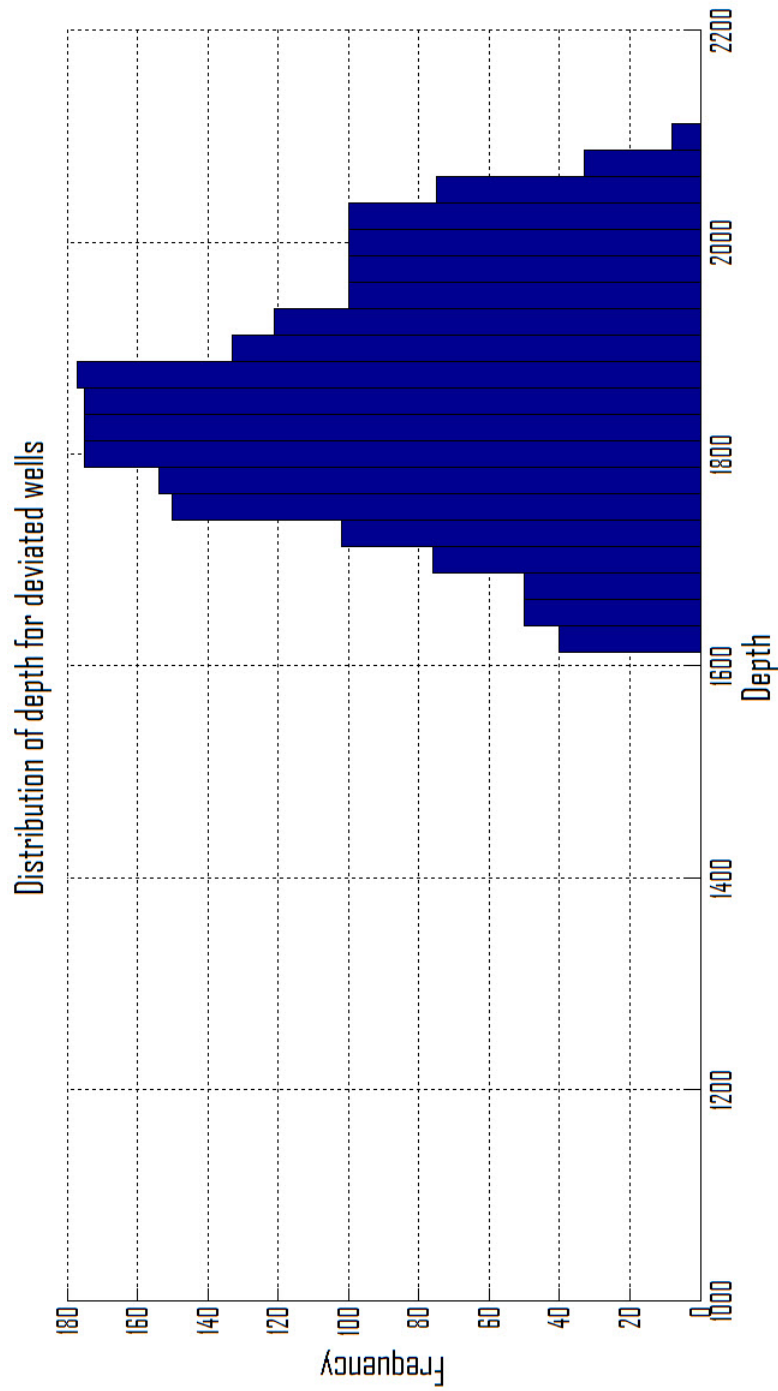
Figure D.5: A histogram showing the distribution of measured depth of the deviated wells in the reservoir interval.

D.2   Histograms for the Draupne Fm.

Figure D.6 shows the distribution of acoustic impedance values in the Draupne Fm. interval. This figure shows that the acoustic impedance for the Draupne Fm. ranges from 3 to 12 km/s $\cdot$ g/cm^3, with a break around 10 km/s $\cdot$ g/cm^3. Most of the values lie between 4.5 and 5.5 km/s $\cdot$ g/cm^3. Seen from this figure, an AI filtering with a range from 4 to 8 km/s $\cdot$ g/cm^3 is reasonable.

The distribution of measured depth of the wells in the Draupne Fm. interval is shown in Figure D.7. This figure shows that the depth ranges from 1425 to 1750 meters MD, with some values around 1850 and 1350 meters. Most of the values lie between 1450 and 1575 meters, but a significant portion of the values also lie between 1650 and 1750 meters.

Figure D.8 shows the distribution of measured depth of the vertical wells in the Draupne Fm. interval. All the wells with inclination angles less than around 4° are taken into account in this plot. The figure shows that the depth of the vertical wells ranges from 1425 to 1750 meters MD, with some values around 1350 meters. Most of the values lie between 1450 and 1575 meters.

The distribution of measured depth of the deviated wells in the Draupne Fm. interval is shown in Figure D.9. All the wells with inclination angle larger than around 40° are taken into account in this plot. Figure D.9 shows that the depth of the horizontal wells lie around 1600, 1700 and 1850 meters MD. Most of the values lie around 1600 meters. When comparing Figure D.8 and Figure D.9 for the Draupne Fm. this also shows that the deviated wells generally lie deeper than the vertical wells. To make sure the depth filtering includes both vertical and horizontal wells, Figure D.7, D.8 and D.9 are compared and concluded from this, a depth filtering with a range from 1450 to 1750 meters is a good choice.
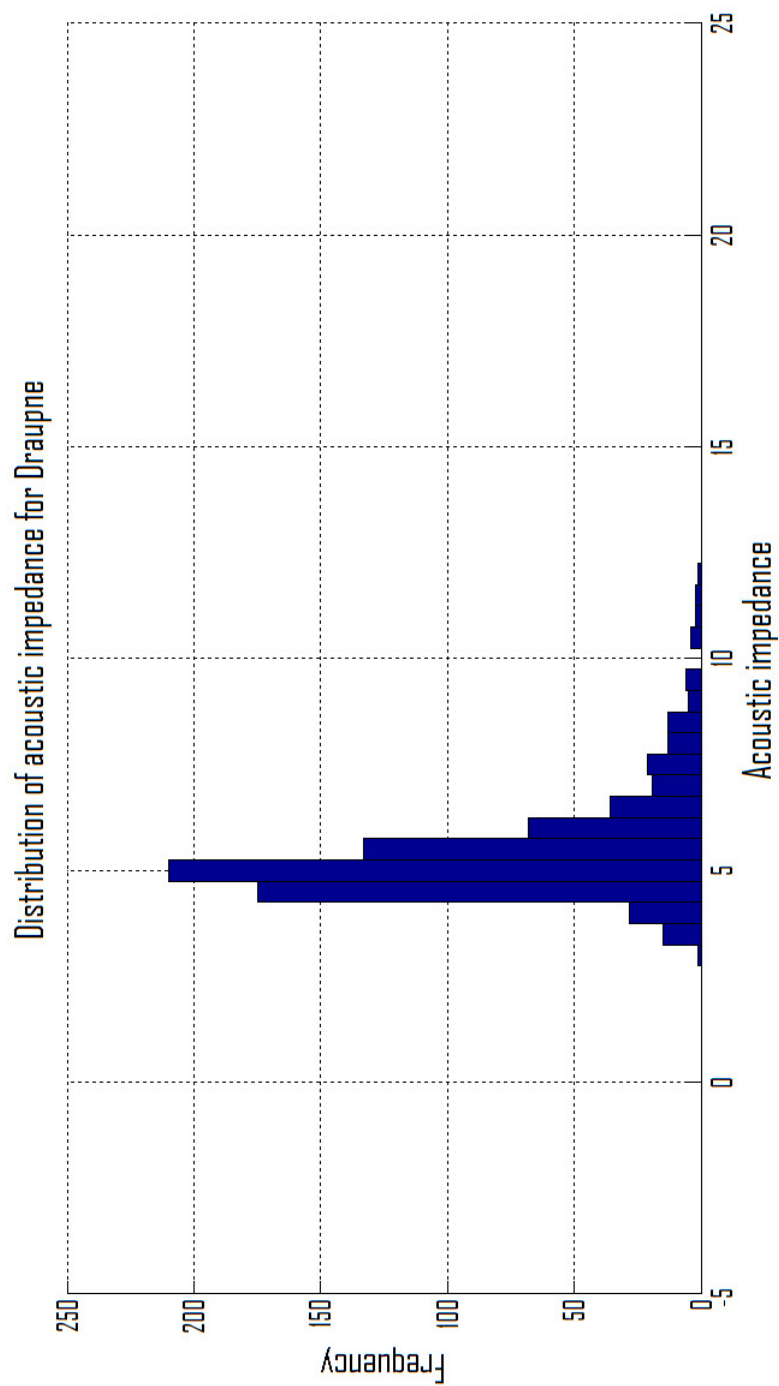
Figure D.6: A histogram showing the distribution of acoustic impedance values in the Draupne Fm. interval.
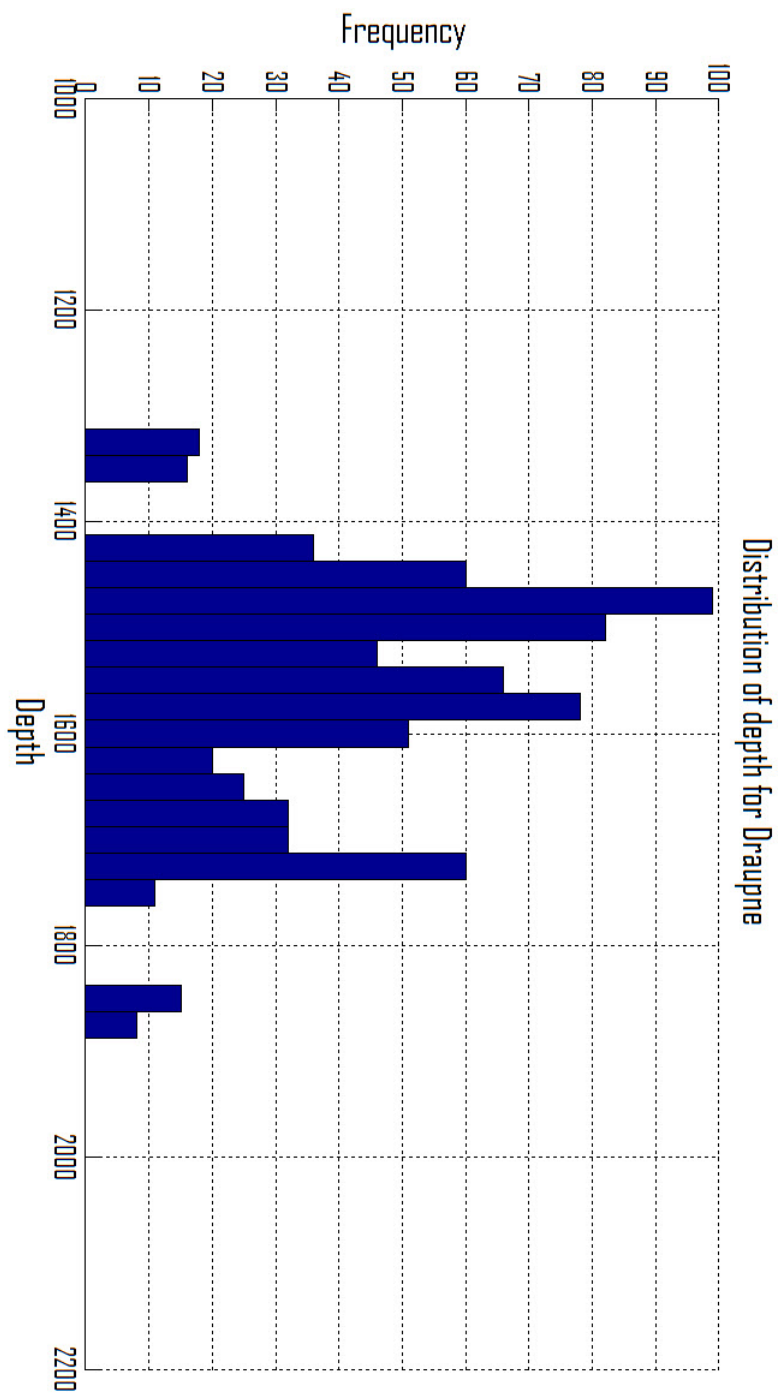
Figure D.7: A histogram showing the distribution of measured depth of the wells in the Draupne Fm. interval.
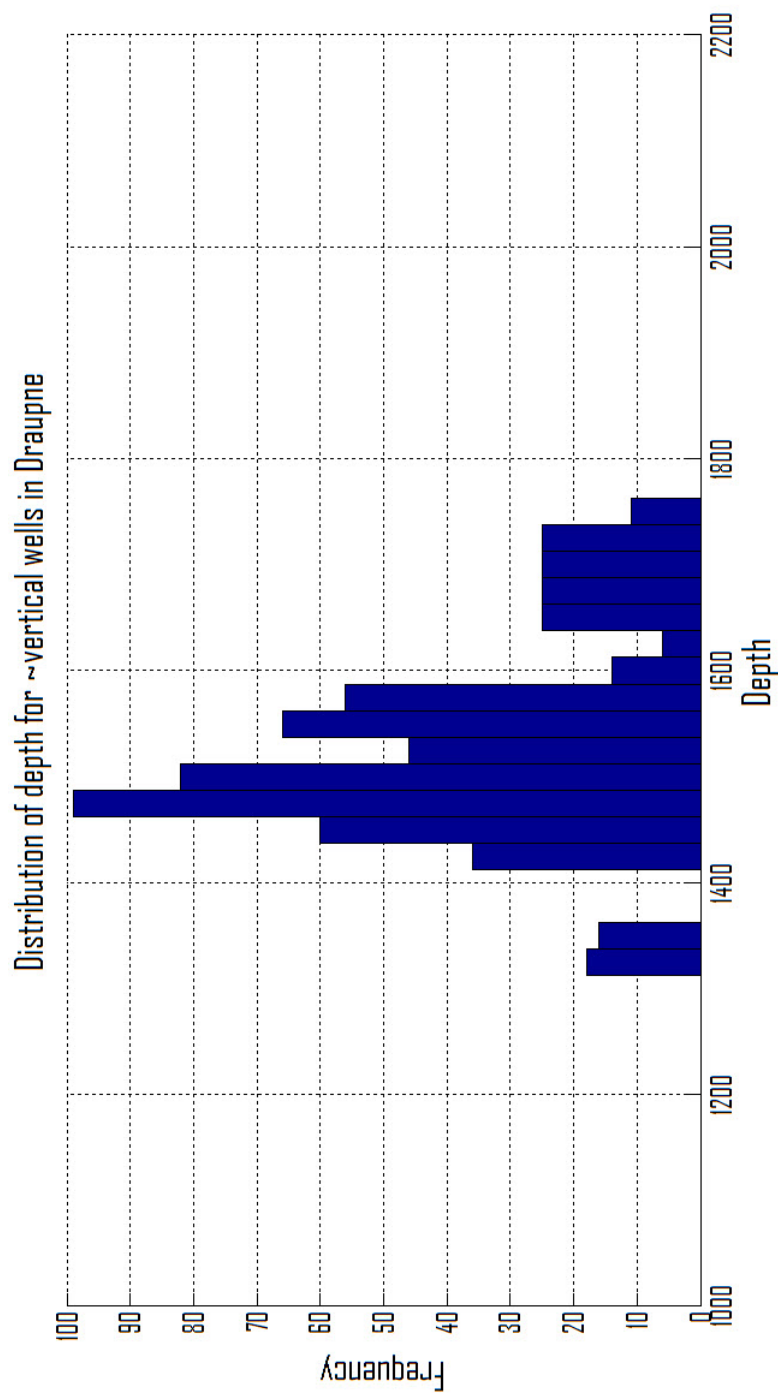
Figure D.8: A histogram showing the distribution of measured depth of the vertical wells in the Draupne Fm. interval.
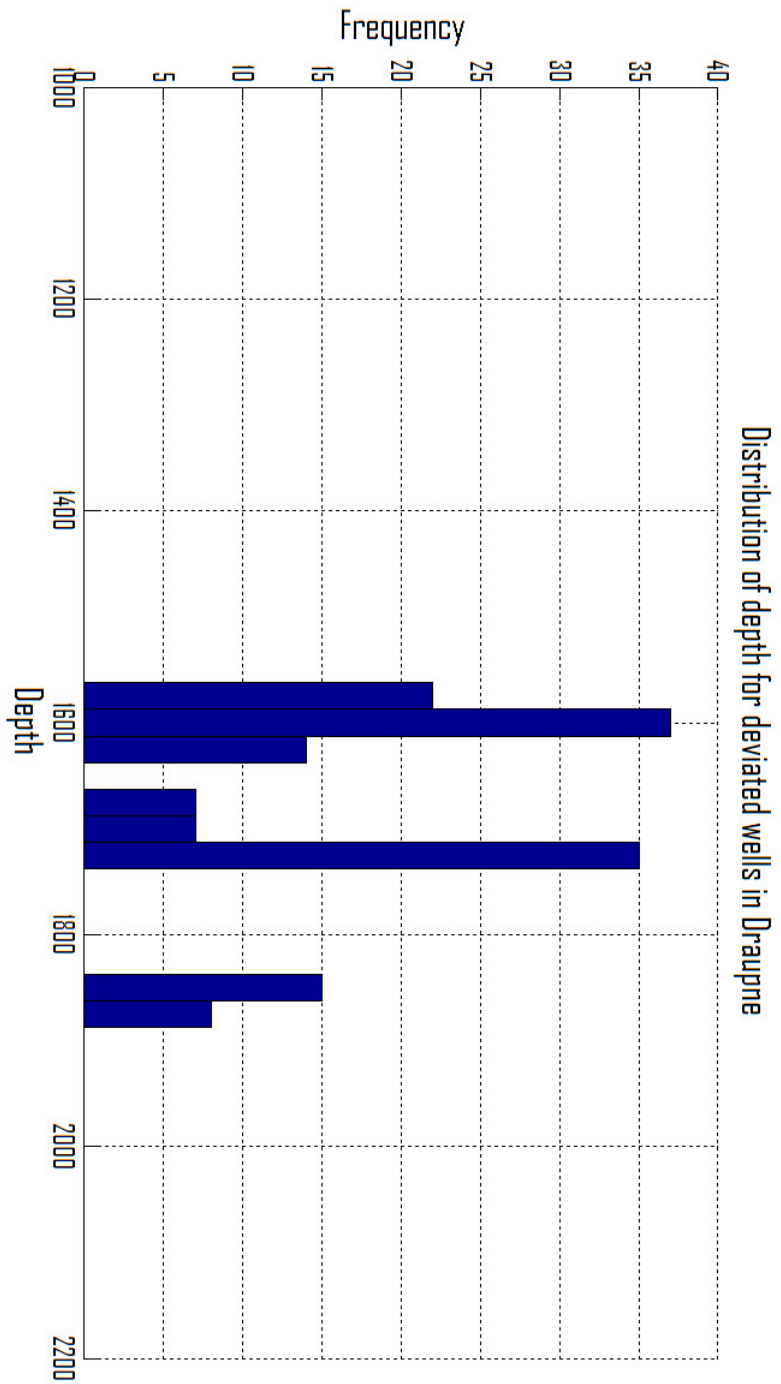
Figure D.9: A histogram showing the distribution of measured depth of the deviated wells in the Draupne Fm. interval.